# OPTIMAL OPERATION AND SECURITY ANALYSIS OF POWER SYSTEMS WITH FLEXIBLE RESOURCES

A Dissertation
Presented to
The Academic Faculty

by

Evangelos Polymeneas

In Partial Fulfillment
Of the Requirements for the Degree
Doctor of Philosophy in the
School of Electrical and Computer Engineering

Georgia Institute of Technology
December 2015

# OPTIMAL OPERATION AND SECURITY ANALYSIS OF POWER SYSTEMS WITH FLEXIBLE RESOURCES

Approved by:


Dr. A.P. Meliopoulos, Advisor
School of ECE
*Georgia Institute of Technology*

Dr. Andy Sun,
School of ISyE
*Georgia Institute of Technology*

Dr. Magnus Egerstedt
School of ECE
*Georgia Institute of Technology*

Dr. Shijie Deng
School of ISyE
*Georgia Institute of Technology*

Dr. Fumin Zhang
School of ECE
*Georgia Institute of Technology*


Date Approved: 09/22/2015

*To my parents, George and Klairi, for teaching me honor*

*and to Eirini, for always being there*

# ACKNOWLEDGEMENTS

This page is too small and the time allotted to its writing too short to find the right words to express gratitude to everyone that impacted the writing of this thesis. Be that as it may, I would first like to thank my advisor and mentor, professor A.P. Meliopoulos, for his feedback, advice and his unrelenting patience in dealing with a rather impatient and stubborn young researcher. His approach to teaching, mentoring and research is truly making the world a better place and it an outmost stroke of luck to have worked by his side.

I would be remiss not to mention the valuable contributions of my esteemed thesis committee. Professors Magnus Egerstedt and Fumin Zhang of my reading committee truly helped shaped this thesis with their precise and comprehensive feedback during my PhD proposal. I would also like to thank Professor Andy Sun, for closely following my work during my studies and for a series of interesting discussions on power system optimization. Furthermore, it is an honor to have professor Shijie Deng on my committee: his academic standing and years of work in our field speak for themselves. Lastly, I would like to thank professor Costas Vournas, from my alma matter, the National Technical University of Athens for his mentoring and guidance in my early years as a student in ECE.

It has been a pleasure and a privilege to have worked alongside such an esteemed group of colleagues at the Power System Control and Automation Lab at Georgia Tech. I would like to thank Evangelos Farantatos for providing me with guidance in my first steps and beyond, and Renke Huang for always being available to help and answer questions. I'm grateful to have worked with current members of the lab, including older friends such

as Liangyi Sun, Zhenyu Tan, Aniemi Umana, Rui Fan and Sanghun Choi and newer members, such as Rohit Jinsiwale, Bai Cui, Wenlu Fu, Yu Liu, Stella Kampezidou, Hussain Albinali and Orestis Vasios.

This thesis would not have been completed without the support of those close to me. I am forever grateful to my parents, George and Klairi and my sister Ioanna for supporting me despite my crazy decisions and to my better half, Eirini. Finally, Thymios, Michael, Christodoulos, Georgios, Yannis, Kostas, Spyros and Mike: thank you for making this journey amazing.

A special mention should go to Onassis Foundation for financially supporting me via an honorary scholarship for all these years.

# TABLE OF CONTENTS

# LIST OF TABLES

# LIST OF FIGURES

# SUMMARY

The objective of this research is to present a comprehensive framework for harnessing the flexibility of power systems in the presence of unforeseen events, such as those associated with component outages or renewable energy variability. Increased penetration of variable resources in the power grid, mainly in the form of wind and solar plants, has resulted in variable power flow patterns, increased thermal unit cycling and higher reserve capacity requirements. Furthermore, the variability of renewable energy output has increased the system's ramping requirements and threatens the system's voltage control capabilities. However, new sources of flexibility and network control are emerging to address these problems. Specifically, energy storage systems, demand side management, distributed energy resources and flexible transmission operation can participate by providing ramping services and/or voltage control, as well as by alleviating transmission congestion. This research focuses on contributing to modeling and optimization approaches for scheduling the operation of these sources of flexibility in a certain look-ahead horizon, ensuring a state of the art level of modeling accuracy, with full inclusion of voltage control considerations which do not exist in current DC-OPF modeling approaches. Also, by including reactive power flows, the network congestion model proposed is above par compared to the current state-of-the-art for look-ahead dispatch literature. Nevertheless, the model is further expanded by including a thermal model for transmission lines, which allows for the implementation of dynamic line ratings in look-ahead economic dispatch. The benefits from these augmented modeling capabilities are documented and compared with current operating practices.

Once an AC-OPF look-ahead optimization problem has been established, and the corresponding components have been modeled, further contributions are made in the area of remedial action schemes. The developed formulations allow for the identification of appropriate corrective actions that will restore feasibility in infeasible cases.

Finally, a combination of contingency filtering and contingency analysis approaches is developed, to allow for fast identification and analysis of critical outages in the transmission system. The filtering approach is based on a basic Taylor expansion of network power flow equations as well as a new formulation of margin indices that directly quantify the proximity to constraint violation in the post-outage system state. The analysis approach is based on low-rank modifications of the Jacobian matrix of network equations, to produce good estimates of post-outage operating states and map the effect on the system's operating constraints. Compared to current state of the art, advances are made both in the speed and the accuracy of the analysis, since the proposed filtering and analysis methods are fully unbalanced. The need for unbalanced security analysis is discussed and justified.

Through the contributions made in this research, a roadmap to increase flexibility in power system operations is developed. Namely, an enhanced modeling capability allows for integration of additional sources of flexibility and voltage control and a highly accurate security analysis and remedial actions formulation allows for improved response to unforeseen critical outages and rapid generation changes.

# Chapter 1. Introduction

## 1.1. Problem Statement

A wide range of newly introduced challenges have increased the complexity of power system operations. Increasing renewable power penetration has exacerbated temporal variations and increased the need for load following reserves. Furthermore, it has increased the uncertainty and has given rise to stochastic operations algorithms, especially for day-ahead planning purposes. Given the finite ramp rate of conventional units, these effects have in turn led to higher operational costs and threats to system reliability due to ramping insufficiencies. In addition, gradually increasing system stress combined with aging transmission infrastructure that was designed for system loading and generation technologies that were prevalent decades ago have increased the potential for transmission line congestion issues, leading to high marginal costs. A closely related issue is the threat to power system reliability, due to the gradual aging and retirement of transmission and generation assets, which is not associated with equally active infrastructure investments. Furthermore, the appearance of large wind farm installations has introduced new power flow patterns and in many cases has brought forth unforeseen congestion issues and potentially negative marginal prices. This issue is expected to unfold in ways that are hard to predict especially as system stress increases and as new load types are widely introduced, such as Electric Vehicles. As renewable and distributed generation gains ground in terms of cost effectiveness, the traditional methodologies for designing and operating the power grid are expected to become less relevant and adequate.

One particular manifestation of the upcoming challenges in the scheduling of power system operation is related to the concept of flexibility. The integration of a large capacity of renewable resources in bulk power systems has given rise to step up and down ramps in active power output (MW) from renewable sources, which, combined with already existing load ramps, translate to large ramps in Net System load. The capability of the system to respond to such large deviations in Net Load in short periods of time is known as the system's flexibility. CAISO's projection for a typical Net Load daily profile curve has become famous as the "duck curve" due to its characteristic shape, shown in Figure 1.1 (re-printed from [1]). An additional complication is the timing of these ramping events during the day cannot be accurately predicted in day-ahead studies, and they typically have to be addressed in shorter planning horizons, when the pool of committed generators with sufficient ramping capabilities may be very restricted. Similar ramping phenomena have been recorded or are expected to appear in other systems, such as the Irish [2] as well as the ERCOT, MISO and NYISO systems [6].

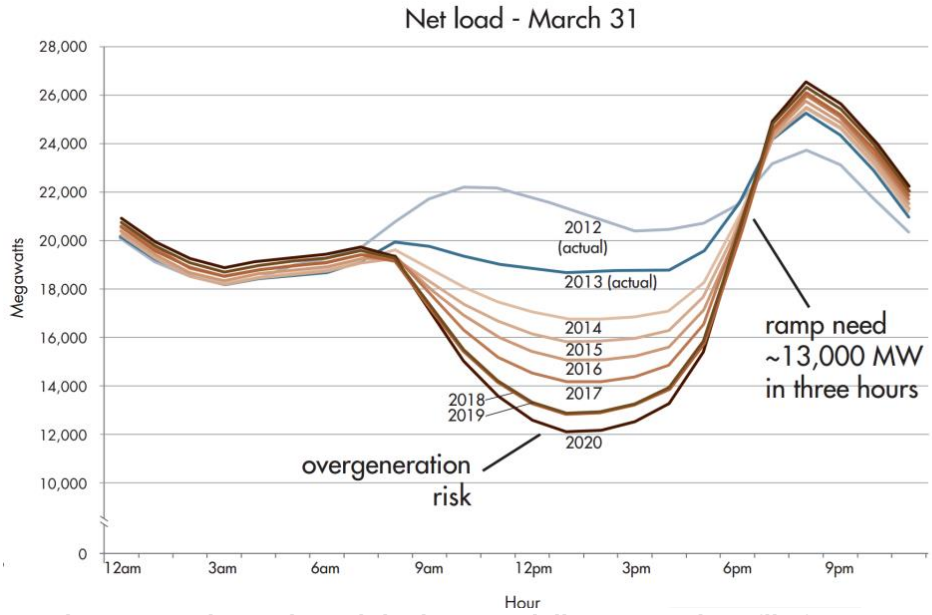


**Figure 1.1: The projected duck-curve daily Net Load profile for CAISO [1].**

However, ramp-rate related flexibility is not the only challenge for power system operations documented in the literature. With higher renewable penetration, voltage control is expected to become more challenging [2], bringing forth the need for including voltage control to the economic dispatch problem. Hence, voltage-agnostic DC-OPF operational tools that are widely used in practice are fundamentally ill-suited to address this challenge. Reactive power capability is expected to fall due to the displacement of synchronous generators by wind farms with reduced reactive support capability [2], while only 27% of wind farms currently offer reactive control dispatch.

Several studies in the recent years have focused on suggesting institutional, technical and infrastructure improvements to address the challenges from renewable integration. A DOE report [3] highlights the need for short term flexibility of generating units and particularly the need for an operational framework that will allow proper incentives and scheduling for this flexibility to be deployed, especially in the real-time operator action domain. Furthermore, the same study identifies that the additional flexibility may not be easily obtainable from conventional generating units, and suggests alternatives, such as demand side resources, energy storage units and Hybrid Electric Vehicles. A more comprehensive list of flexibility-providing technologies, and their maturity level, has been compiled in Table 1.1 [4].

**Table 1.1: Sources of Flexibility, their technical characteristics & maturity level**

| TECHNOLOGY | RAMP RATE / RESPONSE TIME | MATURITY |
|---|---|---|
| **Fossil Fuel Generators** | From 1.5%/min (coal) to 100%/min (internal combustion engines) | Very Mature |
| **Nuclear** | 4%-10% per min | Very Mature |
| **Biogas** | Very fast | Mature |
| **Co-generation** | 5-20%/min | Very Mature |
| **Active Control for wind plants** | 100%/min | Medium |
| **Demand management for industrial installations** | 20-100%/min | Medium-High |
| **Demand Management for households** | 100%/min | Low |
| **PHEV's** | 100%/min | Low-Medium |
| **Pumped Hydro** | 40%-100%/min | High |
| **Compressed Air Energy Storage** | 10-20%/min | Low |
| **Flywheels** | Milliseconds | Low |
| **Batteries** | Seconds | Medium |

An IEA study [5] showed that transforming system operation practices and market operation may mitigate the high costs of increases renewable resources integration. Specifically, moving towards real time operations, where the uncertainty is reduced, is considered very important.

A NERC report on flexibility [6], [7] stresses the need for additional flexibility due to the variability of renewable generation. In ERCOT for example, where wind reaches about 25% of load at times, there exist ramps of about 50% of total wind capacity in an hour. The report also highlights the importance of the capability to respond to extreme weather events that may produce wind cut-outs due to very high wind speeds. According the NERC, the sources of flexibility are:

- Conventional Units with ramping capabilities
- Demand Response

- Variable generation Management (renewable curtailment)
- Energy Storage & PHEV's
- Sub-hourly scheduling (look-ahead dispatch)
- Transmission Planning

An NREL report [8] comments on the needs for increased flexibility due to the increasing integration of renewable energy. NREL identifies the following as potential solutions to this issue:

- Flexible Operations: Move decision making closer to real time
- Flexible Demand Side Resources: Responsive distributed storage, customer load
- Flexible Transmission: Optimize transmission usage & improved access to resources
- Flexible Generation: units with high ramp-up & ramp-down capability

The aim of this research is to develop a framework for real-time power system operations that will address some of the challenges put forth by the studies mentioned above. Such a framework would have to:

- Rely on a real-time look-ahead scheduling formulation that is solvable in realistic time windows and schedules the operation of the system for a certain look-ahead horizon. It would be beneficial to model both ramping & voltage control phenomena.
- Model the novel sources of flexibility mentioned above, including energy storage, responsive demand, distributed energy resources, ramp-constrained generation.
- Include remedial action schemes for unforeseen severe events, such as critical component outages

- Have the capability to model & simulate a large number of potential contingency events that threaten the security of power system operations

This research addresses the challenges above by putting forth contributions in all of these areas. A detailed summary of contributions is offered in the next paragraph.

## 1.2. Research Objectives & Contributions

In order to address the challenges discussed above, especially in the short-term operational time-frame, in this research we focus on expanding the modeling of the short-term look-ahead dispatch to include new flexible components as well as more accurate network models. Once the model formulation has been set up, we modify the model to produce remedial action schemes in infeasible cases. Finally, at a given optimal solution a filtering & analysis framework is developed for identifying critical outages with a lowered computational cost. A summary of contributions in modeling (Distribution, Transmission, Generation & Storage) and in the real time operations & security analysis is given in Figure 1.2.

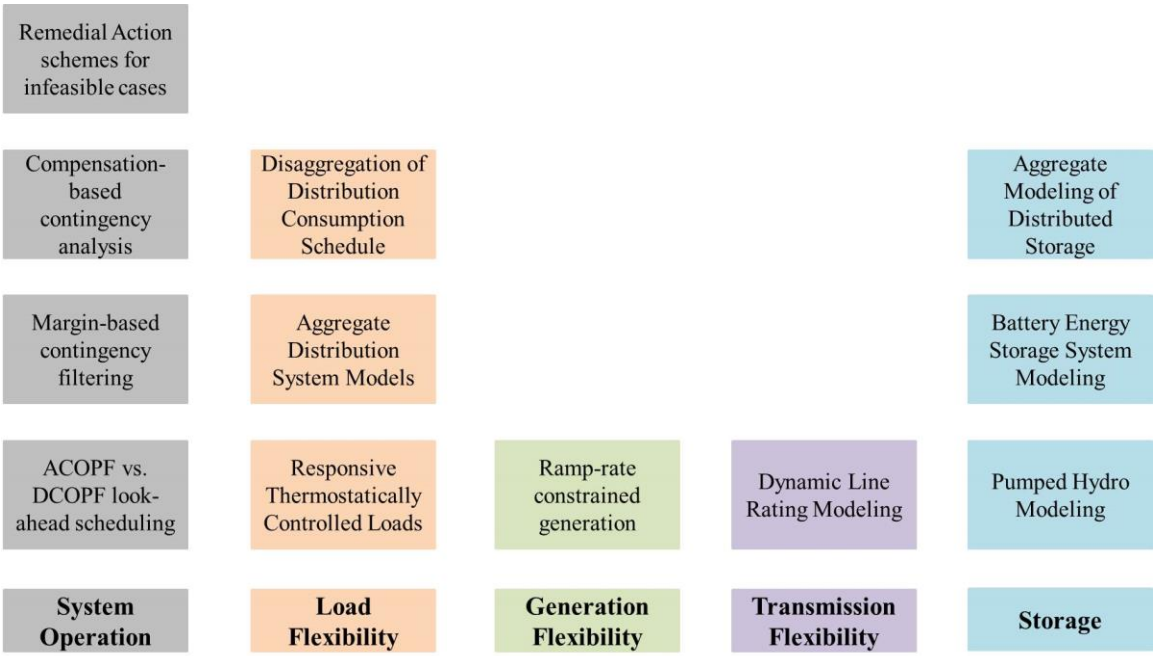


**Figure 1.2: Summary of contributions**

A summary of the outlined contributions is as follows:

**1. An implementation & comparison of AC versus DC look-ahead OPF formulations for scheduling flexible operations in power systems.**

A multi-period look-ahead AC-OPF is cast as a Quadratically Constrained Quadratic Programming (QCQP) problem and solved via primal-dual interior method. The non-convexity of the problem may lead to convergence to local minima. For this purpose, a DC-OPF look-ahead formulation is also put forth. This formulation is solved via Quadratic Programming and exhibits desirable convexity properties. In this research, the advantages and disadvantages of using either approach for real time operations are discussed. It should be stressed that the DC-OPF is the current operating practice. In this research, an effort is made to quantify the drawbacks of this practice due to reduced voltage control capabilities and inaccuracy of congestion modeling.

**2.a. Development of transmission, generation and load models that are currently disregarded in look-ahead OPF formulations.**

It is common for look-ahead scheduling to include standard models such as generators with ramping constraints and static models of network components, such as transmission lines and transformers. However, in this research we introduce physically based models of the following components into the look-ahead OPF:

- Thermal model of transmission line. This model allows for the implementation of dynamic line ratings. The benefits of transitioning from static line ratings to dynamic temperature-based ratings are also quantified.
- Thermostatically Controlled Load with temperature constraints
- Utility-scale Battery Energy Storage System, with separate charge and discharge efficiency

**2.b. Aggregate modeling of active distribution systems for transmission-level look-ahead scheduling algorithms & disaggregation of transmission-level commands to individual distributed energy resources.**

The effort to enrich the available modeling capabilities is extended to the development of an approximate aggregate dynamic model of an active distribution system that can be used to schedule its operation via the transmission-level look-ahead formulation. This addresses the issue of tractability and scalability for the control of small-scale distributed energy resources. By adding their capabilities to the dispatch procedure, a significant source of flexibility is utilized. Furthermore, a semidefinite programming approach for extracting this aggregate model from Distribution System simulation data is also developed. Finally, a Euclidian distance minimization problem is solved to implement the disaggregation of the aggregate distribution system schedule given by the look-ahead OPF in order to obtain the set of individual device controls that will, in aggregate, produce a

consumption pattern as close as possible to the desired one, as given by the look-ahead OPF solution.

**3. Remedial action & load shedding scheme formulation, with minimal load shedding**

The look-ahead OPF formulation, both in its accurate AC form and its approximate DC form can be an infeasible problem. Two algorithms are put forth for the determination of remedial actions, in the form of load shedding, in cases where they are needed, to restore feasibility. The first is an iterative stepwise de-relaxation algorithm where the equality constraints are initially relaxed but gradually enforced at a given maximum rate per step. The second is a direct & non-iterative minimal load shedding algorithm that identifies minimal load shedding actions by adding the load shedding quantities to the objective function and severely penalizing them. The two methods are compared and their applicability in practical test cases is examined

**4. Contingency Filtering & analysis for real time security analysis algorithms**

A real-time security analysis approach must be in place to evaluate the security analysis (N-1 or higher) of a given solution to the scheduling algorithm. In this thesis we develop a two stage (filtering – analysis) framework, where the first step consists of fast contingency filters for critical outages using newly defined margin indices, that quantify overall proximity to constraint violations. A first order Taylor expansion is used to obtain fast margin index estimates after an outage. The second step consists of performing one or more power flow iterations using the Newton method & the post-outage Jacobian matrix. A compensation method, using low-rank Jacobian corrections to increase the speed of these Newton iterations without sacrificing accuracy, is developed and theoretically justified.

The above contributions serve one common goal, whose importance was highlighted in Paragraph 1.1. That goal is to increase available power system flexibility by utilizing a wider range of tools. With the look-ahead dispatch formulation, the security analysis function and the remedial action scheme identification, the decision making is moved closer to real time, which is a key requirement for "flexible operations". Also, by including more resources to the flexibility pool, the overall system flexibility is extended beyond what conventional fossil fuel plants can offer. In particular, aggregate distribution system & dynamic line rating modeling constitute two important modeling options that have largely been ignored in the literature and their importance is highlighted here.

## 1.3. Thesis Outline

The remainder of this thesis is organized as follows. In Chapter 2 a review of related literature is performed and our original contributions are placed within the context of the body of work already available. The look-ahead AC Optimal Power Flow formulation and its solution method are put forth in Chapter 3, and a comparison with the DC-OPF look-ahead problem, which is the current state of the art, is presented. The two methods are compared on the basis of timing & accuracy of scheduling output. The library of dynamic models added to the optimization procedure is presented in Chapter 4, with strong emphasis on Dynamic Line Ratings and Aggregate Distribution System models, which are entirely new concepts in AC look-ahead scheduling. In Chapter 5 the handling of infeasible cases is examined, by proposing and examining two different algorithms to handle such cases, and benchmarking their performance. In Chapter 6 the problem of fast filtering of severe outages at a given candidate solution is examined, and the concept of margin indices is

developed to improve filtering accuracy. In Chapter 7 the related problem of contingency analysis with compensation methods is revisited, and some results are provided that allow for fast implementation of compensation methods, and identification of potentially islanding outages. Conclusions and suggestions for future work are given in Chapter 8.

# Chapter 2. Literature Review & Summary of Contributions

## 2.1. Overview

The increased penetration of variable resources in the Electric Grid is introducing new challenges for power system operation, such as thermal unit cycling [9], increased reserve requirements and thermal unit ramping insufficiencies [10]. These situations are detrimental [11], [12] both for power system reliability and economic operations and have resulted in frequent occurrences of price spikes in power markets. Specifically, in [13] the authors highlight that increased penetration of intermittent energy sources is expected to increase costs through increased reserve requirements and displacement of cheap units to cover the increased ramping needs. They conclude that increased system flexibility is a potential solution to this problem. Thus flexibility has arisen as a key concept in modern power system operation [14]. To formalize this concept, probability of ramping insufficiency has been proposed as a metric that quantifies available power system flexibility [15], [16].

In addition to optimal flexible operation, real time security analysis is also pivotal in addressing the new challenges in the horizon. The changing landscape in the electric power industry is associated with changing requirements in security monitoring and its associated impact on the operational reliability of the system. Gradual load increase, variable

generation (wind, PV), aging infrastructure [17], as well as the restructuring of the electricity markets [18], which is accompanied by strict separation of the power supply, transmission, distribution and operation entities, may threaten the reliable operation of the power system. Online security analysis [19] can be critical to evaluate power system security and prevent potential blackouts [17].

## 2.2. Flexible OPF

Flexible resources, such as large scale and distributed storage as well as responsive load [20] can serve as a solution to the problems mentioned in the overview section [21]. Several efforts to incorporate demand response within unit commitment & dispatch models have been recorded in recent literature [22], [23], [24] and [25]. The impact of demand side management on improving the operation of a grid with high renewable penetration has been demonstrated in the literature [26]. Large storage units, such as pumped hydro, have been shown to reduce costs and improve reliability in systems with considerable renewable penetration [28]. The role of storage in enabling renewable penetration and reducing the required reserves is verified through studies in the California system [27]. In [29] the authors discuss that, under a high wind penetration scenario the Texas ERCOT system is likely to experience high costs and thermal unit ramping insufficiencies that can be largely avoided utilizing storage and flexible system operations. Furthermore, recent studies have shown that modeling transmission constraints when assessing the available operational flexibility is very important for system operators [30].

Various methodologies to address the problem have been introduced in the literature. Significant work has been performed in the Security Constrained Unit Commitment

(SCUC) domain [31], [32], [33]. However, as we discussed in the introduction section, our work is focused on more accurate models than the ones used in simple SCUC and on shorter horizon operational time frames that are closer to real time. Hence, we are solving what is known as a look-ahead dispatch problem.

Research on look-ahead dispatch is not new [34],[35], but it has been gathering increasing attention with the projected increase in renewable penetration. An interior point method for the solution of this problem was provided in 2001 [36]. In [37] the problem is addressed by solving a muli-step DC robust dispatch problem. Although the model used is simple, the robust method offers substantial guarantees with respect to wind uncertainty. In a recent study [38] the authors proposed operating renewable resources with a flexible operating margin (below their maximum power point) with the help of a two stage stochastic optimization problem. Another approach is to relate variable generation with adequate flexible resources in order to address the variable output of the former [39]. A decentralized participation of flexible loads, such as space heaters and electric vehicles, optimized through the technique of lagrangian relaxation is proposed in [40] and a 24 hour horizon is implemented. Model predictive control has also been employed for dispatching demand response assets [41], but the effects of the transmission grid are neglected. In [42] the authors achieve the integration of storage dynamics into the dispatch model by solving a multi-step OPF problem. However, they focus their analysis on storage resources, and use an SDP relaxation for the solution, which is not always characterized by a zero duality gap. A similar problem is solved in [43] and it is solved using particle swarm optimization. PSO is also used in [44] to solve a multi-step optimization problem, but within the context of microgrid scheduling. An efficient PSO algorithm for the dynamic dispatch problem

was proposed in [45]. A hybrid PSO – interior point method has also been proposed for the Dynamic OPF problem [46]. An excellent formulation and solution algorithm for the multi-step optimal power flow using Benders' decomposition to take advantage of parallel computing is given in [47]. A detailed treatment of various multi-step Security Constrained Economic Dispatch problems, including flexible loads is given in [48]. A similar model has also been extended to multi-objective multi-step dispatch [49].

Although most existing approaches are focusing on active power issues, a voltage-stability oriented framework has recently been proposed [50]. The ability of responsive load to provide further ancillary services, such as regulation, has also recently been explored [51].

The need for a multi-period economic dispatch that has a sufficiently long time horizon and incorporates storage and demand response has been recognized by NREL [52]. Despite this fact, the shift towards multi-step OPF research has been relatively recent. In [53], a range of algorithms is proposed for the solution of the multi-step OPF problem. The same problem (although labeled "Dynamic Economic Dispatch"), is solved in [115], and some issues related to heuristic initialization rules are addressed. Our research is aimed at refining and improving recent previous work on the flexible multi-step optimal power flow [54].

The existing approaches either focus on introducing flexible resources to a single-period OPF problem or consider a multi-period unit-commitment type of problem with significant simplifications. In this research, a multi-period Flexible Optimal Power Flow (F-OPF) is proposed. Compared to literature that follows the same route, such as [52] and

[53], the formulation we developed puts forth important contributions to the existing body of work:

**1. AC modeling, with incorporation of system dynamics, nonlinearities & voltage control.** both flexible resources and traditional system components have dynamic constraints. Ramping constraints, storage dynamics and customer inconvenience constraints are such examples. The multi-period F-OPF formulation allows full modeling of these constraints that become particularly relevant in cases of high wind penetration. No linearization of the system model will be assumed, leading in a highly accurate modeling of all types of phenomena pertinent to the dispatch problem. Unlike existing approaches that rely on the DC approximation, our formulation has the capability for voltage control & consideration of reactive power flows.

**2. Significant expansion of the component modeling in the look ahead problem, with physically-based modeling of a wide range of new devices.** In our large-scale F-OPF we use a combination of accurate physically-based models of power system components and aggregate models for the flexible distribution feeders. The latter model itself is derived from high-fidelity physically-based models of customer-owned resources in the feeder, fully considering their constraints, such as customer inconvenience and set points. Due to the physically-based modeling, the extent of the flexibility offered by distributed resources is accurately quantified. Several other models, such as ramp-constrained generation, energy storage systems, thermostatically controlled loads and lines with dynamic thermal limits are also added to the look-ahead dispatch. We find that the flexibility offered by thermal line modeling and responsive loads, which is often neglected in current studies, has extremely important benefits for power system operation.

**3. Comparison with DC-OPF look-ahead dispatch state-of-the-art.** In this research we also implement the current state-of-the-art in look-ahead scheduling of transmission systems, which is a multi-step Quadratic Programming problem. Given that this problem has desirable properties of global optimality but important non-negligible assumptions regarding system modeling & voltage control, in this thesis we examine the cost associated with performing the look-ahead operations with the simplified model and explore the tradeoff between global optimality & speed of solution on the one hand (offered by the DC formulation) and modeling accuracy on the other (offered by our AC formulation).

## 2.3. Aggregate Distribution System Modeling

In order to smoothly incorporate flexible resources within the dispatch problem, the need to transition to a multi-period "flexible optimal power flow" (F-OPF) paradigm is apparent. This multi-period problem will incorporate inherent dynamic constraints in power system assets, such as ramping constraints for conventional generators and customer convenience constraints for responsive loads. One of the problems that needs to be addressed is aggregate modeling of distributed flexible assets. Specifically, each distribution feeder has potentially thousands of flexible (active) resources that cannot possibly be included within the F-OPF solution algorithm for reasons of scale and tractability.

Various efforts to model aggregate flexibility of distributed resources, while observing customer constraints, have been recorded in the literature. A first effort was to model Thermostatically Controlled Load (TCL) uncertainties using a state queuing model [55]. A refined version of this approach resulted in the use of Markov models for TCL state

estimation and control [56]. This framework was later extended to non-homogenous TCL populations [57]. Efforts to quantify TCL sensitivity using aggregate battery models have also been recorded [58]. Other approaches focus on an approximate first order model for TCL loads [59], or even higher order models for estimating ON/OFF populations [60].

Some efforts to implement the virtual power plant approach using physically based models exist in the literature. For example in [61] the authors propose a virtual power plant comprised of several space heaters that is able to track an active power command. However, estimation of the available flexibility is not described. The VPP method is also used in [62], but the proposed method is applicable only to thermal loads and utilizes their specific equation structure. An excellent method to aggregate thermostatically controlled loads is given in [63], but it is specific to TCL loads and it requires the solution of an expensive robust optimization problem in a receding horizon manner. An aggregation methodology is also proposed in [64], but it is proposed specifically for electric vehicle applications. An implementation of the virtual power plant concept using direct load control to dispatch the various responsive loads is given in [65].

On the implementation side, the communication and architecture needed for the realization of the Virtual Power Plant are explored in [66].

In this research we propose an aggregate model for the distribution feeder with flexible resources. Unlike existing research, that has mostly focused on specific resource types (for example only TCL's or only batteries), our model provides a description for the time evolution of the feeder's feasible set for any population of flexible resources. In addition, it is based on physically-based models of individual resources to derive the aggregate

abstract model. Hence, the results concerning the total operational flexibility of the feeder are expected to be very accurate.

In addition, compared to existing literature, the aggregate dynamic model presented here directly quantifies the feasible set for the aggregate active & reactive power consumption of the Distribution System, using a model identification procedure based on system data. The identification procedure is implemented by semidefinite programming, in order to obtain a maximal but conservative ellipsoidal approximation of the feasible set. Existing literature is not concerned with reactive power consumption of the feeder. However, it is necessary in our AC formulation of the look-ahead OPF, which fully considers voltage control.

Finally, an important contribution of this research is that we develop aggregate models purely for introduction to the transmission level optimization problem, not for aggregate control purposes. None of the existing approaches have models for the Distribution System feasible sets, and hence it is very difficult to introduce these aggregate models to the system-wide dispatch problems. In this research we implement both the aggregation, as well as the system-wide optimization and subsequently the disaggregation to each distribution-connected device, thus obtaining a full hierarchical optimization scheme.

## 2.4. Load Shedding & Remedial Action Literature Review

Due to unforeseen events, such as component outages or event extreme weather events and voltage instability situation during high load peaks, a partial curtailment of load may be required, in order to achieve feasible or secure operation of the power system. That action, known as load shedding, is part of a larger literature regarding Remedial Action

Schemes (RAS), which is also referred to as Wide Area Protection Schemes (WAPS) for power systems. Other remedial action schemes can be emergency re-dispatch of generators to modify the flow of power though the network or even emergency control of under-load tap-changers to address voltage stability issues. A relatively exhaustive summary of modern wide area protection controls is given in [67]. The role of such remedial schemes in improving reliability in the face of rising renewable energy penetration is discussed in [68]. Synchrophasor technologies have augmented the system operator's capabilities to implement such Wide Area Control techniques, due to increased observability & highly accurate state estimation techniques [69].

Investigation of load shedding methodologies is a very active area of power system literature. One of the first and very important contributions [70] centered on the solution of a static nonlinear optimization problem in order to minimize total congestion after an outage. Both generator dispatch and load shedding were considered as control variables. A different approach, focusing on addressing under-voltage issues and load recovery dynamics was proposed in [71]. A closely related method, based on continuation power flows and local sensitivities, provides a practical methodology to avoid voltage collapse [72]. These methodologies, and other similar to them, such as [73] and [74] focus on issues of such as the low computational cost or the distributed implementation of the proposed methods.

The research presented in this work is focused on finding the amount of load shedding required in order to restore solvability of the Look-Ahead Optimal Power Flow cases. Literature in this area is also quite rich. The idea to apply an interior point method in order to solve a static AC-OPF formulation with the objective of obtaining a minimum load

shedding required to restore a feasible solution was first proposed in [75]. The proposed approach works well, but it is a static (single-period) problem that cannot schedule load shedding actions in the future. Furthermore, its modeling capabilities are limited, since a simple formulation using only active & reactive power balance is used, ignoring all other complex models and constraints. A practical method to minimize the distance to the closest bifurcation point, in order to arrive to a feasible point is discussed in [76]. The main advantage of the method is the low computational overhead, but it is focused on re-dispatching, not load shedding. A methodology based on the primal-dual interior point method, using a formulation similar to [75], is proposed in [77], although it does not address its outlined disadvantages. An interesting method to schedule load shedding with the objective of minimizing customer interactions is put forth in [78], but it is focused on distribution system applications. A method that features some look-ahead capabilities is shown in [79], and decides both the time and magnitude of the load shedding. However, it is focused on short-term phenomena, such as voltage variations and short term angle oscillations. Furthermore, the algorithm used is a relatively show gradient search algorithm and the modeling capabilities are at the level of a quite simple optimal power flow. A very interesting approach that minimizes load shedding with the help of a static OPF but also gives the capability for short term overloads of transmission lines to decrease load shedding is discussed in [80]. However, a static algorithm is used, missing dynamic effects in transmission lines and the limit relaxation is largely ad hoc, without any modeling of transmission lines.

In this research, the modeling capabilities of the look-ahead OPF are utilized in order to create a minimal load shedding schedule formulation for a future horizon of certain

length. The dynamic nature of the look-ahead OPF allows for the inclusion of dynamic device models that do not exist in similar existing approaches, such as [75] and [80]. In particular, the capability to model dynamic line ratings of transmission lines, which are only modeled ad hoc in [80], but also other dynamic effects such as ramp-constrained generation, are expected to greatly impact load shedding requirements. Furthermore, the multi-period nature of the problem allows for calculation the location, the magnitude and the time of the minimal load-shedding. By appropriately penalizing load shedding, it also allows for prioritizing & scheduling re-dispatch procedures to avoid any load shedding, if it can indeed be avoided.

At the same time, an alternative load shedding calculation algorithm, based on gradually loading the system until further loading is not possible, is also discussed. The gradual-derelaxation algorithm does not achieve minimal magnitude load shedding but it features other advantages such as simplicity and improved convergence performance, as well as equal sharing of load shedding burden by all buses.

## 2.5. Contingency Selection

A basic problem in security assessment is the identification and selection of the contingencies that are critical to system security. The contingency selection problem was introduced in 1979 [81] and its importance to system security was documented [82]. NERC [83] mandates the secure operation of the system under any credible contingency. Solving a full AC power flow for each potential outage may impose a huge computational burden, thus making online security analysis impossible. Contingency selection is a methodology

to identify those contingencies that are potentially hazardous. Contingency selection must be efficient for practical systems. Contingency selection is of paramount importance in making online security assessment feasible [84]. It has been used for screening contingencies in Voltage Security Assessment applications [85] and Dynamic Security Assessment [86]. Fast contingency filters are also extremely important building blocks of algorithms that address the Security Constrained Optimal Power Flow (SCOPF) problem [87].

The contingency selection methods proposed in the literature can be divided into four main categories: i) Performance Index (PI) methods [88], [89] that choose a performance index function that describes a measure of system security and then rank contingencies based on the post contingency performance index value, often using a first-order estimate ii) Concentric Relaxation Methods [90] that are based on the assumption that only a local area around the location of the outage is affected by it, and a subsequent gradual relaxation of that assumption to increase accuracy iii) Bounding Methods [91] and [92] filter out non critical contingencies by incrementally bounding the post-contingency branch flows solving the power flow equations in an appropriately chosen sub-network. iv) Sparsity-oriented compensation methods [93], [94] or partial refactorization methods [95] that find the exact post-contingency solution either by determining the effects of topological changes on the power flow Jacobian using compensation methods or by performing Jacobian re-factorization in an efficient manner. Performance index methods typically require a much smaller number of overall computations, but are plagued by the reduced accuracy of the first-order estimate for the post-contingency value of the performance index. The PI-based technique may be inaccurate because the PI function is a highly

nonlinear function due to the nonlinearity of the power flow equations, and the existence of additional nonlinearities, such as generator reactive limits and Load Tap Changer (LTC) limits [96]. For this purpose, hybrid methods have been proposed, that combine the speed of PI methods with the accuracy of compensation methods [96] and [97].

While the existing literature has covered the topic of contingency selection and analysis for balanced networks, using the Traditional Power Flow (TPF) on single-phase equivalent models for power system components, the application of contingency selection methodologies in unbalanced networks remains an unexplored area. Furthermore, existing PI methods use metrics such as the post contingency real power line flows or the post contingency voltage deviation and reactive power injections [98]. However, for transmission lines, the actual thermal constraint is expressed in terms of line current, and not line apparent power, hence the existing PI methods are potentially inaccurate predictors of post-contingency line limit violations. Finally, existing methods focus on the modeling of traditional power system equipment, such as transmission lines and transformers. However, new components, such as Flexible AC Transmission Systems (FACTS) and Power Electronics Interfaced generation play a significant role in power system security [99], [100] and they need to be included in contingency studies.

The methodologies proposed in this paper combine accuracy and speed and allow reliable selection of critical contingencies. The proposed margin indices: (1) directly quantify the distance from constraint violation and (2) the constraint is expressed in terms of the actual constraint physical quantity, for example electric current for thermal limits. The need for this approach is motivated by the fact that actual power transmission systems exhibit imbalance and they are limited by ampacity.

The three-phase formulation allows separate treatment of each phase, addressing unbalanced cases. Second, the proposed state sensitivity method is characterized by decreased computations, due to the application of the compensation method for low-rank corrections of the Jacobian. Furthermore, the proposed methods assign a different weight to each constraint, based on the pre-outage proximity to the limit. Finally, both the index-based filtering and the state sensitivity indices discussed here constitute an extension and improvement of current filtering techniques, with respect to accuracy and speed.

## 2.6. Contingency Analysis

The aim of this work is to provide a unified and generalized framework for fast contingency analysis, combining concepts from power system modeling & analysis, linear algebra and parallel computing. The idea of using facts from linear algebra to improve the speed of modified network solutions is not new. In fact, the two competing approaches are compensation methods [93], based on the matrix inversion lemma to obtain the new solution of a linear network after a modification, and Partial Matrix Re-factorization [95] that focuses on intelligently re-factorizing the system Jacobian upon the topological change in the network. However, previous contributions focused on solving modified DC power flow equations or obtaining linear distribution factors [102], and do not discuss a general class of outages, focusing mainly on branch outages. More recent efforts to revisit these methods have focused on formulating a Newton-based load flow method for line outage analysis [103], but do not provide a generalized and concise formulation of the problem. Other recent work in contingency analysis has focused on refining the sensitivity-based framework [104] or elegantly addressed the multi-device outage problem [105], without

addressing the computational issues of solving low-rank modifications of AC power flows in the general case.

Inspired by previous work on compensation methods, in this work we develop a modeling and analysis framework that allows very fast solution of AC power flow equations, avoiding the re-factorization of the modified Jacobian. In order to achieve a general method, applicable to contingencies ranging from multiple to single devices and very simple branch models to complex models with intricate internal equation structure, we define a structured model syntax that enables straight-forward reformulation of the power flow equations. From this syntax, the Jacobian updates due to any contingency are readily available, and a compensation-based Newton-Raphson, for both single and full contingency analysis is obtained. As a next step, the issue of device mode transitions (such as PV/PQ transitions) and cascading outages due to device limit violations is addressed, and an algorithm that identifies these violations and incorporates the needed model switches into the fast contingency analysis framework is also developed.

# Chapter 3. Look-ahead economic dispatch through flexible optimal power flow

| | |
|---|---|
| $n_a$ | Number of through (current) variables |
| $n_s$ | Number of states |
| $n_u$ | Number of control variables |
| $n_h$ | Number of inequality constraints |
| $\mathbf{i}_k$ | $n_a$ x 1 vector of through variables (current injection) |
| $\mathbf{x}_k$ | $n_s$ x 1 vector of external (voltage) and internal states |
| $\mathbf{u}_k$ | $n_u$ x 1 vector of control variables |
| $\mathbf{p}_k$ | $n_\mathrm{p}$ x 1 vector of parameters for step $k$ |
| $f$ | Scalar device cost function |
| $\mathbf{g}(\mathbf{x}_{k-1},\mathbf{u}_{k-1},\mathbf{x}_k,\mathbf{u}_k \mid \mathbf{p}_k)$ | Device algebraic equations |
| $\mathbf{h}(\mathbf{x}_{k-1},\mathbf{u}_{k-1},\mathbf{x}_k,\mathbf{u}_k \mid \mathbf{p}_k)$ | Device inequality constraint expressions |
| $f(\mathbf{x}_k,\mathbf{u}_k)$ | Device cost function contribution at step $k$ |
| $\mathbf{a}_{eq}(\mathbf{p}_k)$ | Parameter-dependent function – an additive term participating in the device's algebraic expressions |
| $\mathbf{a}_{ineq}(\mathbf{p}_k)$ | Parameter-dependent function – an additive term participating in the device's inequality expressions |
| $Ind_d^x(\bullet)$ | An integer mapping from device-level state indices of device $d$ to system level state indices |
| $Ind_d^h(\bullet)$ | An integer mapping from device-level inequality indices of device $d$ to system level inequality indices |
| $Ind_d^u(\bullet)$ | An integer mapping from device-level control indices of device $d$ to system level control indices |
| $c(\mathbf{X}_k,\mathbf{U}_k)$ | System level cost function at step $k$ |

## 3.1. Quadratized Dynamic Device Modeling

One of the fundamental challenges in formulating and solving the flexible OPF problem is the capability to model a wide range of power system device models, in addition to the standard models of generators, transmission lines, transformer and loads. Indeed, an effective flexible OPF framework must include models for a wide range of storage technologies, explicit models of responsive loads with customer convenience constraints, as well as new dynamic models for classical devices, such as ramp-limited generators and dynamic thermal line ratings. In the context of this work, this issue is addressed by introducing "object-oriented" device models that describe the dynamics, algebraic equations and constraints of each device. The device modeling is completely decoupled from the algorithms used to handle the device's connectivity in the network, as well as the algorithms for the synthesis and solution of the optimization problem.

A quadratic device model is adopted, with the syntax as shown in (1):

$$\begin{bmatrix} \mathbf{i}_k \\ \mathbf{0} \end{bmatrix} = \mathbf{g}(\mathbf{x}_{k-1}, \mathbf{u}_{k-1}, \mathbf{x}_k, \mathbf{u}_k \mid \mathbf{p}_k) = \mathbf{a}_{eq}(\mathbf{p}_k) + Y_{eqx}\mathbf{x}_k + Y_{equ}\mathbf{u}_k + \begin{bmatrix} \vdots \\ \mathbf{x}_k^T F_{eqxx}^i \mathbf{x}_k^T \\ \vdots \end{bmatrix} + \begin{bmatrix} \vdots \\ \mathbf{u}_k^T F_{equu}^i \mathbf{u}_k^T \\ \vdots \end{bmatrix} + \begin{bmatrix} \vdots \\ \mathbf{x}_k^T F_{eqxu}^i \mathbf{u}_k^T \\ \vdots \end{bmatrix} - \mathbf{B}_{eq}^{k-1} \tag{1a}$$

$$\mathbf{B}_{eq}^{k-1} = -N_{eqx}\mathbf{x}_{k-1} - N_{equ}\mathbf{u}_{k-1} \tag{1b}$$

$$\mathbf{h}(\mathbf{x}_{k-1}, \mathbf{u}_{k-1}, \mathbf{x}_k, \mathbf{u}_k \mid \mathbf{p}_k) = \mathbf{a}_{ineq}(\mathbf{p}_k) + Y_{ineqx}\mathbf{x}_k + Y_{inequ}\mathbf{u}_k + \begin{bmatrix} \vdots \\ \mathbf{x}_k^T F_{ineqxx}^i \mathbf{x}_k^T \\ \vdots \end{bmatrix} + \begin{bmatrix} \vdots \\ \mathbf{u}_k^T F_{inequu}^i \mathbf{u}_k^T \\ \vdots \end{bmatrix} + \begin{bmatrix} \vdots \\ \mathbf{x}_k^T F_{ineqxu}^i \mathbf{u}_k^T \\ \vdots \end{bmatrix} - \mathbf{C}_{ineq}^{k-1} \tag{1c}$$

$$\mathbf{C}_{ineq}^{k-1} = -N_{ineqx}\mathbf{x}_{k-1} - N_{inequ}\mathbf{u}_{k-1} \tag{1d}$$

$$\mathbf{h}(\mathbf{x}_{k-1}, \mathbf{u}_{k-1}, \mathbf{x}_k, \mathbf{u}_k \mid \mathbf{p}_k) \le \mathbf{0} \tag{1e}$$

$$\mathbf{x}_{\min} \le \mathbf{x}_k \le \mathbf{x}_{\max}, \mathbf{u}_{\min} \le \mathbf{u}_k \le \mathbf{u}_{\max} \tag{1f}$$

$$f(\mathbf{x}_k, \mathbf{u}_k) = \mathbf{a}_f + \mathbf{b}_{fx}^T\mathbf{x}_k + \mathbf{b}_{fu}^T\mathbf{u}_k + \mathbf{x}_k^T C_{fxx}\mathbf{x}_k + \mathbf{x}_k^T C_{fxu}\mathbf{u}_k + \mathbf{u}_k^T C_{fuu}\mathbf{u}_k \tag{1g}$$

The constant vectors $\mathbf{a}_{eq}(p)$ and $\mathbf{a}_{ineq}(p)$ are $n_s \times 1$ and $n_h \times 1$ vector functions respectively. The argument of this function is a vector of device parameters at step *k*, to allow for parameter dependent models. $Y_{eqx}, Y_{equ}, Y_{ineqx}, Y_{inequ}$ are appropriately sized matrices defining the linear terms in equations (1a) and (1c). Furthermore, the quadratic terms, if any, are defined by collections of sparse matrices, such as $F_{eqxx}^i$. Finally, lower and upper bounds on the participating variables are treated separately from general constraints ***h***. In cases of variables without lower or upper limits, extremely low or large values are set as the lower and upper bounds respectively.

Without loss of generality, this model can be used to represent any flexible resource. Note that constraints (1a) and (1c) include both static and dynamic equalities and inequalities, respectively. The dynamics are captured by the past history vectors (1b) and (1d). If the equations are static the past history vectors are zero.

The cost of operating the system is assumed to have quadratic structure as well (1g). The matrices $C_{fxx}, C_{fxu}$, and $C_{fuu}$ are stored in sparse format. In the classical OPF problem, it should be expected that, for most devices, the factors involved in (1g) have zero values, except for generators. However, this formulation allows flexibility for experimentation with other objective functions in different settings (such as customer flexibility markets) & future research.

From an implementation perspective, it is worth noting that, while linear and constant terms ($Y_{eqx}$, $Y_{equ}$, $Y_{ineqx}$, $Y_{inequ}$ e.t.c.) can be stored as full matrices, quadratic terms, such as $F^{i}_{eqxx}$, must always be stored in sparse form, for computational and storage economy reasons.

This is a quadratic model that accurately represents each device's dynamics. It is obtained by integrating the corresponding differential-algebraic equations (e.g. through quadratic integration [106]). The main advantage of this sparse quadratic syntax is that it allows an efficient algorithmic computation (object oriented) of Jacobeans, Hessians, etc. of the underlying optimization problem, without compromising the capability of utilizing nonlinear device models.

The device interacts with the rest of the network via its through variables. Specifically, the current equations of all devices that are connected to the same node must sum up to zero, in order to enforce Kirchhoff's Current Law. For this purpose, the device model also contains a $n_s$ x 1 connectivity vector to map from the device-level equations to the network-level equations:

$$Ind^{x}_{d}(m) = n \tag{2}$$

This signifies that the *m*-th equation of device *d* maps to the *n*-th system-level equation.

## 3.2. Equation Synthesis & Problem Formulation

The device data structures defined in Paragraph 3.1 are adequate to synthesize the system-level look-ahead optimization problem in a concise manner. Specifically, the *n*-th equality constraint for the system level flexible optimal power flow is:

$$g_n(\mathbf{X}_{k-1}, \mathbf{U}_{k-1}, \mathbf{X}_k, \mathbf{U}_k) = \sum_{Ind_d^x(m)=n} g^{(d)}(\mathbf{x}_{k-1}, \mathbf{u}_{k-1}, \mathbf{x}_k, \mathbf{u}_k) \tag{3}$$

A similar process is followed to synthesize the system level inequality constraints *h*. Note that, for this framework to be operational, a mapping between the system-level and the device level states, controls and inequalities must also exist. Namely, the *n*-th system level inequality constraints at each step is:

$$h_n(\mathbf{X}_{k-1}, \mathbf{U}_{k-1}, \mathbf{X}_k, \mathbf{U}_k) = \sum_{Ind_d^h(m)=n} h_m^{(d)}(\mathbf{x}_{k-1}, \mathbf{u}_{k-1}, \mathbf{x}_k, \mathbf{u}_k) \tag{4}$$

The objective function for the system at step *k* is given simply as the summation of the individual cost functions for the $N_d$ devices:

$$c(\mathbf{X}_k, \mathbf{U}_k) = \sum_{i=1}^{N_d} \mathbf{f}^{(d)}(\mathbf{x}_k, \mathbf{u}_k) \tag{5}$$

Given the quadratic structure of the device cost functions (1g), the system cost function is also quadratic.

Using these synthesis rules, the following *K*-step problem is defined:

$$
\begin{aligned}
&\min_{\mathbf{X},\mathbf{U}} \sum_{k=1}^{K} c(\mathbf{X}_k, \mathbf{U}_k) \\
&\text{subject to} \\
&\mathbf{g}(\mathbf{X}_{k-1}, \mathbf{U}_{k-1}, \mathbf{X}_k, \mathbf{U}_k \mid \mathbf{P}_k) = 0 \quad k = 1,2,\ldots,K \\
&\mathbf{h}(\mathbf{X}_{k-1}, \mathbf{U}_{k-1}, \mathbf{X}_k, \mathbf{U}_k \mid \mathbf{P}_k) \le 0 \quad k = 1,2,...,K \\
&\mathbf{U}_{\min} \le \mathbf{U}_k \le \mathbf{U}_{\max} \quad k = 1,2,...,K \\
&\mathbf{X}_{\min} \le \mathbf{X}_k \le \mathbf{X}_{\max} \quad k = 1,2,...,K \\
&\mathbf{X}_0 = \mathbf{X}_{init} \\
&\mathbf{U}_0 = \mathbf{U}_{init}
\end{aligned}
\tag{6}
$$

The flexible OPF problem in (6) is a quadratically constrained quadratic program (QCQP). Note that $\mathbf{X}_k$, $\mathbf{U}_k$ and $\mathbf{P}_k$ are the consolidated system state, control and parameter vectors respectively. The parameter vector depends on the particular device models employed, but typical parameters include load active and reactive consumptions & wind speed values. Hence, (6) needs to be solved independently for each possible scenario in the look-ahead *K*-step horizon. This work is focused on the deterministic look-ahead OPF, i.e. solving (6) for a given scenario of parameters.

## 3.3. Solution Method

The look-ahead AC-OPF problem is a non-convex Nonlinear Programming (NLP) problem [107]. Numerical solutions to such problems are plagued by sensitivity to initial guess, lack of global optimality guarantees and potentially lack of global convergence guarantees. Given the large scale of the problems under consideration, the class of algorithms used in this research was the Primal Dual Interior Point method, which is widely used for the AC-OPF problem ([108], [109]). The method is amenable to sparse matrix

techniques, which is consistent with the sparse structure of network equalities and inequalities.

The solver used in this research is IPOPT [110], which comes with global convergence properties, utilizing an interior point method with a filter line search step that guarantees global convergence under mild regularity conditions. Global optimality is not guaranteed; merely convergence to a stationary point for the problem's Lagrangian. Hence, no global optimality claims are made in this research, whenever the AC-OPF look-ahead algorithm is concerned.

The numerical performance of IPOPT is considerably improved if explicit expressions for the constraint & objective gradients, as well as the Lagrangian's Jacobian are provided. The quadratic structure of the flexible OPF enables computationally efficient calculation of sparse Jacobian & Hessians. Namely, problem (6) is structured as follows in our framework:

$$\begin{aligned} &\min_{\mathbf{z}} \; f(z) = \mathbf{z}^{\mathrm{T}} A_f \mathbf{z} + b_f^T \mathbf{z} + c_f \\ &\text{subject to} \\ &\mathbf{z}^T H_{g,i} \mathbf{z} + b_{g,i}^T \mathbf{z} + c_{g,i} + a_{g,i}(\mathbf{P}) = 0 \quad i = 1,\ldots,N_s \\ &\mathbf{z}^T H_{h,i} \mathbf{z} + b_{h,i} \mathbf{z} + c_{h,i} + a_{h,i}(\mathbf{P}) \le 0 \quad i = 1,\ldots,N_h \\ &\mathbf{z}_{\min} \le \mathbf{z} \le \mathbf{z}_{\max} \end{aligned} \tag{7}$$

The problem cast in variables **z**, defined as:

$$\mathbf{z} = \begin{bmatrix} \mathbf{X}_1 \\ \mathbf{U}_1 \\ \vdots \\ \mathbf{X}_k \\ \mathbf{U}_k \end{bmatrix} \tag{8}$$

Hence, the gradients are calculated as follows:

$$\nabla_z f = \mathbf{z}^T (H_f + H_f^T) + b_f^T \tag{9a}$$

$$\nabla_z g_i = \mathbf{z}^T (H_{g,i} + H_{g,i}^T) + b_{g,i}^T \tag{9a}$$

$$\nabla_z h_i = \mathbf{z}^T (H_{h,i} + H_{h,i}^T) + b_{h,i}^T \tag{9c}$$

The Lagrangian hessian is calculated as follows:

$$\nabla_{zz} L(\mathbf{z}, \boldsymbol{\lambda}_g, \boldsymbol{\lambda}_h) = A_f + \sum_{i=1}^{N_s} \lambda_{g,i} H_{g,i} + \sum_{i=1}^{N_h} \lambda_{h,i} H_{h,i} \tag{10}$$

The sparse structure of $H_f, H_g, H_h$ and $b_f, b_g, b_h$ allows for quick calculation of the sparse gradients and hessians This allows, from an implementation perspective, use of IPOPT with relatively small external overhead for obtaining Jacobians and Hessians. This is the primary benefit the Quadratic formulation of the look-ahead AC-OPF developed in this research.

### 3.4. The DC-OPF look-ahead dispatch

The DCOPF look-ahead dispatch is a version of the look-ahead problem that relies on the DC Optimal Power Flow at each step [48], [49]. In turn, the DC-OPF is based on the assumption that branch resistances can be neglected, and that voltage magnitudes remain constant at unity. Hence the power flows on lines depend on the voltage phasor angles, which become the only variables in the DC-OPF. In order to implement this approach and compare with the AC-OPF look-ahead dispatch developed in this work, additional dynamic models of devices, consistent with the DC assumptions were developed. In these models:

- The interface variables with the point of connection of each device are the node's angle $\theta$ and the incoming (absorbed) active power by the device, instead of $I_r^k, I_i^k$ and $V_r^k, V_i^k$ respectively.
- Kirchoff's current law is enforced by requiring that the sum of active power in a node be zero, instead of currents in the AC-OPF.
- Any reactive power aspects of connected devices are neglected. Indeed, the DC-OPF does not consider reactive power dispatch in any way
- To maintain the main linearity advantage of the DC-OPF, all device models used were linear.

With the above developments, the DC-OPF look-ahead dispatch becomes a Quadratic Programming problem (convex quadratic cost function with linear constraints). This problem is now essentially a succession of DC-OPF's with transition constraints for all dynamic devices:

$$\min_{\theta_i, X_i} \left\{ \sum_{j=1}^{N_g} a_{g,i} P_{g,i}^2 + b_{g,i} P_{g,i} + c_{g,i} \right\}$$

subject to

$$\begin{aligned} &\sum_{j \in N_i} P_j(\theta_i^k, X_j^k, \theta_i^{k-1}, X_j^{k-1}) = 0 && \forall i = \in \{1, \dots N_b\}, \forall k \in \{1, \dots K\} \\ &A_j \theta_i^k + B_j X_j^k + C_j \theta_i^{k-1} + D_j X_j^{k-1} \le b_j && \forall j = \in \{1, \dots N_d\}, \forall k \in \{2, \dots K\} \\ &E_j \theta_i^k + F_j X_j^k + G_j \theta_i^{k-1} + H_j X_j^{k-1} = 0 && \forall j = \in \{1, \dots N_d\}, \forall k \in \{2, \dots K\} \end{aligned} \tag{11}$$

The DC-OPF look-ahead dispatch problem is a quadratic programming (QP) problem [111]. Assuming the problem is feasible and bounded, as is the case in Optimal Power Flow problems, (11) is solvable by mature Interior Point Methods. Primal-Dual interior point method is a mature method to solve such convex problems to global optimality [111]. The

Interior Point solver used in this research is IPOPT [110], however the results are also verified using MIPS, which is part of the MATPOWER package [112], in the MATLAB environment.

Given that the AC-OPF look-ahead dispatch is a non-convex formulation and the PDIPM algorithm may converge to local minima, it is of interest to compare its output with the results of the DC-OPF look-ahead dispatch, which is a convex formulation that uses less accurate linearized models for the system's devices.

**Table 3.1: AC-OPF vs. DC-OPF look-ahead dispatch features**

| FEATURES | DC-OPF LOOK AHEAD DISPATCH | AC-OPF LOOK-AHEAD DISPATCH |
|---|---|---|
| TRACTABILITY | Smaller Size<br>QP Problem | Larger Size<br>Non-convex problem |
| GLOBAL OPTIMALITY | Solved to global optimality | Global optimality not guaranteed |
| CONVERGENCE GUARANTEES | Always converges (under mild regularity conditions) | Convergence sensitive to initial guess |
| MODELING ACCURACY | Approximate Models<br>Inaccurate Congestion Modeling | Physically Based & Accurate Models<br>Models non-linear phenomena |
| QUALITY OF DISPATCH | Only active power dispatch | Full active-reactive dispatch |
| FEASIBILITY OF REAL-TIME DISPATCH | Static AC-OPF dispatch may be infeasible | Guarantees feasibility |

The difference between the two formulations is summarized in Table 3.1. The DC-OPF is a convex problem, with strong convergence and global optimality guarantees. However, unlike the AC-OPF look-ahead dispatch, it utilizes the DC approximation which may misrepresent the actual behavior of the electric grid. As such, if dynamic devices (such as storage or ramp-constrained generation) are scheduled using the DC-OPF, then any errors introduced by the DC approximation will have to be corrected in the clearing of the

real-time (static) operation of the system, either through out-of-market actions or a corrective dispatch using more accurate models. These actions may carry more cost or may even be insufficient to restore feasibility, under extreme conditions. Hence, the inaccuracy of the DC-OPF problem may lead to higher costs or even infeasibility of the real-time dispatch. Finally, unlike the AC-OPF, the DC-OPF clearly ignores all non-linear effects and all control variables except for active power dispatch. Thus, it does not perform or account for reactive dispatch, load tap changing mechanisms e.t.c..

In order to explore the tradeoff between the globally optimal DC-OPF and the more accurate AC-OPF model, tests were performed in various standard test cases. The same scenarios (load variation & renewables output) were solved using a DC-OPF and an AC-OPF look-ahead dispatch. In order to consider the corrective dispatch issues of the DC-OPF, the dispatch schedules produced by this method were used to schedule the dynamic resources (ramp-constrained generation and storage in this case) and a static corrective AC-OPF was solved at each step, by keeping the dynamic dispatch fixed to the output of the DC-OPF, in a two stage fashion. On the other hand, the look-ahead flexible AC-OPF output was used for the scheduling of all control variables, and no static dispatch was needed for that case. The comparison methodology for the two different look-ahead formulations is shown in Figure 3.1 .

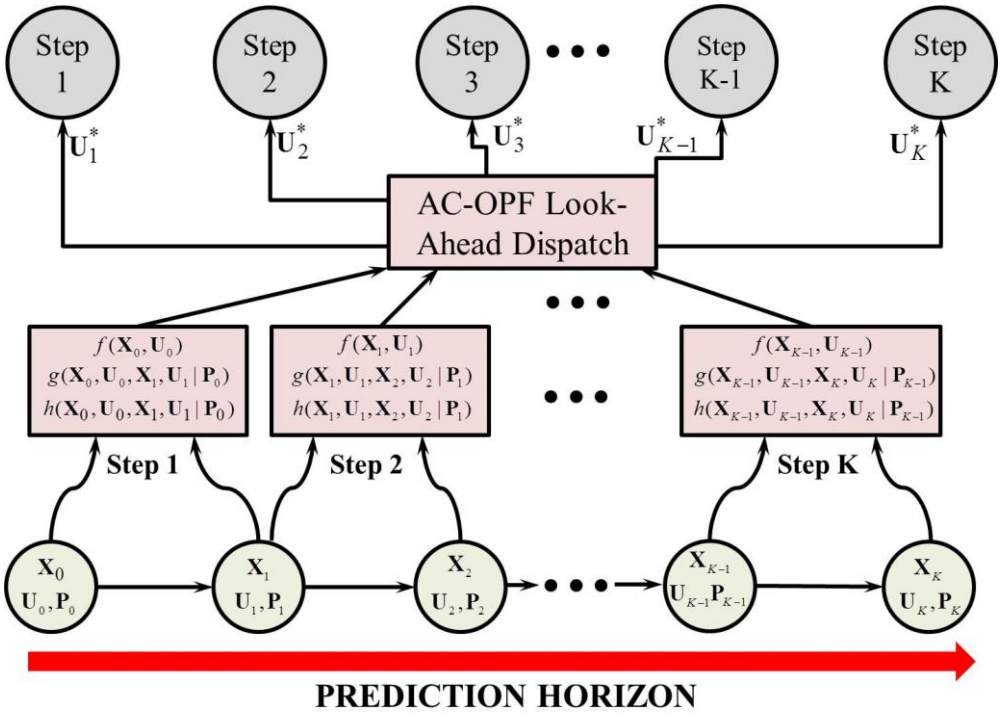


(a)

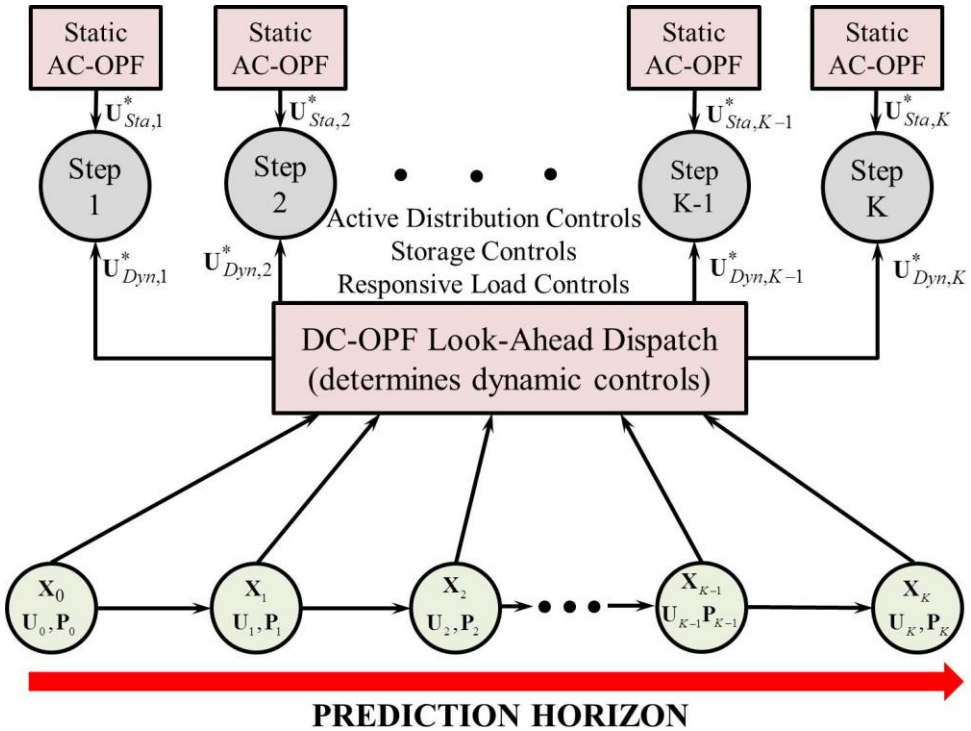


(b)

**Figure 3.1: AC-OPF versus DC-OPF evaluation method (a) AC-OPF (b) DC-OPF**

The total operating cost of these two different frameworks was recorded for each case. The first case study used was the IEEE 30 bus system (Figure 3.2). A wind farm with a base case capacity of 35MW and a storage unit with base case capacity of 50MW, 100MWh were placed in bus 6. The transmission corridor 6-8, which is a 32MVA, 135KV line, is congested in this particular system. Because of different congestion models used by the AC-OPF and the DC-OPF we expect significant variations in the dispatch results. A summary of different scenarios examined, and the corresponding operating cost yielded by the two different look-ahead dispatch frameworks under examination is given in Table 3.2.

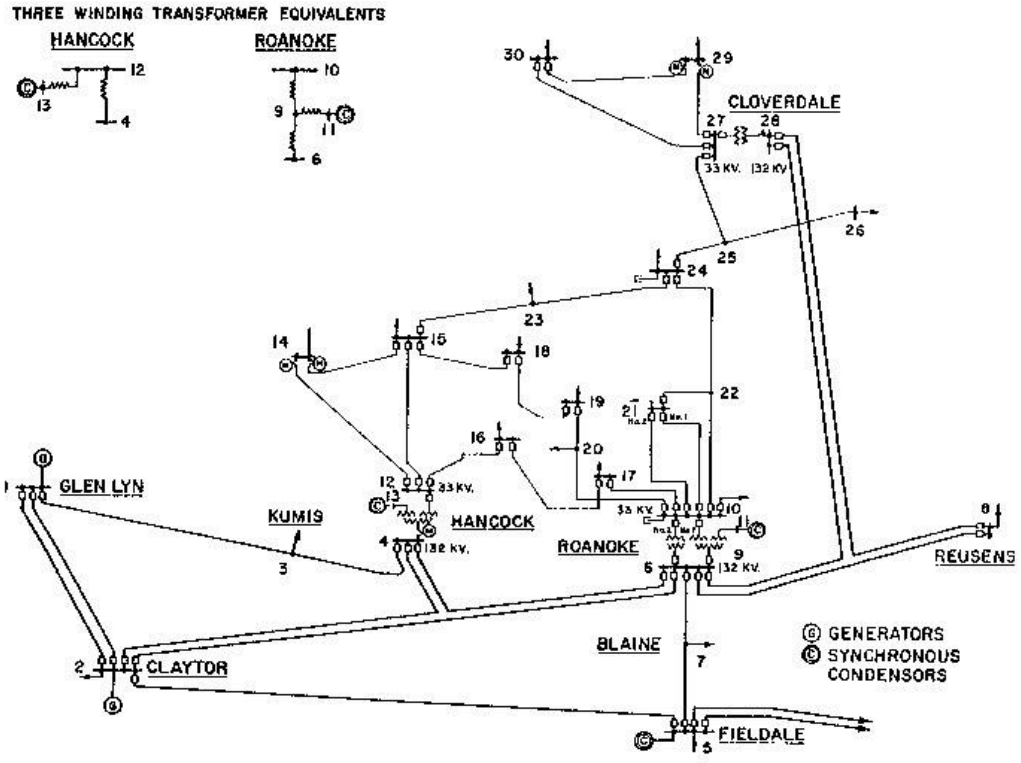


**Figure 3.2: IEEE 30-bus system**

**Table 3.2: AC-OPF versus DC-OPF dispatch operating cost results – IEEE 30 bus**

| Scenario | Storage Energy | Storage Power | Wind Penetration | DC-OPF Cost | AC-OPF Cost | Cost w/o storage |
|---|---|---|---|---|---|---|
| A | 100MWh | 50MW | 35MW | 5.6228e+04 | 5.5623e+04 | 5.6381e+04 |
| B | 200MWh | 100 MW | 35MW | 5.6095e+04 | 5.5068e+04 | 5.6381e+04 |
| C | 50MWh | 25MW | 35MW | 5.6313e+04 | 5.6048e+04 | 5.6381e+04 |
| D | 300MWh | 150MW | 35MW | 5.5479e+04 | 5.4618e+04 | 5.6381e+04 |
| E | 100MWh | 50MW | 70MW | 4.8897e+04 | 4.8281e+04 | 4.9142e+04 |
| F | 100MWh | 50MW | 135MW | 4.2105e+04 | 4.1348e+04 | 4.2448e+04 |

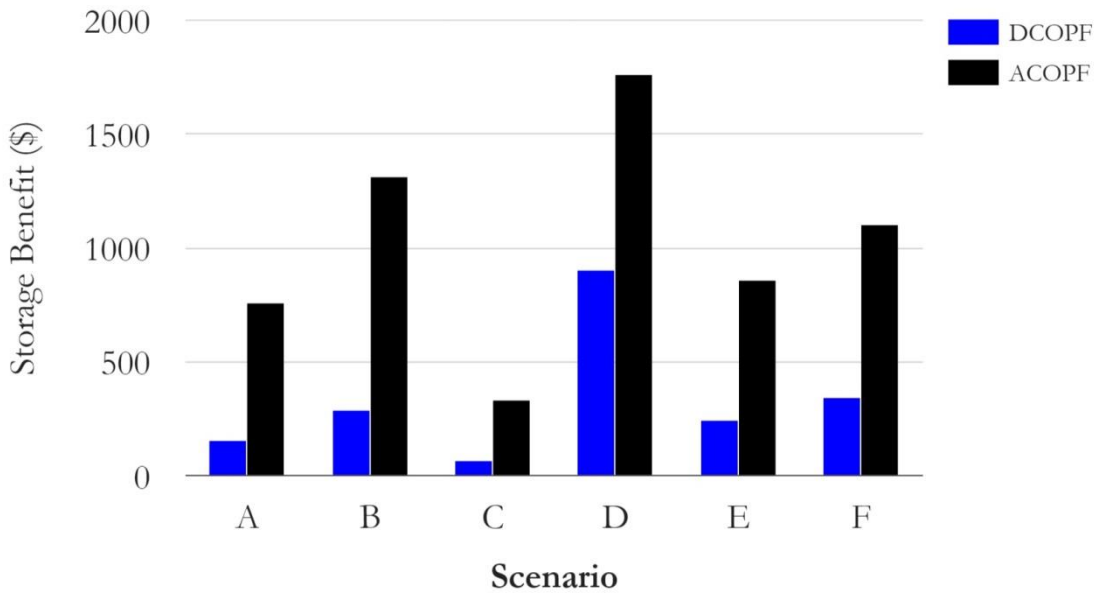


**Figure 3.3: Cost Reduction from Battery Operation – ACOPF vs. DCOPF in 30 Bus Case**

As shown in Table 3.2, for the scenarios under examination, the AC-OPF dispatch yields lower operational cost than the DC-OPF dispatch with AC-OPF corrective actions. Although this case study does not allow for general conclusions to be drawn, in this particular case the AC-OPF look-ahead dispatch is preferable since it allows more efficient

utilization of installed storage capacity. In order to further quantify this, Figure 3.3 shows the *Storage Cost Reduction*, i.e. the reduction in operating cost compared to what the cost would be if storage was completely removed from the system, for the two different look-ahead dispatch procedures. For completeness, that cost value is given in the last column of Table 3.2. It is clear that in all cases the AC-OPF look-ahead dispatch allows better utilization of the storage installed in bus 6. This is attributed mostly to the more accurate modeling of the congestion in line 6-8 in the AC formulation.

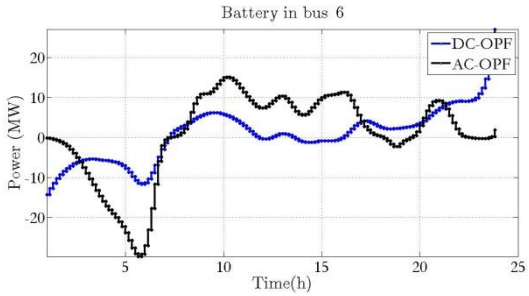


(a) Case A - Battery Power

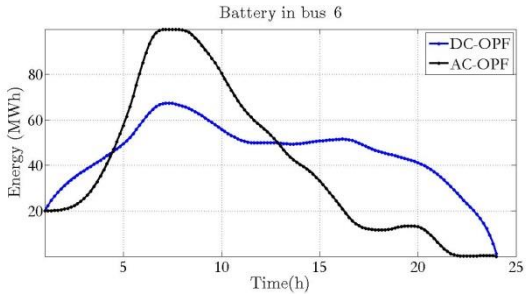


(b) Case A- Battery Energy

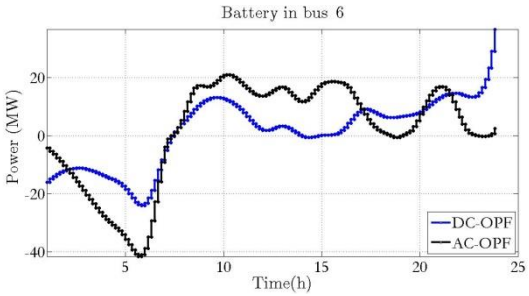


(c) Case B – Battery Power

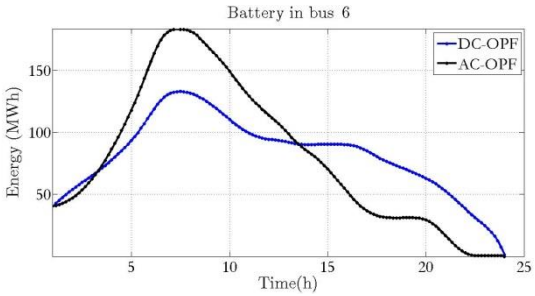


(d) Case B – Battery energy

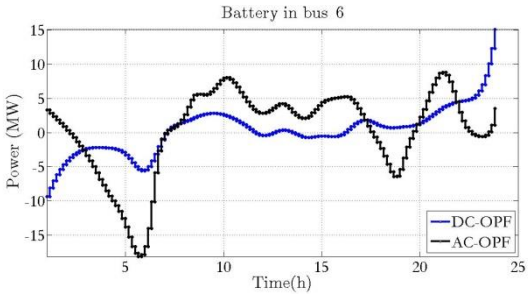


(e) Case C – Battery Power

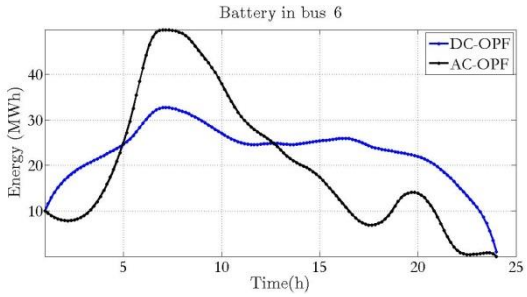


(f) Case C – Battery Energy

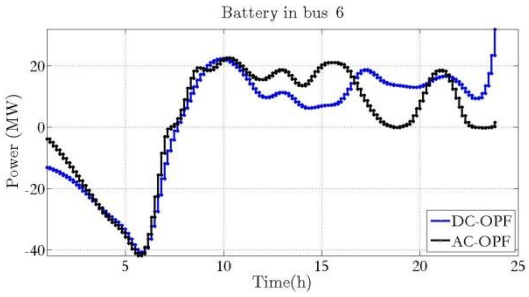


(f) Case D – Battery Power

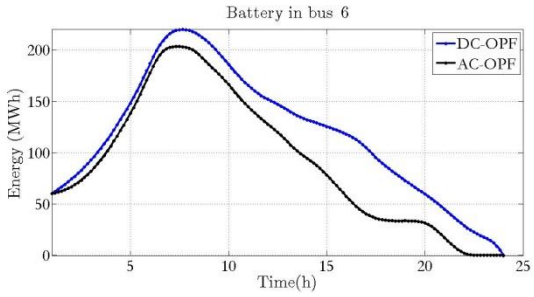


(g) Case D – Battery Energy

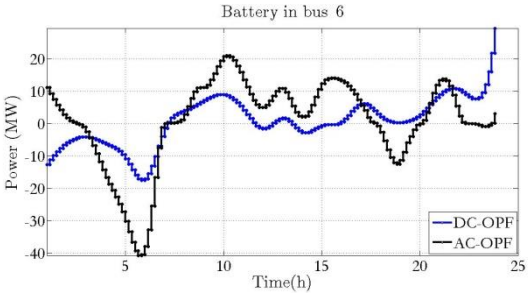


(h) Case E – Battery Power

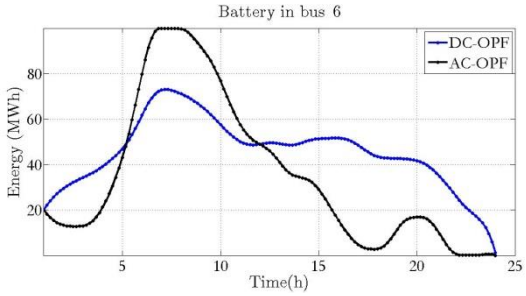


(i) Case E – Battery Energy

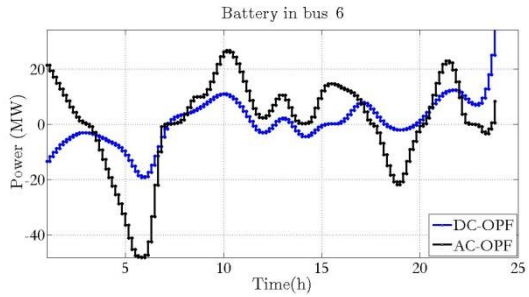


(j) Case F – Battery Power

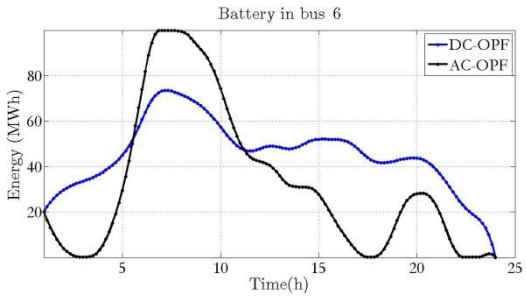


(k) Case F – Battery Energy

**Figure 3.4: Storage Dispatch Patterns – Cases A - F**

The different dispatch patterns of the storage unit schedules via the look-ahead problems are shown in Figure 3.4, where the differences between the two dispatch results are clearly shown.

However, the IEEE 30 bus system is a small test case and all storage capacity was placed near a congested transmission corridor. By repeating this test in a 2383 bus of the Polish Test system, we can draw some conclusion regarding larger, more realistic systems.

The results are shown in Table 3.3 and the cost reduction comparison results are shown in Figure 3.5.

**Table 3.3: AC-OPF versus DC-OPF dispatch operating cost results – Polish 2383 bus**

| Scenario | Storage Energy | Storage Power | Wind Penetration | DC-OPF Cost | AC-OPF Cost | Cost w/o storage |
|---|---|---|---|---|---|---|
| A | 24 GWh | 8GW | 3.21GW | 4.2674e+07 | 4.2568e+07 | 4.8148e+07 |
| B | 46GWh | 12 GW | 3.21GW | 4.1034e+07 | 4.0886e+07 | 4.8148e+07 |
| C | 12 GWh | 4GW | 3.21GW | 4.4763e+07 | 4.4700e+07 | 4.8148e+07 |
| D | 46GWh | 12GW | 4.1730 | 4.0057e+07 | 3.9901e+07 | 4.7169e+07 |

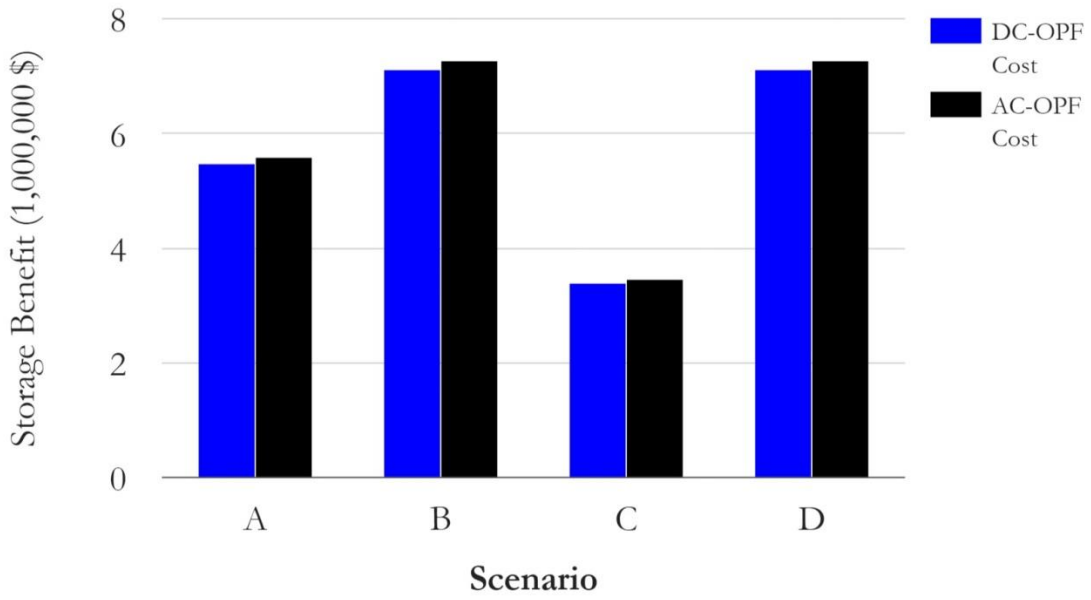


**Figure 3.5. Cost Reduction from Battery Operation – ACOPF vs. DCOPF in 2383 Bus Case**

From the results in Figure 3.5 it is evident that, while the cost reduction is still greater in the AC-OPF look-ahead case, the difference is much less pronounced (not exceeding 2%) than the 30 bus case.

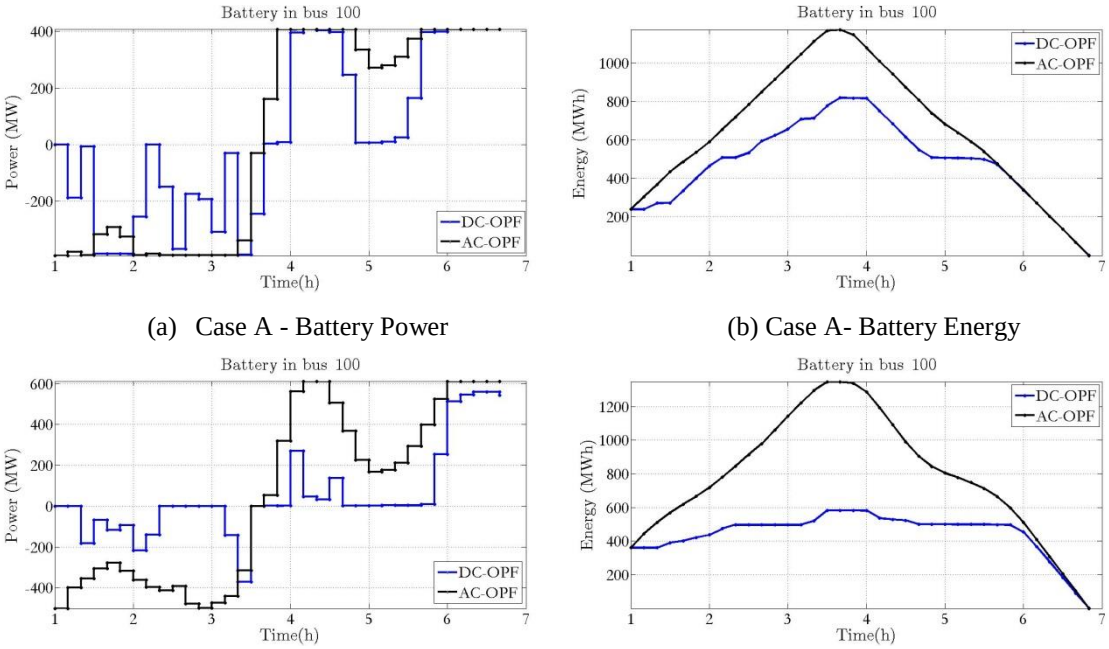


(a) Case A - Battery Power

(b) Case A- Battery Energy

(c) Case B – Battery Power

(d) Case B – Battery energy

**Figure 3.6: Storage Dispatch Patterns – Bus 100**

In order to demonstrate a sample of the different dispatch patterns that result from the two look-ahead dispatch paradigms, the power and energy plots for the storage unit in bus 100 are provided in Figure 3.6.

## 3.5. Sample Timing Results

The AC-OPF look-ahead dispatch was tested on various standard power system test cases, using an 1-hour look-ahead horizon. The timing results, on an un-optimized personal computer with an Inter Core i7-4510U 2GHz processor are reported in Table 3.4. It should be noted that convergence speed relies heavily on initialization and algorithm parameters, such as the Hessian scaling parameter in the PDIPM algorithm. Hence, timing results are only indicative and not definitive.

**Table 3.4: Timing Results for Various Case Data – 1 hour look-ahead horizon**

| SYSTEM CASE | STATE VARIABLES | CONTROL VARIABLES | INEQUALITY CONSTRAINT | AC-OPF EXECUTION TIME (S) | DC-OPF EXECUTION TIME |
|---|---|---|---|---|---|
| **IEEE 24 Bus** | 288 | 396 | 516 | 0.1960 | 0.1050 |
| **IEEE 118 Bus** | 1,416 | 648 | 2,532 | 0.7780 | 0.0760 |
| **IEEE 300 Bus** | 3,600 | 828 | 6,066 | 2.0280 | 0.0960 |
| **PEGASE 1354** | 16,248 | 3,120 | 28,194 | 17.1200 | 0.3030 |
| **2383 Polish System (Winter Peak)** | 28,596 | 3,924 | 45,972 | 53.3560 | 2.9174 |
| **PEGASE 2869** | 34,428 | 6,120 | 61,920 | 59.5810 | 0.7120 |
| **3120 Polish System (Spring Peak)** | 37,440 | 3,576 | 59,598 | 48.5290 | 2.8620 |
| **British 2224 System** | 26,688 | 4,728 | 45,930 | 33.1470 | 0.8620 |
| **PEGASE 9241** | 110,892 | 17,340 | 207,186 | 235.8153 | 10.3530 |

However, timing results serve to indicate that the look-ahead dispatch problem is solvable within reasonable time frames, even in a retail machine, with average computational power. For the larger test case, the PEGASE 9241 system, a 1-hour look-ahead problem was solved within less than 4 minutes. For reference, the DC-OPF look-ahead timing results are also provided. They are obviously advantageous compared to the AC-OPF formulation, given the strong convergence properties of the QP formulation and the smaller size of the problem, due to the modeling restrictions of the DC-OPF formulation.

# Chapter 4. Dynamic Models for Flexible Power System Dispatch

| | |
|---|---|
| $g_d + jb_d$ | Generator direct-axis admittance |
| $\tilde{V}^k = V_r^k + jV_i^k$ | Device Terminal Voltage phasor at step *k* in Cartesian Coordinates |
| $\tilde{E}^k = E_r^k + jE_i^k$ | Generator internal EMF phasor at step *k* in Cartesian Coordinates |
| $\tilde{I}^k = I_r^k + jI_i^k$ | Device *incoming* current in Cartesian Coordinates |
| $R$ | Generator Ramp Rate in MW/min |
| $\Delta t$ | Chosen step size for look-ahead FOPF |
| $a_g, b_g, c_g$ | Generator's quadratic cost function coefficients |
| $K_1, K_2, K_3$ | Line thermal model coefficients |
| $T^k$ | Line average conductor temperature at step *k* |
| $T_{amb}^k$ | Ambient Temperature at step *k* |
| $Q_{th}^k$ | Heating / cooling rate from TCL at step *k* |
| $a_{tcl}$ | TCL efficiency factor |

| | |
|---|---|
| $R_{tcl}, C_{tcl}$ | TCL parameters – Conditioned Space to Ambient thermal resistance and Conditioned Space thermal capacitance |
| $u_{tcl}$ | TCL duty cycle |
| $g_s + jb_s$ | Admittance of Battery Energy Storage System |
| $E_{\max}, E_{\min}$ | Maximum and Minimum Energy of Battery Energy Storage System |
| $P_k^+$ | Battery charge power |
| $P_k^-$ | Battery discharge power |
| $n_s^+, n_s^-$ | Battery charging and discharging efficiency respectively |
| $SOC^k$ | Battery State of Charge, at step $k$ |
| $a_s, b_s, c_s$ | Storage quadratic cost function coefficients |
| $P_d^k$ | Active Power Consumed by Aggregate Distribution System at step $k$ |
| $Q_d^k$ | Reactive Power Consumed by Aggregate Distribution System at step $k$ |
| $B^k$ | Positive Definite Matrix defining the ellipsoidal feasible region of the Aggregate Distribution System at step $k$ |
| $d^k$ | Vector defining the ellipsoidal feasible region of the Aggregate Distribution System at step $k$ |
| $\Delta B_p, \Delta B_q, \Delta B_{par}^+, \Delta B_{par}^-$ | $2 \times 2$ matrices, defining the Active Distribution System state transition model |
| $\Delta d_p, \Delta d_q, \Delta d_{par}^+, \Delta d_{par}^-$ | $2 \times 1$ vectors, defining the Active Distribution System state transition model |
| $p_j^k$ | Value of $j$-th parameter of device model at step $k$ |

## 4.1. Introduction

The formulation of the look-ahead dispatch problem as a multi-step optimal power flow was discussed in Chapter 3. Similarly to a static Optimal Power Flow, this formulation enforces the network power flow equations as an equality constraint in each step. In addition, if dynamic device models are present their discrete time state transition equations are also enforced as equality constraints between adjacent time steps. However, existing formulations of the OPF problem are not look-ahead and rely on static device models. Any dynamic effects, such as storage state of charge or generator ramping constraints, are typically modeled by the Unit Commitment problem (day ahead scheduling) which uses a DC optimal power flow approximation. Hence, dynamic device models suitable for a multi-step AC-OPF formulation are not available in the literature.

In this Chapter a set of dynamic device models suitable for this use are described & validated. All the models proposed are compatible with the quadratized state & control syntax x of 0. The models to be covered are: i) Ramp-rate constrained generator ii) Thermostatically Controlled Responsive Load iii) Transmission Line with Dynamic Line Rating iv) Energy Storage System and v) Active Aggregate Distribution System. Models (i) – (iv) are relatively simple physically-based models. However, the Aggregate Distribution System Model is a completely new model developed in this research, and issues such as parameter identification and model derivation are more extensively discussed. Dispatch results, implementation issues and limitations are presented & discussed for all models under examination.

## 4.2. Ramp-Rate Constrained Generation

The effect of ramp-up and ramp-down constraints in the economic operation of power systems are very well studied for the unit-commitment problem [113], [114] and the look-ahead dispatch problem [115]. The inclusion of this model is particularly important in systems with high penetration of renewable energy sources. The quadratized model for the ramp-rate constrained generators used in this research is obtained by combining the steady-state single-axis model [116] with the addition of a ramp constraint:

$$\begin{bmatrix} I_r^k \\ I_i^k \\ 0 \\ 0 \end{bmatrix} = \begin{bmatrix} -g_d(E_r^k - V_r^k) + b_d(E_i^k - V_i^k) \\ -b_d(E_r^k - V_r^k) - g_d(E_i^k - V_i^k) \\ g_d E_r^k V_r^k - b_d V_r^k E_i^k + g_d V_i^k E_i^k + b_d V_i^k E_r^k - g_d\left(V_r^k\right)^2 - g_d\left(V_i^k\right)^2 - P_k \\ -g_d V_r^k E_i^k - b_d V_r^k E_r^k + g_d V_i^k E_r^k - b_d V_i^k E_i^k + b_d\left(V_r^k\right)^2 + b_d\left(V_i^k\right)^2 - Q_k \end{bmatrix} \quad (12a)$$

$$\begin{bmatrix} 0 \\ 0 \end{bmatrix} \geq \begin{bmatrix} P_k - P_{k-1} - R\Delta t \\ -P_k + P_{k-1} - R\Delta t \end{bmatrix} \quad (12b)$$

$$\begin{bmatrix} P_{\min} \\ Q_{\min} \end{bmatrix} \leq \begin{bmatrix} P_k \\ Q_k \end{bmatrix} \leq \begin{bmatrix} P_{\max} \\ Q_{\max} \end{bmatrix} \quad (12c)$$

Where the state and controls vectors are given as:

$$\mathbf{x}_k = \begin{bmatrix} V_r^k \\ V_i^k \\ E_r^k \\ E_i^k \end{bmatrix} \quad (13a)$$

$$\mathbf{u}_k = \begin{bmatrix} P_k \\ Q_k \end{bmatrix} \quad (13b)$$

The objective function contribution at each step can be a quadratic cost function of the active power control variable:

$$f(\mathbf{x}_k, \mathbf{u}_k) = a_g P_k^2 + b_g P_k + c_g \tag{14}$$

Where *a, b, c* are cost coefficients provided by each generator's cost curve.

### 4.3. Transmission Line with Dynamic Line Rating

Transmission line current magnitude is typically constrained due to the heat generated by Ohmic losses within the conductor. Such thermal limits are considered essential in virtually all Optimal Power Flow formulations and are usually treated as static maximum current magnitude limits. However, the observation has been made that the actual physical constraint with regard to this phenomenon is the transmission line's temperature, and not its current. This gave rise to increasing interest in thermal modeling of transmission lines [117]. More recently, an IEEE Standard [118] was published, detailing a comprehensive line temperature model, including meteorological effects, such as ambient temperature, precipitation, solar irradiation and prevailing winds, all of which affect the dynamic thermal model of the transmission line. It has been recorded that static line ratings often underestimate the actual loading capability of the line by as much as 15% and that higher reliability can be attained if dynamic line ratings of lines are monitored [119]. Further work has focused on actual implementations of real-time dynamic rating monitoring installations [120].

The dynamic thermal model of transmission lines is a good candidate for addition to the flexible dispatch formulation. Benefits in operating cost and reliability have been recorded in cases where dynamic ratings are taken into account in system operation.

Furthermore, the dynamic nature of the flexible dispatch procedure of Chapter 3 allows the modeling of phenomena such as "temporary" overloading of critical lines, which a static OPF dispatch fails to capture. The hard constraint on line current magnitude can be removed, in favor of the actual conductor temperature limit.

A model for dynamic line rating can be incorporated in the flexible OPF dispatch by using the simplified first-order model put forth in [118] that assumes the conductor temperature model is a first order linear ODE with the line current magnitude as an input. It must be stressed that a fully detailed model of conductor temperature variations is nonlinear and convoluted, but the first order approximation, derived from [117] and [121] and mentioned in the standard is adequate for the purposes of this research. In fact, a linear model is obtained by linearizing the radiation heat losses from the line, which is itself a less significant factor in the model, which strengthens the validity of the approximation used here. The fact that the time constant for the thermal phenomena in a transmission line is approximately 10-15 minutes means that a look-ahead dispatch with 5 minute time steps should be adequate to capture the underlying phenomena.

The thermal model of the transmission line is as follows:

$$\begin{bmatrix} I_{1,r}^k \\ I_{1,i}^k \\ I_{2,r}^k \\ I_{2,i}^k \\ 0 \\ 0 \end{bmatrix} = \begin{bmatrix} (g+g_s)V_{1,r}^k + (-b-b_s)V_{1,i}^k - gV_{2,r}^k + bV_{2,i}^k \\ (b+b_s)V_{1,r}^k + (g+g_s)V_{1,i}^k - bV_{2,r}^k - gV_{2,i}^k \\ -gV_{1,r}^k + bV_{1,i}^k - (g+g_s)V_{2,r}^k + (b+b_s)V_{2,i}^k \\ -bV_{1,r}^k - gV_{1,i}^k + (b+b_s)V_{2,r}^k + (g+g_s)V_{2,i}^k \\ z_1^k - (g^2+b^2)\left[\left(V_{1,r}^k\right)^2 + \left(V_{1,i}^k\right)^2 + \left(V_{2,r}^k\right)^2 + \left(V_{2,i}^k\right)^2\right] + (2g^2+2b^2)\left(V_{1,r}^k V_{2,r}^k + V_{1,i}^k V_{2,i}^k\right) \\ T^k - T^{k-1} - K_1\left(T^{k-1} - T_{amb}^k\right) - K_2 z_1^{k-1} + K_3 \end{bmatrix} \quad (15a)$$

$$T^k \le T^{\max} \quad (15b)$$

The state vector is given as:

$$\mathbf{x}_k = \begin{bmatrix} V_{1,r}^k \\ V_{1,i}^k \\ V_{2,r}^k \\ V_{2,i}^k \\ z_1^k \\ T^k \end{bmatrix} \tag{16}$$

Where $z_1^k$ is an auxiliary variable, representing the line current magnitude squared. It was introduced for quadratization purposes. The last equation in (15a) is a simple Euler integration of the simplified thermal dynamics of the line:

$$\frac{dT}{dt} = K_1(T - T_{amb}) + K_2\|I\|^2 + K_3 \tag{17}$$

Note that $K_3$ depends on solar heating of the line (and hence depends on metrological conditions). Hence, it is treated as a parameter for this model, extracted from the meteorological forecast. The term $K_1$ depends on convection heat loss of the line, as well as the line's thermal capacitance and a linearized version of radiation heat loss. Hence variable wind speed & direction is to be considered, then $K_1$ is also a parameter, whose value for the look-ahead horizon depends on the weather forecast, which in turn affects the forced convective heat loss due to the wind. A simplified version of this model, with constant $K_1$ can be extracted, if constant wind pattern is assumed for the look-ahead horizon, or if the convective losses due to wind are altogether neglected. The latter will result in an overly conservative dynamic line rating model, because forced convection always has a cooling effect for the line. Finally, $K_2$ is due to ohmic effects within the line and it depends on conductor material only. Hence, it can always be considered constant.

## 4.4. Thermostatically Controlled Responsive Loads

A responsive TCL load is defined as a power consumption device whose primary purpose is to regulate the temperature of a monitored space so that it lies within a pre-determined tolerable range: $T_{in} \in [T_{\min}, T_{\max}]$. Space air conditioning, electric water heaters and freezers are some prominent examples. The common characteristic of such loads is that the binding hard constraint on their operation is the minimum and maximum temperature of the regulated space. Hence, their operation can be scheduled by a look-ahead dispatch, so as to consume / refrain from consuming in order to support economic and reliable operation of the system.

It should be noted that the provided system by such loads does not come at the expense of the customer. Since the temperature constraint is explicitly modeled, the load's main function is served without customer inconvenience and any system support provided is within the capabilities of the load.

The model employed for responsive TCL's is:

$$\begin{bmatrix} I_r^k \\ I_i^k \\ 0 \\ 0 \\ 0 \end{bmatrix} = \begin{bmatrix} u_{tcl}^k (g_{tcl} V_r^k - b_{tcl} V_i^k) \\ u_{tcl}^k (b_{tcl} V_r^k + g_{tcl} V_i^k) \\ P_{tcl}^k - g\left(V_r^k\right)^2 - g\left(V_i^k\right)^2 \\ Q_{th}^k - \frac{a_{tcl}}{50}\left[T^k - T_{amb}^k\right] P_{tcl}^k \\ T^k - T^{k-1} - \frac{1}{C_{tcl} R_{tcl}}\left(T_{amb}^k - T^{k-1}\right) - \frac{1}{C_{tcl}} u_{tcl}^k Q_{tcl}^k \end{bmatrix} \tag{18a}$$

$$\begin{gathered} T^{\min} \le T^k \le T^{\max} \\ 0 \le u_{tcl} \le 1 \end{gathered} \tag{18b}$$

Where the state and controls vectors are given as:

$$\mathbf{x}_k = \begin{bmatrix} V_r^k \\ V_i^k \\ P_{tcl}^k \\ Q_{th}^k \\ T^k \end{bmatrix} \tag{19a}$$

$$\mathbf{u}_k = \begin{bmatrix} u_{tcl}^k \end{bmatrix} \tag{19b}$$

The ambient temperature is a time-varying parameter for this model, provided by the weather forecast.

For our purposes, the electrical behavior of the TCL is modeled as a constant impedance load $g_{tcl} + jb_{tcl}$. The thermal model includes the effect of ambient temperature and space temperature on the efficiency of the thermodynamic cycle and the temperature dynamics are modeled using a simple first-order model. Note that the duty cycle control variable $u_{tcl}^k$ is factored in when evaluating the device absorbed current, as well as the actual heat/cool rate in (18a). The equations in (18a) are obtained from a quadratization of the following equations:

$$\begin{aligned} \tilde{\mathbf{I}} &= u_{tcl} Y \tilde{\mathbf{V}} \\ P_e &= \mathrm{Re}\left\{\mathbf{V}\mathbf{I}^*\right\} \\ Q_{th} &= \frac{a}{50}\left[T_{amb} - T\right] P_e \\ C\frac{dT(t)}{dt} &= \frac{1}{R}\left[T_{amb}(t) - T(t)\right] + u_{tcl} Q_{th} \end{aligned} \tag{20}$$

This model captures both the active and reactive consumption of TCL's, as well as the thermal losses of the house and the effects of control actions on TCL efficiency.

## 4.5. Energy Storage System

The value of energy storage in addressing issues arising from renewable penetration, and providing ramping, regulation or peak shaving services has been recognized in the literature [122], [123]. Hence, consideration of high-accuracy energy storage models is a salient feature of the look-ahead dispatch framework. The energy storage model considers charging and discharging losses, as well as the capability of the storage plant to provide reactive power support. Obviously, the dynamic aspects of the battery's state of charge, as well as the limitations in active power and energy capacity must be included in the model.

The quadratized model for the battery energy storage system is as follows:

$$\begin{bmatrix} I_r^k \\ I_i^k \\ 0 \\ 0 \\ 0 \end{bmatrix} = \begin{bmatrix} -g_s(E_r^k - V_r^k) + b_s(E_i^k - V_i^k) \\ -b_s(E_r^k - V_r^k) - g_s(E_i^k - V_i^k) \\ -g_s E_r^k V_r^k - b_s V_r^k E_i^k - g_s V_i^k E_i^k + b_s V_i^k E_r^k + g_s\left(E_r^k\right)^2 + g_s\left(E_i^k\right)^2 - P_k^- + P_k^+ \\ -g_s V_r^k E_i^k + b_s V_r^k E_r^k + g_s V_i^k E_r^k + b_s V_i^k E_i^k - b_s\left(V_r^k\right)^2 - b_s\left(V_i^k\right)^2 - Q_k \\ SOC_k - SOC_{k-1} + \frac{1}{E^{\max}} \frac{1}{n_s^-} P_k^- \Delta t - \frac{1}{E^{\max}} n_s^+ P_k^+ \end{bmatrix} \quad (21a)$$

$$\begin{aligned} 0 \le P_k^+ &\le P^{\max} \\ 0 \le P_k^- &\le P^{\max} \\ Q^{\min} \le Q^k &\le Q^{\max} \\ 0 \le SOC^k &\le 1 \end{aligned} \quad (21b)$$

The state and control vectors for this model are:

$$\mathbf{x}_k = \begin{bmatrix} V_r^k \\ V_i^k \\ E_r^k \\ E_i^k \\ SOC^k \end{bmatrix} \tag{22a}$$

$$\mathbf{u}_k = \begin{bmatrix} P_k^+ \\ P_k^- \\ Q_k \end{bmatrix} \tag{22b}$$

This battery model includes losses in the electrical subsystem (through the admittance $g_s + jb_s$ as well as internal losses in the battery. In fact, discharge efficiency $n_s^-$ may be different from charging efficiency $n_s^+$, and this phenomenon is appropriately modeled. For this purpose, charging power $P_k^+$ is treated as a separate control variable from discharge power $P_k^-$, each with their own control bounds. Note that $n_s^-$ and $n_s^+$ are constant parameters with a positive value less than one. Furthermore, the state of charge variable *SOC* is between zero and one and expresses the level of charge of the battery. Note that it is simply a scaled version of the battery's currently stored power.

In case it is desirable, the charge/discharge control terms can also participate in the objective function for this device:

$$f(\mathbf{x}_k, \mathbf{u}_k) = a_g \left(P_k^- - P_k^+\right)^2 + b_g \left(P_k^- - P_k^+\right) + c_g \tag{23}$$

Note that the net power output from the battery is $P_k^- - P_k^+$. Also note that, unlike generating plants whose cost is non-negative in every period, storage plants are characterized by a negative cost when they are charging.

## 4.6. Active Distribution System

A large number of distributed active devices are expected to be connected in the future distribution feeder, including rooftop solar, plug-in hybrid electric vehicles, small scale storage and responsive loads. Each of these devices may be small in rating (a few kW), serving individual residential or small commercial customers. While it would be beneficial to include them in the transmission-level look-ahead dispatch formulation, such a choice is faced with important hurdles:

- The transmission level dispatch is concerned with optimizing large transmission and generation assets, whose typical magnitudes are in the order of several Megawatts. Hence, a scaling issue arises, if all distribution devices are included individually in the dispatch
- Thousands of these devices may be connected to each feeder, and the typical distribution system may be composed of hundreds of such feeders. Hence, individual consideration of every active device will require the full inclusion of millions of state-space models in the look-ahead dispatch, thus increasing considerably the size of the look-ahead dispatch, which is already a computationally challenging problem, as discussed in Chapter 3.
- The devices connected to the distribution system have their own set of binding constraints that need to be considered. Specifically, responsive loads must serve their main function without exception (no customer inconvenience), storage devices must remain within their physical limits etc.

In order to solve the scaling and tractability issues that arise from introducing distributed resources to transmission-level dispatch, one approach is to obtain an aggregate representation of the distribution system. In this paragraph we formulate an aggregate model that relies on the description of the feasible set for the aggregate active and reactive power consumption of the active distribution system. Furthermore, a time-domain model is developed, that provides a description for the feasible *P*-*Q* set in period *t* given the power consumption in period *t*-1. Since this model aggregates a multitude of distributed resources that add up to several Megawatts of capacity, this approach addresses both the scale and the tractability issue.

### 4.6.1. Ellipsoidal Model for Active Distribution System

The adopted model for the active distribution system represents a compromise between tractability, simplicity and accuracy. To represent the available control capability in terms of active & reactive consumption of the distribution feeder, we assume that the feasible region of this feeder is an ellipsoid in the *P*-*Q* plane:

$$F_{pq} = \left\{ \begin{bmatrix} P_d \\ Q_d \end{bmatrix} \in R^2 : \begin{bmatrix} P_d \\ Q_d \end{bmatrix} = Bu + d, u^T u \le 1 \right\} \tag{24}$$

Where $B \succ 0$ is a $2 \times 2$ symmetric matrix and $d \in R^2$ .

An example of such a feasible region for a representative feeder with 800 8kW Air-Conditioned Homes and 200 4.4kW, 6kWh batteries is shown in Figure 4.1. The physical meaning of this representation is that the center *d* of the ellipsoid is the "base case" consumption of the feeder – equivalent to a static representation of the feeder as a constant PQ load, and *B* represents the active-reactive control capabilities of the feeder.

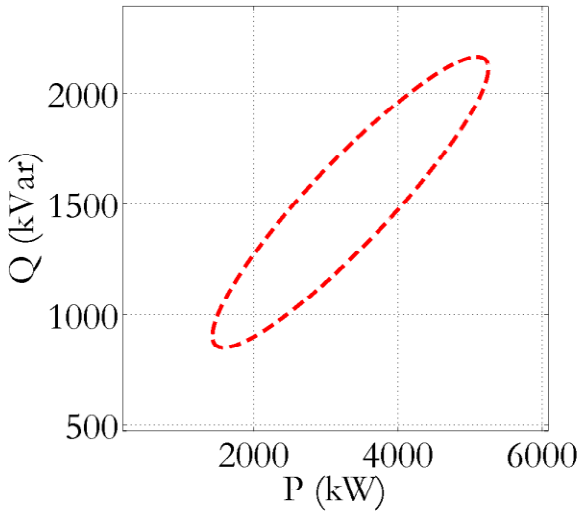


**Figure 4.1: *P-Q* feasible region for a sample feeder**

However, given that dynamic devices are connected to the feeder, the feeder's consumption at one period affects the feasible consumption in the next. Intuitively, in a feeder with responsive loads, increased consumption in one period leads to reduced feasible consumption region in the next step and vice versa. For this purpose, the following time-domain ellipsoidal model for the active distribution feeder is adopted:

$$\begin{bmatrix} P_d^k \\ Q_d^k \end{bmatrix} = B^k u^k + d^k$$

$$B^k = B^{k-1} + P_d^{k-1}\Delta B_p + Q_d^{k-1}\Delta B_q + \sum_{j=1}^{n_p} p_j^{k-1}\Delta B_{par}^{-} + \sum_{j=1}^{n_p} p_j^{k}\Delta B_{par}^{+} \tag{25a}$$

$$d^k = d^{k-1} + P_d^{k-1}\Delta d_p + Q_d^{k-1}\Delta d_q + \sum_{j=1}^{n_p} p_j^{k}\Delta d_{par}^{-} + \sum_{j=1}^{n_p} p_j^{k}\Delta d_{par}^{+}$$

$$\left\| u^k \right\|_2 \le 1 \tag{25b}$$

The model defined in (25a)-(25b) defines an ellipsoidal feasible region for the active and reactive power consumption in the *k*-th step, as well as a linear update for the matrix $B^k$ and the vector $d^k$ defining the feasible ellipsoid at step *k*. The linear update depends

on the consumptions at step *k*-1, as well as the value of the *exiting parameter* $p_j^{k-1}$ and the *entering parameter* $p_j^k$. Notice that the exiting parameter models the prevailing conditions determining the feasible region at the previous step, while the entering parameter models the prevailing conditions at the current step, hence it is conceptually reasonable to include both in the state transition model linking the two steps.

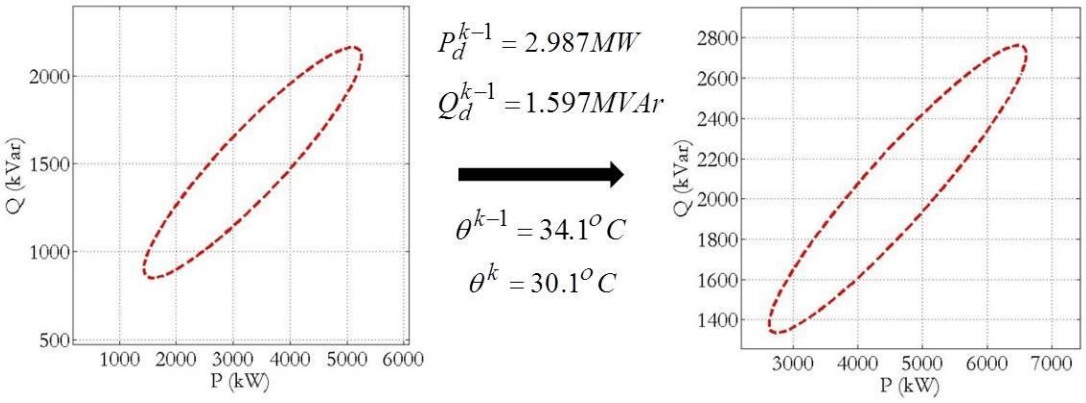


**Figure 4.2. Feasible Region Transition for aggregate distribution system**

An example of feasible region transition for the same sample feeder is shown in Figure 4.2.

The model of (25a)-(25b) is already in quadratic form. It is not given exactly in the form presented in Chapter 3, as the expressions for the currents are missing. However, these are straight-forward to obtain. Even though the implementation of this model in the look-ahead OPF dispatch includes the current equations, this model is not given here in the interest of conciseness.

The values for $\Delta B_p, \Delta B_q, \Delta B_{par}^+, \Delta B_{par}^-$ and $\Delta d_p, \Delta d_q, \Delta d_{par}^+, \Delta d_{par}^-$ are constant parameters for this model, as well as the initial values for *B* and *d*. Their choice seems

arbitrary at this point. However, a procedure for their data-driven derivation will be outlined in the upcoming paragraphs.

### 4.6.2. The inner ellipsoidal approximation of Convex Polyhedra

Let us define the representation of the ellipsoid $E(B,d)$ with $B$ positive semidefinite as the image of the unit ball under an affine mapping.

$$E(B,b) = \{x : x = Bu + d, \|u\|_2 \le 1\} \tag{26}$$

The ellipsoid $E(B,b)$ has a non-empty interior iff $B \succ 0$ [126]. Let $X \subset R^n$ be a nonempty convex set. The inner approximation problem consists of finding the *maximal* ellipsoid contained in *X*. There can be several measures for "size" of an ellipsoid, including the determinant or the sum of the eigenvalues of *B* [126].

The following facts are known:

**Fact 1** [124**],** [125**].** Let $X \subset R^n$ be a nonempty convex set. Then the set of parameters $(B,b)$ of image representation of ellipsoids that are contained in *X* is convex (i.e. the set $Y = \{(B,d) : E(B,d) \subset X\}$).

**Fact 2.** The following functions are concave in $(B,d)$:

- $Vol^{\,p}(E) = \prod_{i=1}^{n} \lambda_i(B), 0 < p \le 1/n$
- $\sum_{i=1}^{n} \lambda_i^p(B), 0 < p \le 1$

Where $\lambda_i^p(B)$ represents the *i*-th eigenvalue of *B.*

The first fact means that the set of image representations of ellipsoids that are contained in *X* is convex, and thus tractable in theory, and the second fact means that some common measures of "size" of an ellipsoid, given its image representation are easy-to-maximize functions of the image representation. This leads us to the following result [124], given without proof:

**Fact 3** [124**].** Let $P = \{x \in R^n : a_i^T x \le b_i, i = 1, \ldots, m\}$ be a nonempty polyhedral set. Then, the maximal volume ellipsoid $E(B,d)$ contained in *P* can be found by the following problem:

$$\begin{aligned} &\max_{B,d} \; Det(B) \\ &\text{subject to} \\ &\|Ba_i\| + a_i^T d \le b_i \end{aligned} \tag{27}$$

This is a solvable semidefinite program.

Note that the constraints in (27) guarantee that the ellipsoid $E(B,b)$ is contained in *X* and the maximization of the determinant yields the maximum volume ellipsoid contained in *X*.

### 4.6.3. Data-Driven Identification of Aggregate Distribution System Model

Consider a simulation of the Active Distribution System for *S* steps. Suppose that for each step we have a polyhedral description of the feasible set in the *P*-*Q* domain, given by $A^{(k)}$ and $b^{(k)}$:

$$F^{(k)} = \left\{ x \in R^2 : A^{(k)} x \le b^{(k)} \right\} \tag{28}$$

Furthermore, suppose that the consumption of the active distribution feeder between step $k$ and $k$+1 is $P_d^k$ for active power and $Q_d^k$ for reactive power, given as the sum of active and reactive power consumption by all devices in the feeder:

$$P_d^k = \sum_{j=1}^{N_d} P_j^k \tag{29a}$$

$$Q_d^k = \sum_{j=1}^{N_d} Q_j^k \tag{29b}$$

Suppose that the parameter vectors $p_j^k$, the consumption values (29a), (29b) and the polyhedral descriptions of feasible sets (28) are known at each step. Then, the unknown parameters of the aggregate ellipsoidal model can be obtained by the following problem.

$$\begin{aligned}
&\max_{B_k, d_k, \Delta B_p, \Delta B_q, \Delta B_{par}^-, \Delta B_{par}^+} \left\{ \sum_{k=1}^{S} \sum_{i=1}^{2} \sqrt{\lambda_i(B_k)} \right\} \\
&\text{subject to} \\
&\left\| B_k a_i^{(k)} \right\| + a_i^{(k)T} d_k \le b_i^{(k)} \qquad \forall i = 1,2 \ \& \ \forall k \in \{1, \dots S\} \\
&B_k = B_{k-1} + P_d^{k-1} \Delta B_p + Q_d^{k-1} \Delta B_q + \sum_{j=1}^{n_p} p_j^{k-1} \Delta B_{par}^- + \sum_{j=1}^{n_p} p_j^k \Delta B_{par}^+ \qquad \forall k \in \{2, \dots S\} \\
&d^k = d^{k-1} + P_d^{k-1} \Delta d_p + Q_d^{k-1} \Delta d_q + \sum_{j=1}^{n_p} p_j^k \Delta d_{par}^- + \sum_{j=1}^{n_p} p_j^k \Delta d_{par}^+ \qquad \forall k \in \{2, \dots S\}
\end{aligned} \tag{30}$$

The problem in (30) is semidefinite programming problem, since the added equality constraints with respect to (27) are linear in the decision variables. However, this problem can potentially be infeasible, i.e. such $B^k$ and $d^k$ may not exist. For this purpose, it is best to relax the ellipsoid inclusion constraints using variables $\mu_{ik}$ and penalize their value by the norm of $\mu_k$:

$$\max_{B_k, d_k, \Delta B_p, \Delta B_q, \Delta B^-_{par}, \Delta B^+_{par}, \lambda_{ik}} \left\{ \sum_{k=1}^{K} \sum_{i=1}^{2} \sqrt{\lambda_i (B_k)} + \mu \sum_{k=1}^{K} \left\| \mu_k \right\|_1 \right\}$$

subject to

$$\left\| B_k a_i^{(k)} \right\| + a_i^{(k)T} d_k - \mu_{ik} \le b_i^{(k)} \qquad \forall i = 1,2 \ \& \ \forall k \in \{1, \dots K\} \tag{31}$$

$$B_k = B_{k-1} + P_d^{k-1} \Delta B_p + Q_d^{k-1} \Delta B_q + \sum_{j=1}^{n_p} p_j^{k-1} \Delta B^-_{par} + \sum_{j=1}^{n_p} p_j^k \Delta B^+_{par} \qquad \forall k \in \{2, \dots K\}$$

$$d^k = d^{k-1} + P_d^{k-1} \Delta d_p + Q_d^{k-1} \Delta d_q + \sum_{j=1}^{n_p} p_j^k \Delta d^-_{par} + \sum_{j=1}^{n_p} p_j^k \Delta d^+_{par} \qquad \forall k \in \{2, \dots K\}$$

It is worth noting that, unlike (27), the problems (30) and (31) do not maximize the sum of the determinants of $B^k$, i.e. are not volume maximization problems. However, since the eigenvalues of $B^k$ are the magnitudes of the half-axes [126], the objective function remains a measure of "size" of the ellipsoid, and hence the purpose of the inner ellipsoidal approximation remains. This choice is made for reasons of numerical stability, since the numerical experiments with the chosen objective function proved much more reliable compared to the ones using the determinant objective.

### 4.6.4. Hierarchical Receding Horizon Control of Aggregate Distribution System

The linear update assumption for the aggregate distribution system model, used in (25) allows for the formulation of a tractable SDP problem (31), but it is not necessarily accurate. It is, in essence, a simplification of the problem which does not necessarily guarantee accurate modeling of the aggregate behavior of the distribution system. Especially as the prediction horizon increases, larger errors are expected to accumulate due to the approximation. For this reason, a receding horizon control of the distribution system is developed here. The main idea is to use the *K*-step look-ahead OPF problem to determine

the control (P-Q commands) of the distribution system over a smaller number of *M* steps. A disaggregation algorithm is used to distribute the P-Q commands to individual devices. Subsequently, the new state of the distribution system is used to re-extract the aggregate model after the *M* steps conclude. This results in an aggregation – dispatch – disaggregation feedback loop.

The aggregate distribution model is used in a multi-step look-ahead optimal power flow problem, which includes AC power flow & dynamic transition constraints and minimizes the cost over a horizon of *K* steps. Upon convergence, the active and reactive dispatch of a smaller number of *M* steps ($M<K$) is taken as the distribution system's dispatch for the dispatch horizon. This dispatch is then disaggregated to individual devices in the distribution system by solving an $L_2$ norm minimization of the distance between the actual consumption of the feeder for the next *M* steps from the target dispatch, subject to device constraints. This results in individual device-level commands for thousands of devices. The approach is depicted in Figure 4.3. It is important to note that the method has been developed on the assumption that an infrastructure of data acquisition and control capability exists at the distribution level to implement approach [127].

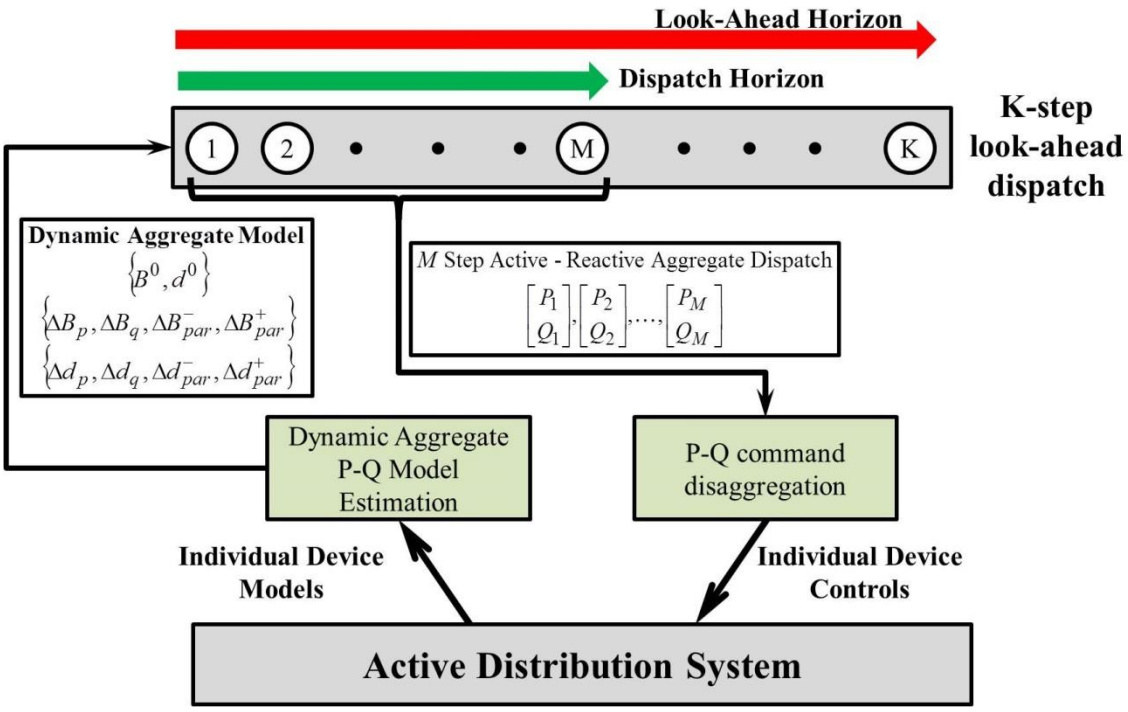


**Figure 4.3: Two Level Distribution System Scheduling**

The aggregation phase consists of a solution of the SDP problem (31). The data for the problem come from a *S*-step simulation of the Active Distribution System. While this simulation is performed, the aggregate power consumption $P_d^k$ at step *k*, the aggregate reactive power consumption $Q_d^k$ as well as the parameters $p_j^k$ are recorded. Furthermore, the feasible P-Q polyhedron for the aggregate consumption of the Distribution Network at each step are also recorded, i.e. a 2x2 matrix $A^{(k)}$ and a 2x1 vector $d^{(k)}$. This simulation is deployed randomly, i.e. the control inputs at each step are drawn randomly from a uniform distribution. Upon collection of that data, an Aggregate Distribution System Ellipsoidal model (25) is fit to this data using (31).

This model is subsequently added to the look-ahead OPF formulation (6) for a chosen look-ahead horizon of *K* steps. Solution of this problem yields a P and Q time series target for the distribution system for the next *K* steps, which is the desirable aggregate consumption of the Distribution System. However, only *M* of these steps are committed as the actual target consumption.

This commitment is realized by solving a disaggregation problem, whereby the aggregate P-Q commands $\hat{P}_d^k$ and $\hat{Q}_d^k$ are distributed to the multitudes of devices connected to the distribution system. Because an approximate aggregate Distribution System P-Q model was used in the look-ahead OPF, there are no guarantees that these P-Q targets are actually feasible. For this reason, the disaggregation problem is cast as an $L_2$ norm minimization problem, where the normalized distance between the actual consumption and the target consumption over the next *M* steps is minimized. This problem is formulated as:

$$\min_{\mathbf{x}_j^k,\mathbf{u}_j^k}\left\{\sum_{k=1}^{M}\left\|\frac{P_d^k-\hat{P}_d^k}{\hat{P}_d^k}\right\|_2+\lambda\sum_{k=0}^{M}\left\|\frac{Q_d^k-\hat{Q}_d^k}{\hat{Q}_d^k}\right\|_2\right\}$$

s.t.

$$\begin{aligned}
P_d^k &= \sum_{j=1}^{N_d} P_j^k && \forall k\in\{1,\ldots,M\}\\
Q_d^k &= \sum_{j=1}^{N_d} Q_j^k && \forall k\in\{1,\ldots,M\}\\
\mathbf{x}_j^{k+1} &= A_j\mathbf{x}_j^k+B_j\mathbf{u}_j^k+D_j\mathbf{p}^k && \forall k\in\{1,\ldots,M-1\},\forall j\in\{1,\ldots,N_d\}\\
\begin{bmatrix}P_j^k\\Q_j^k\end{bmatrix} &= C_j\mathbf{x}_j^k+E_j\mathbf{u}_j^k+F_j\mathbf{p}^k && \forall k\in\{1,\ldots,M\},\forall j\in\{1,\ldots,N_d\}\\
H_j\mathbf{x}_j^k+G_j\mathbf{u}_j^k &\le \mathbf{r}_j && \forall k\in\{1,\ldots,M\},\forall j\in\{1,\ldots,N_d\}\\
\mathbf{x}_j^1 &= \bar{\mathbf{x}}_j^1 && \forall j\in\{1,\ldots,N_d\}
\end{aligned} \tag{32}$$

Where:

| | |
|---|---|
| $\hat{P}_d^k$ , $\hat{Q}_d^k$ | Target aggregate consumption of active and reactive power at step $k$ |
| $\lambda$ | Reactive fitting importance parameter |
| $P_j^k, Q_j^k$ | Active and reactive power consumption of device $j$ at step $k$ |
| $\mathbf{x}_j^k$ | State vector of device $j$ at step $k$ |
| $\mathbf{u}_j^k$ | Controls of device $j$ at step $k$ |
| $\mathbf{p}^k$ | Parameter vector (shared by all devices) at step $k$ |
| $A_j, B_j, D_j$ | Matrices defining the state update model of device $j$ in the discrete time domain |
| $C_j, E_j, F_j$ | Matrices defining the output model of device $j$ |
| $H_j, G_j, \mathbf{r}_j$ | Matrices and vector defining the inequality constraint model of device $j$ |
| $\bar{\mathbf{x}}_j^1$ | Initial state of device $j$, which is given |

A weighting factor $\lambda$ multiplies the normalized error of the reactive power in (32). This is used to regulate the relative importance of reactive power fitting with respect to active power fitting. Because the two commands are possibly conflicting, it is of interest to explore the tradeoff between them. More importantly, a greater weight should be given to active power, since errors in reactive power dispatch can cause serious mismatches between generation and load in the system, and this power will need to be provided by a

standby generator, forcing an out-of-market action. Hence, ensuring perfect tracking of the active power commands provided by the look-ahead OPF is more important than tracking reactive power commands. This is the reason why a value of $\lambda$ smaller than one is typically chosen in our applications.

Note that all device models in (32) are linear, with linear constraints. This is an obvious simplification. However, it is necessary to maintain the polyhedral assumption for the feasible set $F^{(k)}$ of the active and reactive power at step *k*, as well as the tractability of the $L_2$ norm minimization problem. The inequality constraints represent limits of device operation or customer inconvenience constraints. The latter are very important when considering active load devices, such as Thermostatically Controlled Loads of residential houses. Such devices must participate in active-reactive control without disruption of customer temperature requirements.

The formulation in (32) is perhaps too high level and vague. In order to facilitate understanding for the interested reader, we provide a specific example with $N_{TCL}$ air-conditioners and $N_{BATT}$ batteries. A simple linear first-order model is used for both devices. Each house air-conditioner *j* is assumed to have a constant reactive-to-active power ratio $\varphi_j$. For batteries a charging efficiency of $n_{c,i}$ and a discharging efficiency of $n_{d,i}$ is assumed for battery *i*. A separate active and reactive power control is assumed for each battery device, subject to maximum and minimum active/reactive limits. Note that temperature limits $\theta_{\min}$ and $\theta_{\max}$ are enforced for each house, as well as energy limits $E_{\min}$ and $E_{\max}$ for each battery. The control variables for the air-conditioner is the duty

cycle of operation $u_{T,j}^{k}$ of device *j* for period *k* and the control variables for batteries are $u_{P+,j}^{k}, u_{P-,j}^{k}$ and $u_{Q,j}^{k}$, the power charge, power discharge and reactive consumption per period. Negative values for these control variables correspond to active and reactive power generation by the battery. The only parameter involved here is $\theta_{out}$, the ambient temperature, which is common for all thermal house models. The thermal parameters of the first-order thermal model for the residential house are $a_j$ and $b_j$.

The disaggregation problem now becomes:

$$\min_{\mathbf{x}_j^k,\mathbf{u}_j^k}\left\{\sum_{k=1}^{M}\left\|\frac{P_d^k-\hat{P}_d^k}{\hat{P}_d^k}\right\|_2+\lambda\sum_{k=0}^{M}\left\|\frac{Q_d^k-\hat{Q}_d^k}{\hat{Q}_d^k}\right\|_2\right\}$$

s.t.

$$\begin{aligned}
P_d^k &= \sum_{j=1}^{N_{BATT}} P_{B,j}^k + \sum_{j=1}^{N_{TCL}} P_{T,j}^k && \forall k\in\{1,\ldots,M\}\\
Q_d^k &= \sum_{j=1}^{N_{BATT}} Q_{B,j}^k + \sum_{j=1}^{N_{TCL}} Q_{T,j}^k && \forall k\in\{1,\ldots,M\}\\
\theta_j^{k+1} &= a_j(\theta_{out}-\theta_j^k)+b_j u_{T,j}^k n_j P_j^{rated} && \forall k\in\{1,\ldots,M-1\},\forall j\in\{1,\ldots,N_{TCL}\}\\
P_{T,j}^k &= u_{T,j}^k P_j^{rated} && \forall k\in\{1,\ldots,M\},\forall j\in\{1,\ldots,N_{TCL}\}\\
Q_{T,j}^k &= \phi_j u_{T,j}^k P_j^{rated} && \forall k\in\{1,\ldots,M\},\forall j\in\{1,\ldots,N_{TCL}\}\\
0 &\le u_{T,j}^k \le 1 && \forall k\in\{1,\ldots,M\},\forall j\in\{1,\ldots,N_{TCL}\}\\
\theta_{\min} &\le \theta_j^k \le \theta_{\max} && \forall k\in\{1,\ldots,M\},\forall j\in\{1,\ldots,N_{TCL}\}\\
E_j^{k+1} &= E_j^k + n_{c,j}u_{P+,j}^k\Delta t - \frac{1}{n_{d,j}}u_{P-,j}^k\Delta t && \forall k\in\{1,\ldots,M-1\},\forall j\in\{1,\ldots,N_{BATT}\}\\
P_{B,j}^k &= u_{P,j}^k && \forall k\in\{1,\ldots,M\},\forall j\in\{1,\ldots,N_{BATT}\}\\
Q_{B,j}^k &= u_{Q,j}^k && \forall k\in\{1,\ldots,M\},\forall j\in\{1,\ldots,N_{BATT}\}\\
Q_{\min} &\le u_{Q,j}^k \le Q_{\max} && \forall k\in\{1,\ldots,M\},\forall j\in\{1,\ldots,N_{BATT}\}\\
P_{\min} &\le u_{P,j}^k \le P_{\max} && \forall k\in\{1,\ldots,M\},\forall j\in\{1,\ldots,N_{BATT}\}\\
E_{\min} &\le E_j^k \le E_{\max} && \forall k\in\{1,\ldots,M\},\forall j\in\{1,\ldots,N_{BATT}\}\\
\theta_j^1 &= \bar{\theta}_j^1 && \forall j\in\{1,\ldots,N_{TCL}\}\\
E_j^1 &= \bar{E}_j^1 && \forall j\in\{1,\ldots,N_{BATT}\}
\end{aligned} \tag{33}$$

Note that the above formulation in (33) is consistent with the high-level framework in (32).

Upon solution of (32), the actual controls $\left(\mathbf{u}_j^k\right)^*$ for each device *j* and each step *k* are obtained. These controls minimize the distance between the desired aggregate consumption and the actual consumption of the distribution feeder. This explains the use of the term "disaggregation problem" for (32). The value of the objective is a good metric for the

performance of the ellipsoidal approximate model for the aggregate distribution system. Since this model approximates the feasible region of the aggregation, we expect the aggregate commands to be close to feasible. However, such guarantees cannot be provided, since the SDP fitting problem (31) is only a data fitting problem and does not ensure inclusion of the resulting feasible region within the actual polyhedral feasible region of the Distribution System. Hence, infeasibilities of the aggregate commands can and do occur in practice. They manifest as nonzero objective values for (32). The performance of the framework will be evaluated in the results section.

Once the distance-minimizing controls $\left(\mathbf{u}_j^k\right)^*$ for the next $M$ steps have been applied, the Distribution System will reside in a new state. Leveraging data acquisition and state estimation techniques that have been described in prior works [127], the new state is extracted, and a new simulation is performed, to obtain data for a new solution of the SDP problem (31). This results in a new aggregate model for the feasible region of the Distribution Network, and subsequently a new solution of the Transmission-Level look-ahead OPF. Note that each time, the OPF commands after the $M$-th step are discarded and are never applied as Distribution-Level commands.

## 4.7. Numerical Results and Examples

This paragraph is dedicated to results from the application of the models formulated in paragraphs 4.2 - 4.6 and the execution of the corresponding AC-OPF look-ahead dispatch formulated in Chapter 3. Various test cases, ranging from small instructive examples to larger, more realistic systems, are studied. Emphasis is given in the Active

Distribution System Case, and the accuracy and limitations of the aggregate modeling procedure outlined in paragraph 4.6.

### 4.7.1. Energy Storage Results

Energy storage system dispatch is, from an applications perspective, one of the most important justifications behind the look-ahead dispatch formulations discussed in this chapter. Detailed results from the dispatching of storage units in the IEEE 30 Bus system and the Polish 2383 Winter Peak systems were presented in Paragraph 3.4, where the comparison of storage dispatch between AC-OPF and DC-OPF methodologies was discussed. Hence, this result section will focus mostly on a sensitivity analysis of System Cost as a function of storage penetration for various renewable energy scenarios.

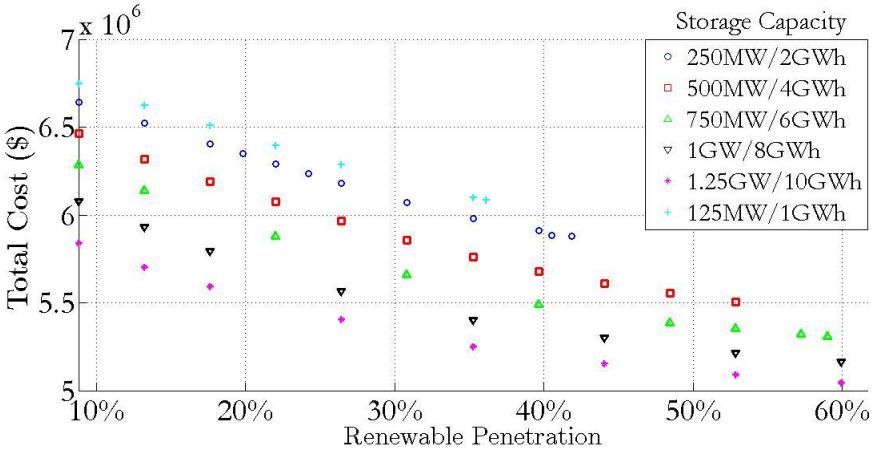


**Figure 4.4: IEEE RTS 24 Bus Total System Cost under various storage scenario**

The AC-OPF look-ahead methodology was applied to the small-size IEEE 24 Bus test case, for a given loading scenario, and various renewable and storage penetration scenarios. The scatter plot of operating costs for various scenarios is shown in Figure 4.4. Note that, for each storage penetration scenario, renewable penetration was increased up to the point that no feasible solution with full absorption of wind (no wind shedding) could be attained.

The maximum feasible wind penetration for each storage penetration scenario is given in Table 4.1

The following conclusions can be drawn from this small case study: 1. Maximum Feasible Wind Penetration increased with wind penetration, but at a decreasing rate, and saturates at some point. This is due to the fact that after a given penetration of storage, issues arise that storage penetration cannot address (for example congestion patterns not affected by the current location of storage). 2. Total cost decreases with storage for all scenarios. The marginal value of storage (the decrease in total cost for a small change in storage) seems to be initially roughly the same for small renewable capacity (roughly 0.2$/MW/day), but it gradually decreases, in extreme levels of renewable penetration.

**Table 4.1: Maximum Feasible Wind as Function of Storage Capacity**

| Storage Power Capacity (MW) | Storage Energy Capacity (MWh) | Maximum Feasible Wind Penetration (MW) |
|---|---|---|
| 126 | 984 | 1,230 |
| 252 | 1,968 | 1,425 |
| 504 | 3,936 | 1,800 |
| 756 | 5,904 | 2,010 |
| 1,008 | 7,872 | 2,040 |
| 1,260 | 9,840 | 2,040 |

### 4.7.2. Thermostatically Controlled Loads

For the purposes of investigating the potential applicability of the Thermostatically Controlled Active load introduced in Paragraph 4.4, we vary the level of penetration of TCL's as a percentage of system load and record the results in terms of total operational cost as well as total energy consumption by thermostatically controlled loads. Subsequently, a version of the dispatch problems were TCL's are passive (not under

centralized dispatch) and the same quantities are monitored. The purpose of the comparison is to investigate whether a decrease in cost runs a risk of increase in energy consumption, due to less efficient operation of TCL's.

**Table 4.2: Effect of TCL control on Cost & TCL Consumption**

| | With TCL Control | | Without TCL Control | |
|---|---|---|---|---|
| **TCL LOAD (%)** | **Total Operating Cost ($)** | **TCL Energy Consumption (MWh)** | **Total Operating Cost ($)** | **TCL Energy Consumption (MWh)** |
| **5%** | 6.9788e+06 | 959.5052 | 6.9966e+06 | 904.1704 |
| **7.5%** | 7.0496e+06 | 1.4421e+03 | 7.0711e+06 | 1.3560e+03 |
| **10%** | 7.1257e+06 | 1.9269e+03 | 7.1502e+06 | 1.8080e+03 |
| **12.5%** | 7.2048e+06 | 2.4113e+03 | 7.2344e+06 | 2.2601e+03 |
| **15%** | 7.2874e+06 | 2.8950e+03 | 7.3230e+06 | 2.7121e+03 |

The test was run in the 24 Bus IEEE Reliability Test system and the results are shown in Table 4.2. It is interesting to note that centralized TCL dispatch achieves important cost reductions, reaching up to 0.7% reduction in total cost for a 15% penetration of controllable TCL loads. This reduction potential in total cost, coming exclusively from a small change in system operations, i.e. the inclusion of TCL's in centralized dispatch, seems extremely attractive. However, it should be noted that significant investments in real-time TCL monitoring and communication equipment are needed to achieve their inclusion to the dispatch procedure. Nevertheless, the existence of this untapped potential is worth noting.

Another significant observation is that the TCL dispatch comes at a cost of less efficient operation of these loads, as their total energy consumption is evidently higher in all cases, if they are under centralized dispatch. Even though total energy consumed increases, total cost is lower. This means that, while TCL dispatch has value for the system,

appropriate incentives must be designed for customers to participate in TCL dispatch, given that their individual consumption will actually increase.

Sample results for the effect of centralized TCL dispatch are shown in Figure 4.5. The total system load with and without centralized dispatch, as shown in Figure 4.5a, is characterized by a smaller peak load in the dispatched case. Of course, increased consumption is required in earlier periods to pre-cool the air-conditioned space and avoid temperature violations. The duty cycle (dispatch decisions) and the corresponding temperatures for three sample TCL's are shown in Figure 4.5b,c, where the pre-cooling effect is evident.

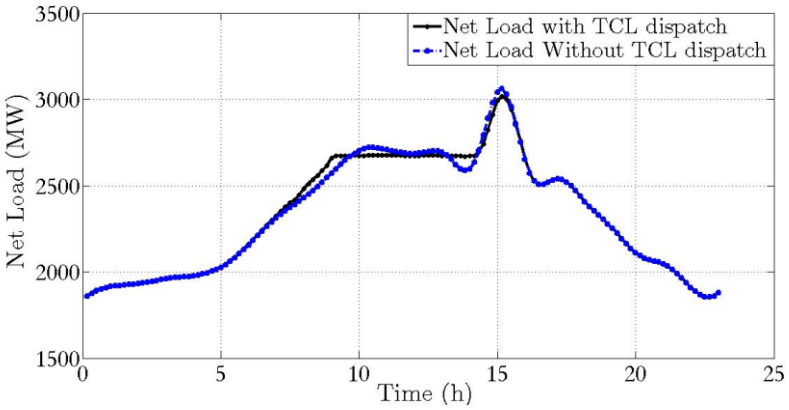


(a)

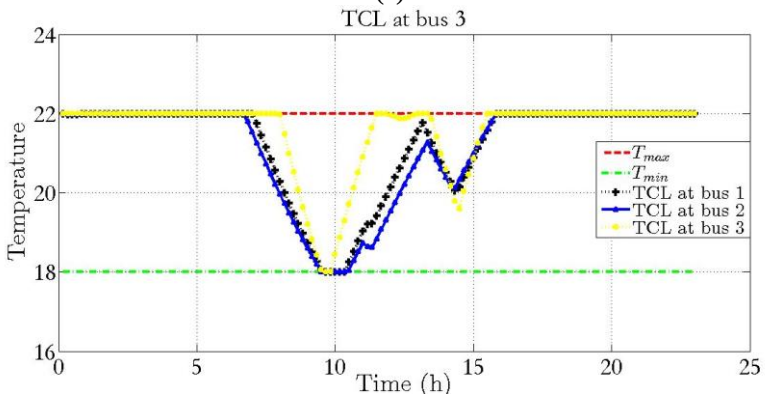


(b)

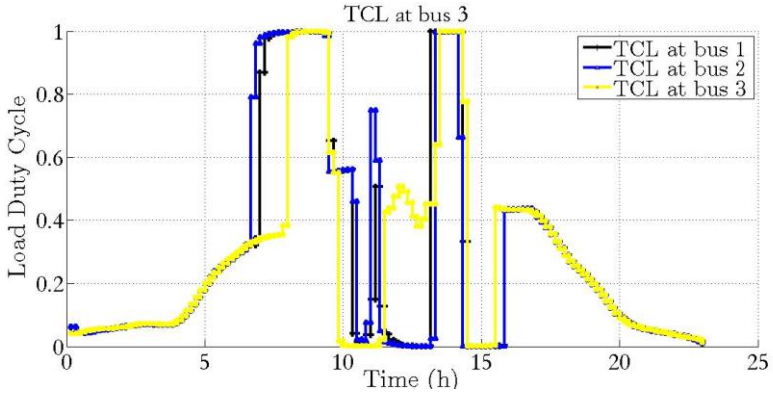

(c)

**Figure 4.5: TCL dispatch results (a) Net Load (b) Sample TCL temperatures (c) Sample TCL controls**

### 4.7.3. Dynamic Line Ratings

The purpose of this case study is to investigate the effects of dynamic line rating used in conjunction with the look-ahead AC-OPF formulation. Namely, we will focus on the comparison between static (MVA based) line ratings and dynamic (temperature based) line ratings. Dynamic line ratings provide additional flexibility, since they provide the capability to plan ahead the overload of a certain transmission line, either to maintain feasibility of the OPF, or simply to reduce cost. In this paragraph, we will compare results for two power systems that are identical in all aspects except one: in System A, all transmission line models feature static ratings, whereas in System B, transmission lines are modeled using the dynamic line rating model of Paragraph 4.3.

It should be noted that, whenever feasibility of the OPF cannot be achieved in a certain period, load shedding (rejection) is required in that period to attain a feasible solution. Load shedding consists of selectively reducing loads in specific buses. In order to highlight the capabilities of the Dynamic Line Rating model in guaranteeing feasibility in otherwise infeasible cases, minimal load shedding, for both active and reactive load, will be reported

for each system. Minimal load shedding results are obtained a relevant look-ahead AC-OPF formulation that is interesting in its own accord and is discussed at length in Chapter 3. For feasible cases (where no load shedding is needed), cost results will also be reported.

**Table 4.3: Comparison of Static versus Dynamic Line Ratings for IEEE 30 Bus System**

| | STATIC RATING (SYSTEM A) | | | DYNAMIC RATING (SYSTEM B) | | |
|---|---|---|---|---|---|---|
| **LOAD (% OF BASE)** | **$P_{shed}$ (MW)** | **$Q_{shed}$ (MVAr)** | **Total Operating Cost ($)** | **$P_{shed}$ (MW)** | **$Q_{shed}$ (MVAr)** | **Total Operating Cost ($)** |
| **94** | 0.0640 | 0.0306 | 6.4518e+04 | 3.3191e-04 | 1.5907e-04 | 6.4515e+04 |
| **96** | 0.4301 | 0.1974 | 6.6281e+04 | 0.0015 | 7.3634e-04 | 6.6271e+04 |
| **98** | 1.9291 | 1.6880 | N/A | 0.0034 | 0.0016 | N/A |
| **100** | 6.4477 | 6.1939 | N/A | 0.0983 | 0.0951 | N/A |
| **102** | 18.2616 | 18.0085 | N/A | 1.9294 | 1.9291 | N/A |
| **104** | 35.9374 | 35.6559 | N/A | 5.4511 | 5.4506 | N/A |

**Table 4.4: Maximum Lagrange Multiplier – IEEE 30 Bus System**

| **LOAD (% OF BASE)** | **STATIC RATING** | **DYNAMIC RATING** |
|---|---|---|
| | $\lambda_{max}$ | $\lambda_{max}$ |
| **94** | 535.3731 | 395.2749 |
| **96** | 712.6980 | 398.4069 |
| **98** | 988.0519 | 569.3133 |
| **100** | 1.0088e+03 | 803.4572 |
| **102** | 1.0297e+03 | 995.6196 |
| **104** | 1.0506e+03 | 1.0195e+03 |

Our first system of interest is the IEEE 30 bus system. The results for System A and System B are presented in Table 4.3 and Table 4.4. The results verify that the magnitude of load shedding is reduced if Dynamic Line Ratings are used, compared to the static ratings case. Furthermore, the total operating cost, for cases where load shedding is not needed, is reduced in the case of System B. It should be noted that reporting operational cost in cases where load shedding is required would not be meaningful, because the removal of load is bound to lead to reduced operational cost, due to the reduction of net

load. Furthermore, the Lagrange multiplier at bus 8, which is the highest Lagrange multiplier for equality constraints, is evidently smaller in the dynamic ratings case.

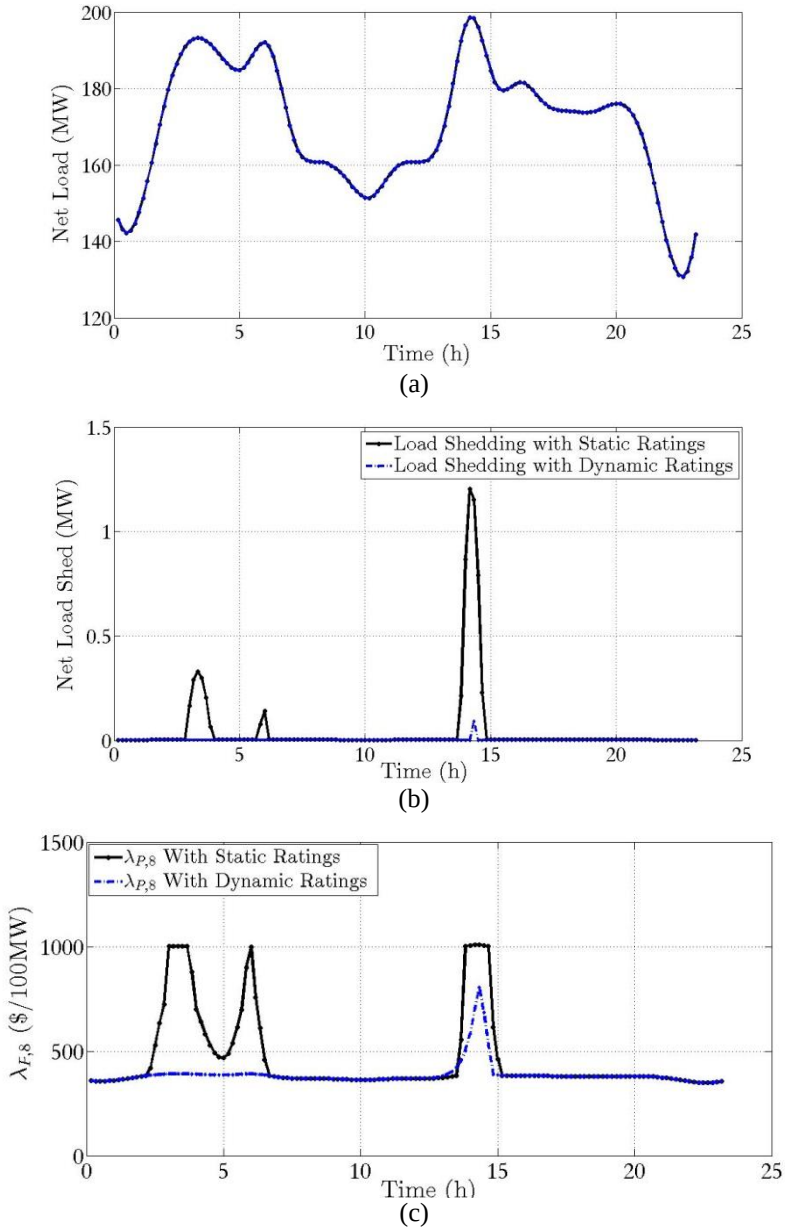


**Figure 4.6: Results for base case scenario a. Load Pattern b. Load Shedding Schedule c. Lagrange Multiplier at bus 8**

The reasons behind the results of Table 4.3 and Table 4.4 can be explained with the help of Figure 4.6. In this figure it is evident that, in case A, load shedding is needed during all peak load periods. On the other hand, load shedding is largely avoided in the dynamic

rating case, except for a minor load shedding needed during the largest peak. Finally, the Lagrangian multiplier in bus 8, shown in Figure 4.6c, is evidently larger during the critical periods for the static ratings case. If the interpretation of the Lagrangian multiplier as a marginal cost of electric power is used ($/MW), this means that dynamic line rating has a sizeable effect in reducing the Locational Marginal Price (LMP) in the most constrained region of the system. The reason of the high LMP in bus 8 is due to the congestion of line 6 – 8. Thus Figure 4.6c highlights the capability of this modeling technique to stabilize electricity prices and alleviate the negative effects of congestion.

Some details regarding the first order dynamic transmission line rating model are shown in Figure 4.7. The two congested lines in the system, line 6-8 (135kV, 35 MVA) & line 25-27 (135kV, 16MVA) are examined. As shown in Figure 4.7a,c, use of the dynamic line rating allows temporary overload of both lines, in order to service the load, contrary to the static line rating methodology. As shown in Figure 4.7b,d the first order dynamic line model indicates that this mode of operation will not, in fact, violate the thermal limit of the line.

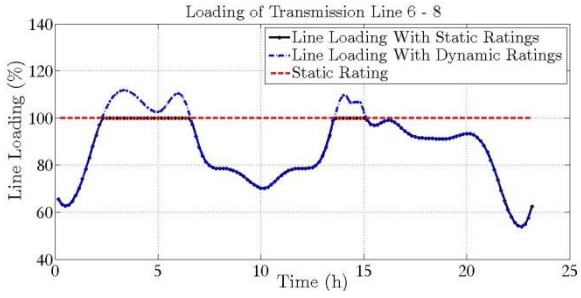


(a)

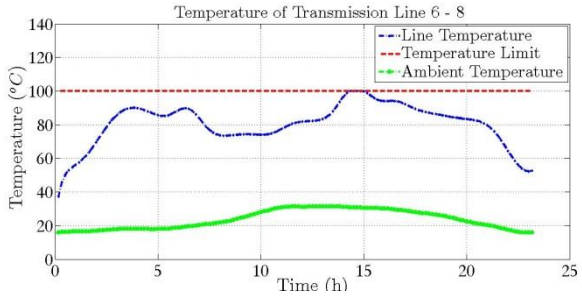


(b)

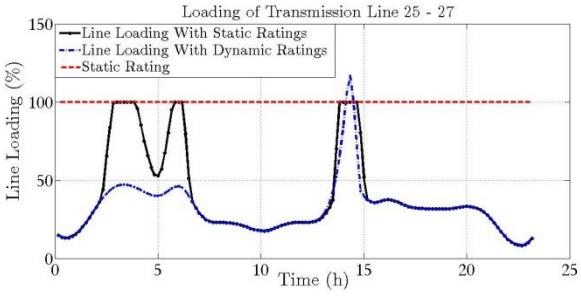


(c)

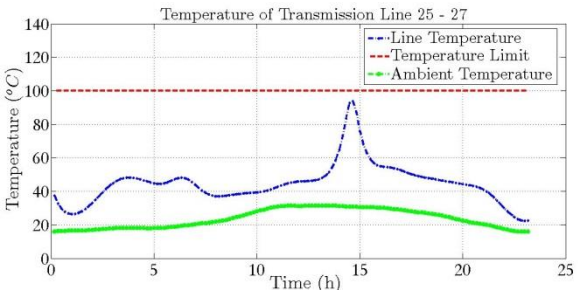


(d)

**Figure 4.7: Dynamic Line Rating Results in base case scenario**

The above observations were made on a rather simplified sample IEEE standard case with a small number of buses. In order to more properly study the benefits of dynamic line rating modeling in a realistic system, a similar testing methodology was applied to the PEGASE 1354 system, a reduced equivalent of the entire European interconnected system, complete with comprehensive line rating data [128]. Unfortunately, dynamic line rating data was not readily available. As a result, realistic line parameters and thermal constant were assumed, using the corresponding IEEE standard [118]. A 7 hour loading scenario, with peak load 80,365MW was tested. This results in a look-ahead AC-OPF model with 223,482 variables and equality constraints and 195,804 inequality constraints. The results are summarized in Table 4.5 and Table 4.6.

**Table 4.5: Comparison of Static versus Dynamic Line Ratings for the PEGASE 1354 System**

| | STATIC RATING (SYSTEM A) | | | DYNAMIC RATING (SYSTEM B) | | |
|---|---|---|---|---|---|---|
| **LOAD (% OF BASE)** | **$P_{shed}$ (MW)** | **$Q_{shed}$ (MVAr)** | **Total Operating Cost ($)** | **$P_{shed}$ (MW)** | **$Q_{shed}$ (MVAr)** | **Total Operating Cost ($)** |
| **96** | 1.5245 | -0.1705 | 2.8679e+06 | 1.6513 | -0.2097 | 2.8678e+06 |
| **100** | 1.6754 | -0.1109 | 2.9893e+06 | 1.3256 | -0.1858 | 2.9891e+06 |
| **104** | 1.4186 | -0.1155 | 3.1109e+06 | 1.6530 | -0.1069 | 3.1107e+06 |
| **110** | 3.6608 | 0.2000 | 3.2940e+06 | 2.2641 | 0.0131 | 3.2936e+06 |
| **115** | 314.4635 | 45.4552 | N/A | 3.7350 | 0.2812 | N/A |
| **120** | 2.7904e+03 | 459.3964 | N/A | 694.0905 | 136.8818 | |

**Table 4.6: Maximum Lagrange Multiplier – PEGASE 1354 System**

| LOAD (% OF BASE) | STATIC RATING $\lambda_{max}$ | DYNAMIC RATING $\lambda_{max}$ |
|---|---|---|
| **96** | 113.7307 | 112.9966 |
| **100** | 115.131 | 114.3696 |
| **104** | 116.7387 | 115.8559 |
| **110** | 121.6062 | 120.3828 |
| **115** | 515.8255 | 190.2477 |
| **120** | 537.3071 | 523.1247 |

The results indicate that a negligible amount of load shedding is required in the base case (indicating a feasible solution). The effects of Dynamic Line Ratings in total system operating cost seem to be negligible, less that 0.1%. However, if load is gradually increased (in an effort to increase system stress) the load shedding required in order to restore feasibility is evidently less if Dynamic Line Ratings are considered in the look-ahead formulation. In fact, at 115% loading, load shedding can be largely avoided and at 120% loading it can be greatly reduced by introducing dynamic line ratings. The same picture can be painted by looking at maximum Lagrangian multipliers. Indeed, these multipliers are consistently larger for the static line rating case. As constraints become binding and load shedding is required, Lagrange multipliers in the corresponding buses abruptly rise. If dynamic line rating is modeled, however, congestion can be relieved, thus reducing the Lagrange multipliers in the neighboring buses. If these lagrangian multipliers are used for pricing, the beneficial effect of dynamic line ratings in mitigating price spikes is, once again, apparent.

### 4.7.4. Active Distribution System

The active distribution system modeling methodology was applied to a sample active distribution system. The distribution system consists of a population of thermostatically

controlled loads and battery storage systems, which means that the disaggregation of P-Q commands is eventually cast as the least squares problem given in (32).

To test the generality of results, the parameters of all devices are drawn from a uniform random distribution around certain chosen central values. The various classes of devices are defined as shown in Table 4.7.

**Table 4.7: Devices in Sample Feeder**

| DEVICE | PARAMETERS | | | | | | |
|---|---|---|---|---|---|---|---|
| **Thermostatically controlled loads** | **R (kW)** | **C (kWs/$^0$C)** | **$P_{rated}$ (kW)** | **$n_{TCL}$** | **Power Factor** | **$\theta_{min}$ ($^0$C)** | **$\theta_{max}$ ($^0$C)** |
| **Class A TCL** | 2.9±5% | 350±10% | 8.0±10% | 0.95 | 0.91±10% | 18.0 | 24.0 |
| **Class B TCL** | 3.4±5% | 350±10% | 8.0±10% | 0.95 | 0.94±10% | 17.0 | 23.0 |
| **Class C TCL** | 2.9±5% | 450±10% | 8.0±10% | 0.95 | 0.88±10% | 18.5 | 24.5 |
| **Class D TCL** | 3.4±5% | 450±10% | 8.0±10% | 0.95 | 0.91±10% | 17.5 | 23.5 |
| **Batteries** | **$n_c$** | **$n_d$** | **$P_{max}$ (kW)** | **$E_{max}$ (kWh)** | **$E_{min}$ (kWh)** | | |
| **Class A Battery** | 0.9±1% | 0.9±1% | 4.4±1% | 0.1±1% | 6±1% | | |

A test feeder of 1,000 active devices, consisting of 200 TCL's from each class and 200 batteries was created. The maximum consumption of the feeder is approximately 7MW. A scatterplot with R & C values in the feeder considered in this Chapter is shown in Figure 4.8.

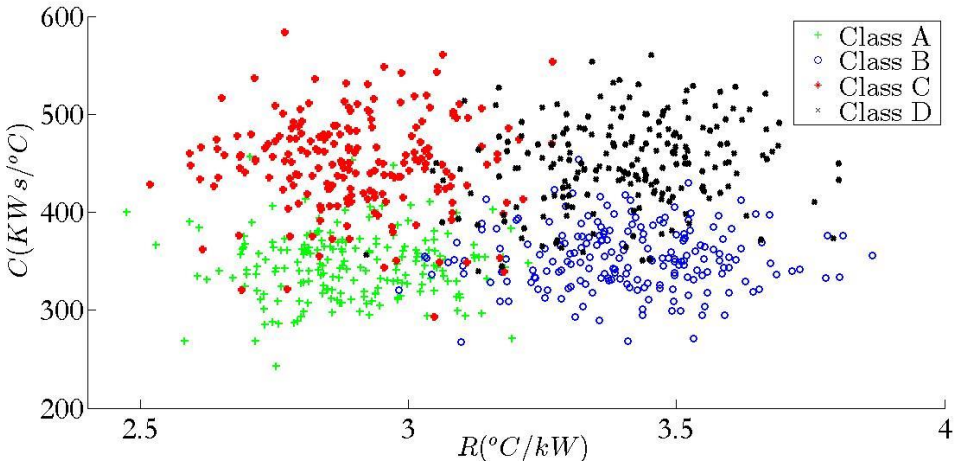


**Figure 4.8: TCL Classes in Sample Feeder**

The aggregation problem for this feeder is addressed by solving the ellipsoidal feasible region approximation problem (31). The data for this problem comes from a simulation of the feeder, where the inputs for the batteries and TCL's are randomly decided. A sample execution of this "aggregation phase" is shown in Figure 4.9. The choice of penalty factor $\gamma$ in (31) crucially affects the resulting model. A smaller $\gamma$ yields a larger feasible ellipsoid, but may overestimate the actual polyhedral feasible region, while the a larger $\gamma$ will yield a more conservative approximation and may lead to severe contraction of the feasible set if the number of steps increases. We consider erring on the conservative side is always preferred, and a penalty factor $\gamma = 200$ is chosen for the remaining results in this chapter, unless otherwise stated.

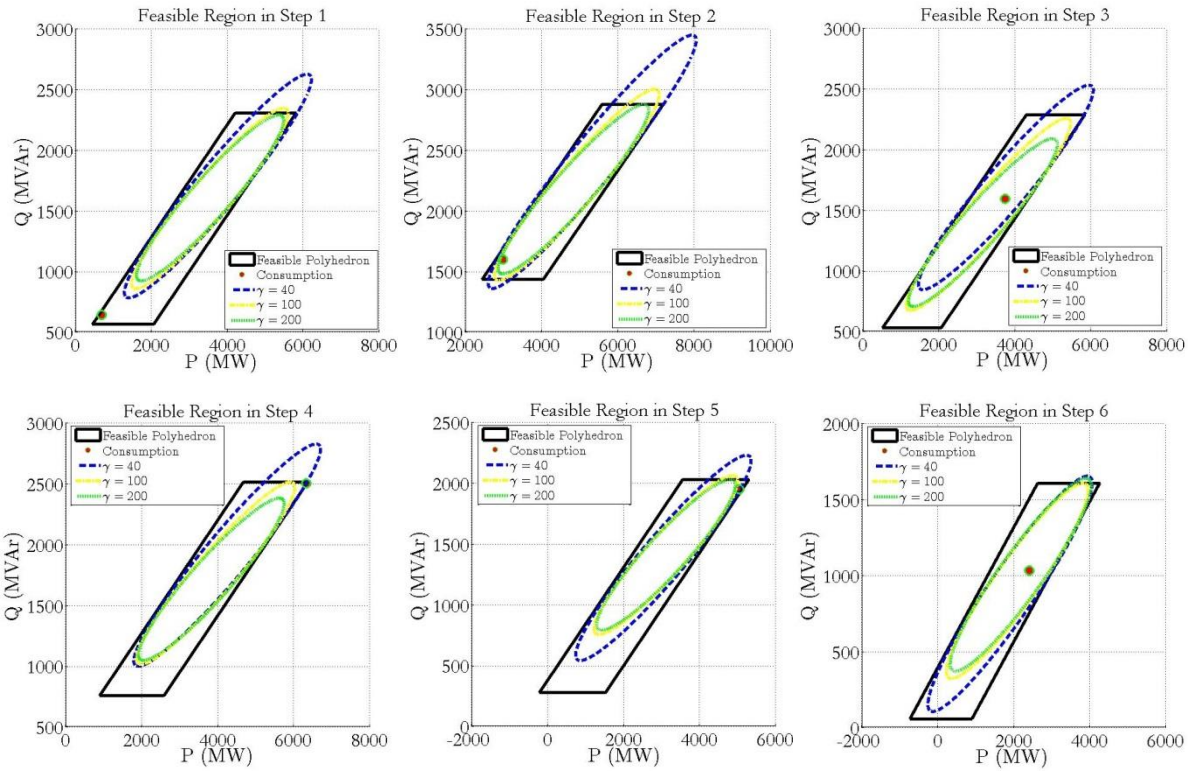

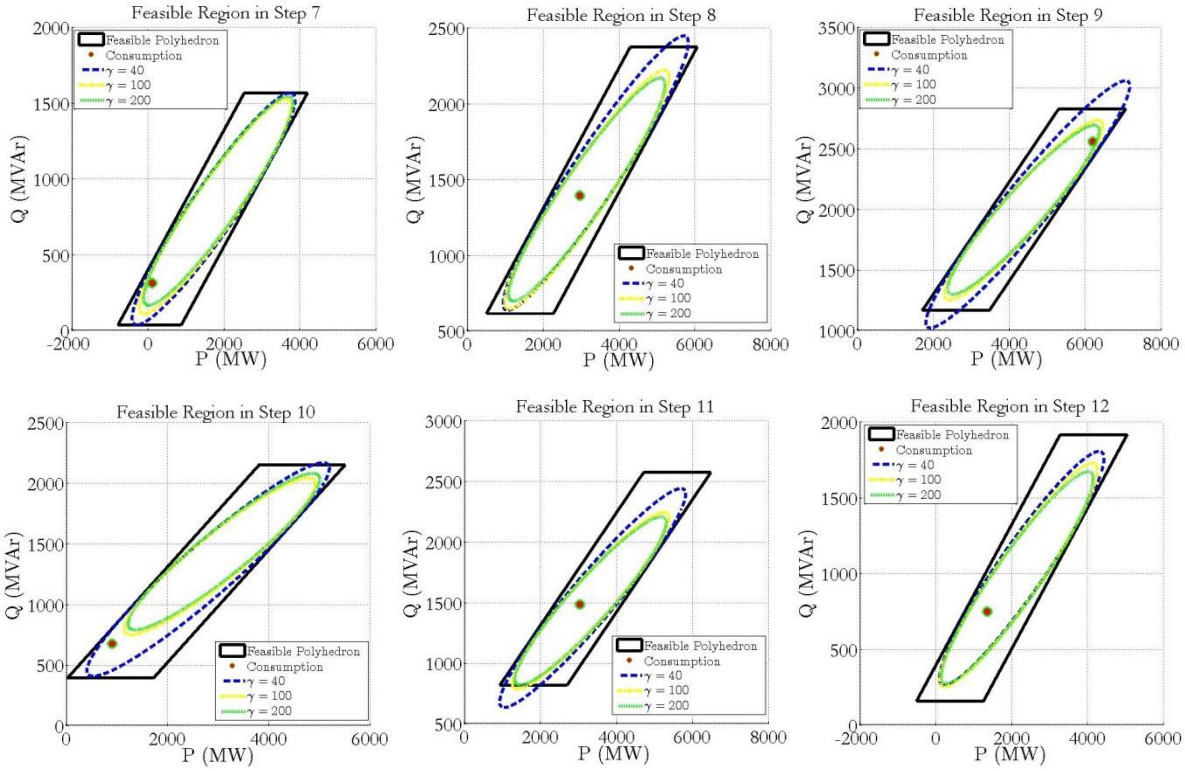


**Figure 4.9: Feasible Polyhedron versus Ellipsoidal approximation for various penalty terms**

As a first numerical experiment, we run a 100-step random simulation of this feeder and obtain an aggregate model by solving (31). Subsequently, we connect this feeder to bus 17 of the IEEE RTS 24 bus system and run the look-ahead OPF with a 10 minute interval to schedule this distribution system. The results are shown below:

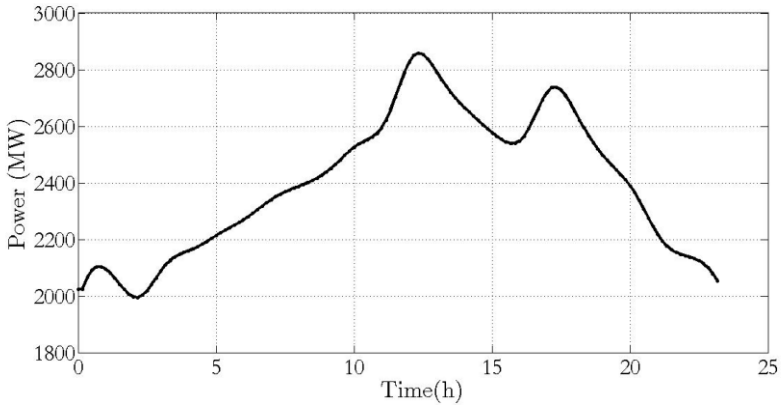


(a)

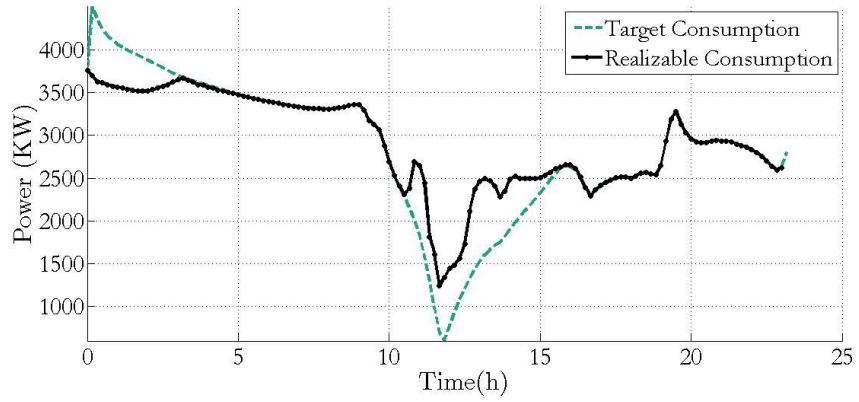


(b)

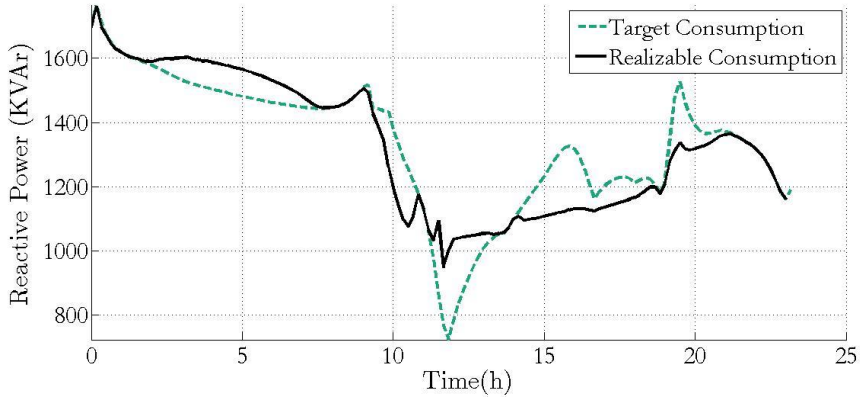


(c)

**Figure 4.10. Single-Run Distribution System Scheduling a. Net System Load b. Active Power Schedule c. Reactive Power Schedule**

It should be noted that for this first experiment, we do not implement the receding horizon scheme of Figure 4.3. Instead, we perform a single run of the optimization algorithm for the entire day, and then we fit the operation of the feeder to the look-ahead OPF result, using the minimization scheme of (33). As shown in Figure 4.10b, the algorithm manages to schedule the distribution system so that consumption is reduced during the peak load of the system, at around 12pm. The dashed line at Figure 4.10b is the schedule provided by the solution of the look-ahead OPF with the aggregate model obtained by the simulation data, while the solid black line is the closest $L2$ norm fit resulting from the solution of (33). Hence, even though the model proves useful in scheduling the distribution system using the look-ahead algorithm, it does not guarantee

feasibility of the target schedule (i.e. the objective of (33) is not zero). This was expected, since our aggregate model is an approximation to allow for transmission system optimization, not an exact modeling approach. This suggests the need for the receding horizon optimization approach of Figure 4.3. The TCL schedules for four TCL's of different classes, which result from the solution of the L2 norm fit problem are shown in Figure 4.11.

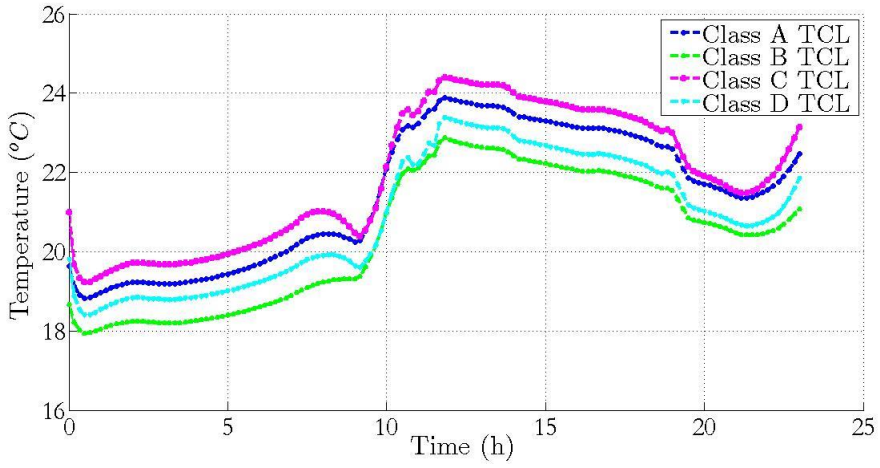


**Figure 4.11: TCL temperature for the consumption schedule of Figure 4.10.**

Note that, according to Figure 4.11 all TCL's are turned OFF during the peak times, in order to reduce distribution feeder consumption, which explains the temperature rise. Furthermore, their temperature does not violate the maximum temperature settings for each class, which are shown in Table 4.7. This is due to the constraints enforced in the fit problem (33).

If the target dispatch is not realizable, this is a significant problem for the decision-maker (e.g. the balancing authority of the transmission system), especially if the active power consumption is different from the scheduled one. Large errors, such as the one showed in Figure 4.10 should be unacceptable. Use of the receding horizon framework is suggested as a solution of the modeling accuracy problem. Renewal of the model at

specified intervals and re-solving of the look-ahead scheduling algorithm will allow a reduction of the inaccuracies, because it allows extraction of renewed state information for all TCL's and Batteries in the system and obtaining of a renewed aggregate model, thus not allowing an accumulation of errors in the aggregate model.

The results for the distribution system scheduling, for the same net load pattern as Figure 4.10a, in the same transmission system (RTS '79) and the same feeder composition as in Figure 4.8, are shown in Figure 4.12. The dashed lines denote the target consumption schedules given for the rest of the day by the look-ahead OPF. There are 10 different dashed lines, each corresponding to a different target schedule, as the look-ahead OPF is solved every two hours. The black line corresponds to the actual consumption, given by the solution of the L2 norm minimization problem. Note that only two hours of each target set point are committed.

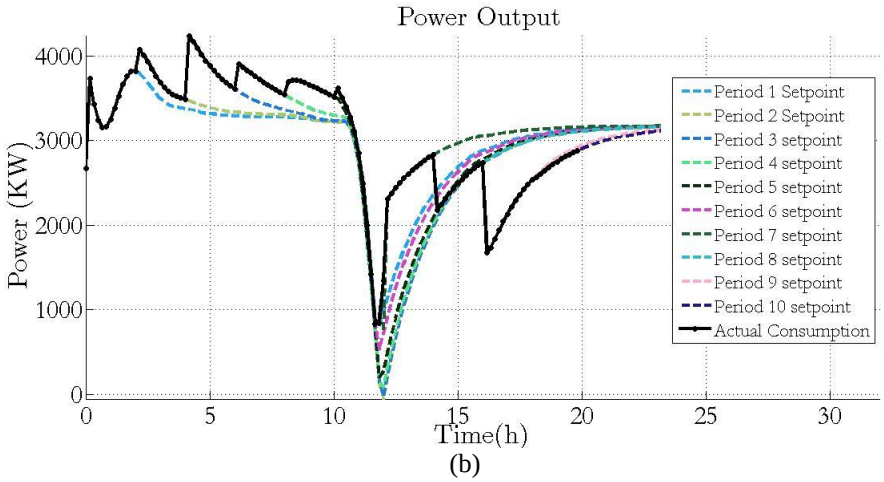

(b)

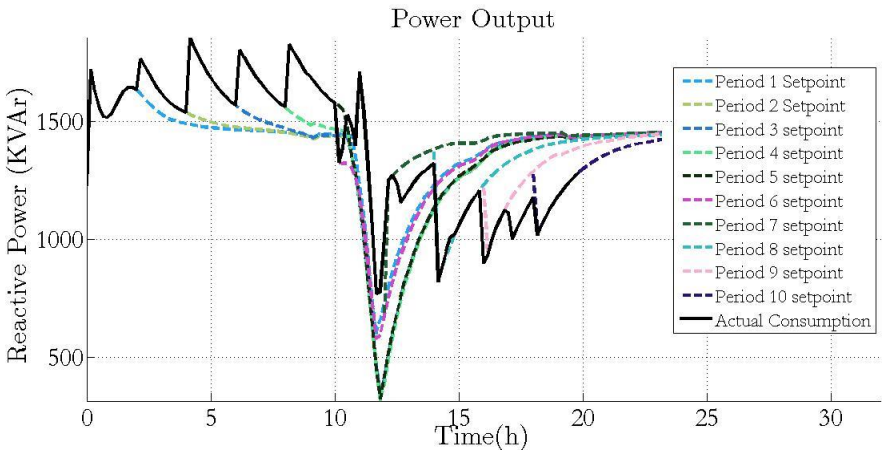


(c)

**Figure 4.12: Aggregate Distribution System Scheduling for a 2h Dispatch Horizon**

From Figure 4.12a it should be noted that there is no error between the target active power consumption and the actual consumption. However, there is some error in the reactive power consumption, due to the small weight factor $\lambda$=0.3 used in (32), to reduce the importance of reactive power fitting. Active power mismatches can be much more threatening to power system operation than reactive power imbalances. It is also of note that, as shown in Figure 4.12, the schedule shows abrupt changes every two hours, as the model is updated, as expected. Note that the general schedule pattern is quite similar to the one yielded by the single-pass approach in Figure 4.10.

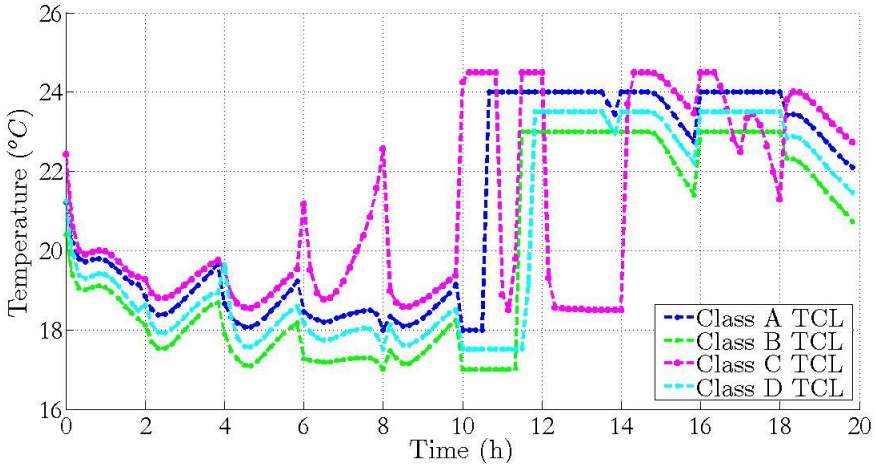


**Figure 4.13: TCL temperature for the aggregate consumption of Figure 4.12**

Figure 4.13 shows the result of the L2 norm fit problem when it comes to the home temperature for four different TCL classes, in order to get the response shown in Figure 4.12. Note the general pattern of pre-cooling the houses in the early off-peak hours and turning-off the air-conditioners in peak times. Furthermore, note that different TCL classes have different thermal models, and are scheduled in different manners by the L2 norm minimization algorithm.

In the final results for this section, we will show the operation of the distribution system with a receding horizon dispatch, and a 1h dispatch horizon. This results in 20 different dispatch schedules within our 20h period of consideration. The results are shown in Figure 4.14. We see that we achieve a zero error between target and realizable dispatch for active power (Figure 4.14a), but occasional errors exist again in the reactive power scheduling (Figure 4.14b).

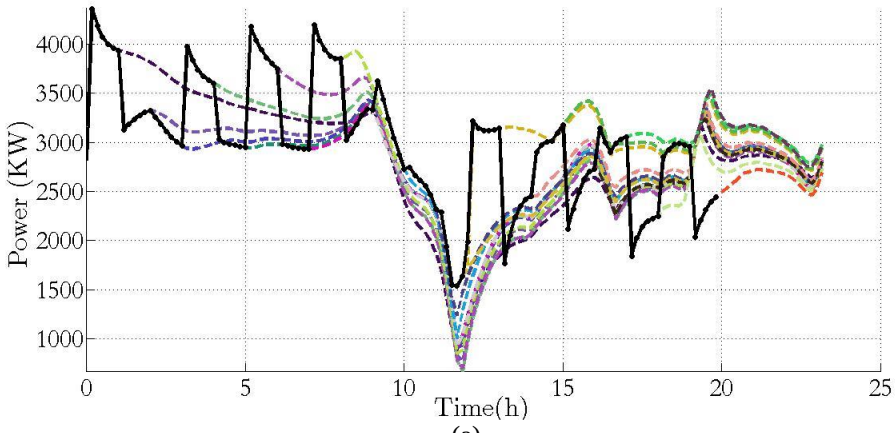

(a)

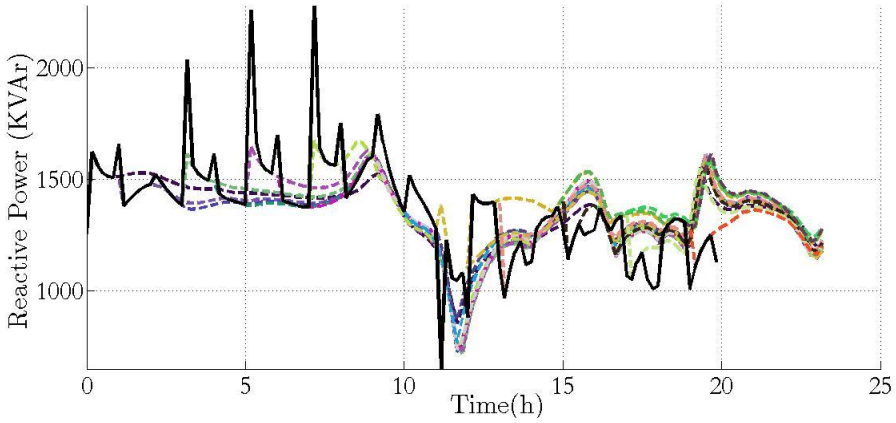


(b)

**Figure 4.14: Aggregate Distribution System Scheduling for a 1h Dispatch Horizon**

In an effort to explain the operation of this framework, we accompany Figure 4.14 with Figure 4.15. In Figure 4.15 we show the feasible region the approximate aggregate model yields with a dashed black line. The circle shows the look-ahead OPF target consumption, as given by the dashed lines of Figure 4.14, while the square shows the realizable consumption given by the solid black line of Figure 4.14, which is the result of the L2 minimization scheme. Only 12 steps (the first two dispatch horizons) are shown in Figure 4.15.

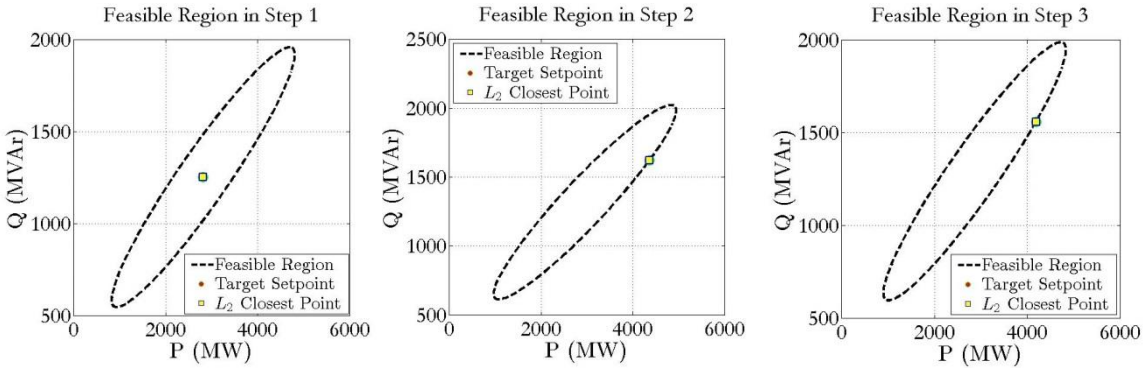

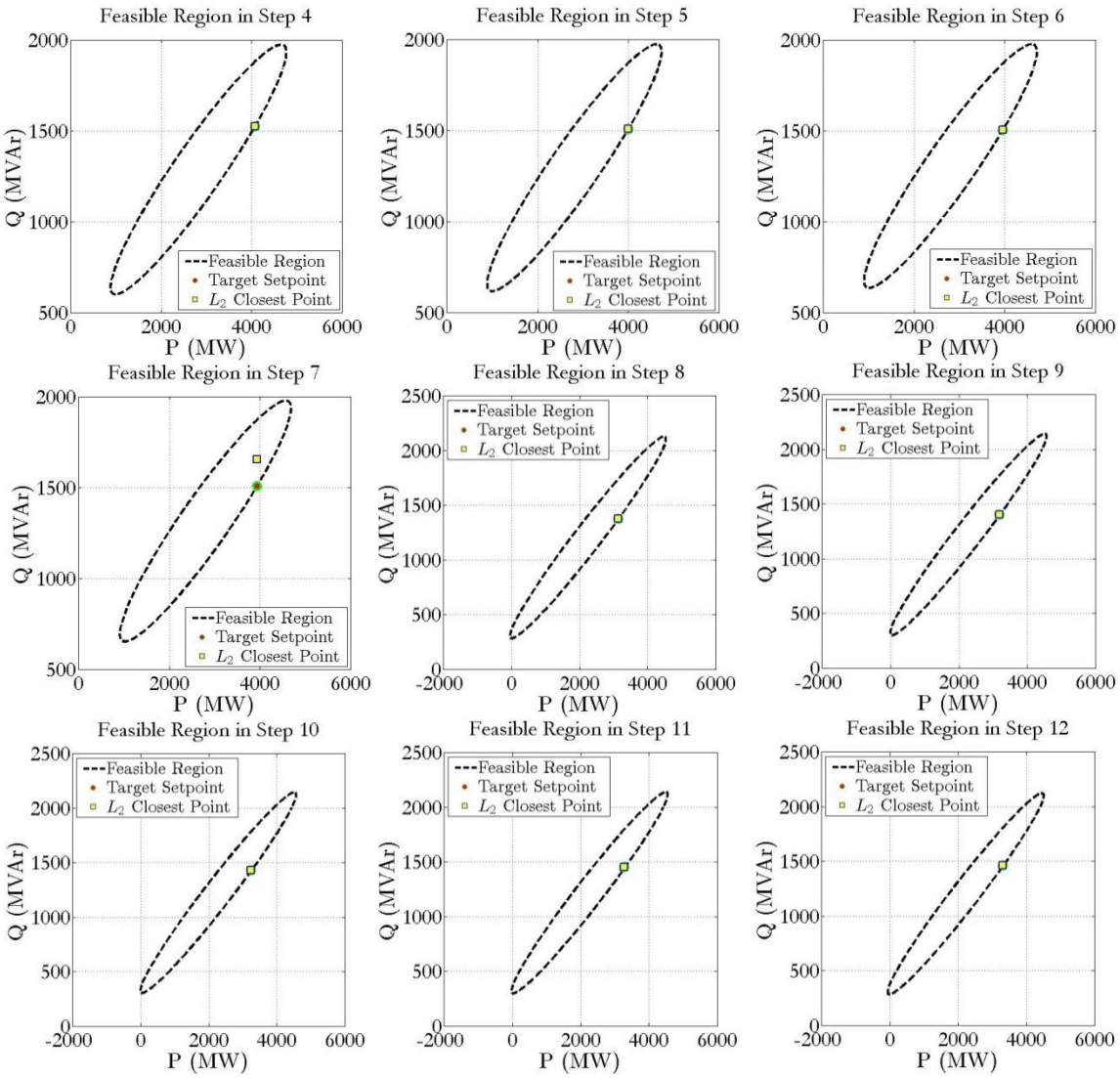


**Figure 4.15: Feasible regions of the aggregate model, target consumption & L2 closest consumption per step, for the results of Figure 4.14**

It is evident that the two points overlap in most cases, showing a zero error between target consumption and actual consumption, verifying the applicability of the approach. However, in some cases such as step 7, the two points do not overlap, allowing for an error in reactive power consumption, which is also shown in Figure 4.14b.

It should be noted that the following tools were used in this chapter. The L2 norm minimization problem was modeled using YALMIP [129] and the polyhedral feasible regions of distribution systems were obtained using the MPT toolbox [130]. The SDP

problem to obtain the parameters for the aggregate modeling of distribution systems was solved using the SDPT solver [131], but the modeling was done using CVX [132] in MATLAB.

# Chapter 5. Stepwise De-Relaxation Algorithm & Minimal Load Shedding

| | |
|---|---|
| $\mathbf{I}_{mk}^{i}$ | Artificial mismatch variable vector at step *k* and iteration *i* of the algorithm |
| $\mu$ | Mismatch penalty factor |
| $\nu_k$ | Mismatch scaling variable at step *k* of the look-ahead OPF |
| $\nu_{\max}$ | Maximum value of mismatch scaling variable at each step |
| $\alpha_i$ | Active constraint set at iteration *i* of the algorithm |
| $s^k$ | Load shedding percentage at step *k*, in the Sheddable load model |
| $g_L + jb_L$ | Nominal impedance of sheddable load model |
| $a_{sh}$ | Quadratic load shedding penalty factor |
| $b_{sh}$ | Linear load shedding penalty factor |
| $G$ | Set of generators in the transmission system |
| $L$ | Set of loads in the system |
| $\kappa$ | Margin of safety for load shedding cost factors |

## 5.1. Introduction

Feasibility of the look-ahead flexible OPF is not always guaranteed. Various issues may be to blame, such as heavy loading of the system and loss of static feasibility of power

flow equations and insufficient ramping capability of conventional generation. Such examples of infeasible situations were also discussed in the results section of Chapter 4. Such situations are likely to occur in the aftermath of a critical outage of a transmission line or a large generating unit. In those cases Remedial Action Schemes (RAS) need to be deployed to restore feasibility. Whenever possible, such actions should be limited to rescheduling of normal operating controls, such as generator re-dispatch and adjustment of transformer tap-settings to regulate voltages in the grid. However, whenever feasibility cannot be restored thusly, emergency actions such as load shedding must be deployed. Load shedding is a very undesirable course of action and its magnitude must be minimized to the least amount possible to attain feasibility.

For this purpose, in order to complete the look-ahead OPF framework, we must develop formulations and methods to calculate remedial actions. These algorithms should allow for the possibility of load shedding, i.e. reducing system load to guarantee feasibility. Two methodologies are discussed in this Chapter to achieve this. The first is an iterative algorithm consisting of initially relaxing power flow equality constraints (thus removing loads from the system) and gradually de-relaxing the equalities and stressing the system until infeasibility is detected or convergence is achieved. The second is an alternative implementation of the look-ahead problem with the addition of a sheddable load model. This results in a composite objective function that aims to achieve a trade-off between minimal load shedding and minimal operating cost. The benefits and disadvantages of those two methods, as well as potential applications are also discussed, and a direct comparison is performed.

## 5.2. Stepwise De-Relaxation Approach

One way to allow for localized remedial actions schemes is to allow for a relaxation of power flow equations at each step. Power flow equations are included in the equality constraints of model (6). Hence, their relaxation consists of introduction of artificial mismatch variables $\mathbf{I}_m$. Since equality constraints are enforced separately at each step in (6), a different mismatch variable $\mathbf{I}_{m,k}$ is introduced for each step *k*. The main idea of the approach discussed in this chapter is to not enforce equality constraints at zero at each iteration *i*, but allow a deviation from zero equal to $\mathbf{I}^i_{m,k}$ at each step *k*. The magnitude of mismatch variables is also penalized in the objective function with a penalty factor of $\mu$.

However, this approach would not guarantee convergence to small enough equality constraint values in feasible cases, since the value of $\mu$ that is large enough to guarantee that is unknown. For this purpose, an iterative approach is adopted. Namely, at each iteration *i*, the value of the mismatch variables is multiplied by a variable $\nu_k$, smaller than 1, which is part of the optimization problem. In order to enforce a certain rate of reduction of mismatches at each iteration, this variable is constrained to be less than $\nu_{\max}$ This guarantees an upper bound on the rate of reduction of the mismatches to zero as iterations progress.

If we initialize the mismatches $\mathbf{I}^0_{m,k}$ to values such that loads are zero, which means that $\mathbf{I}^0_{m,k}$ is equal to the loads at each bus, then the above approach is equivalent to gradual loading of the system, whereby the load at each bus is increased by at least a fixed percentage at each iteration. No inequality constraints are explained to be violated at zero

load, since flows in lines and transformers will be zero. Empirical observation suggests that, as system loading increases in the course of algorithm execution, more constraints will be violated, as line limits are exceeded. Hence, the algorithm is modified to begin with an empty set of enforced inequality constraints, and adaptively add constraints to the enforced set as constraints are violated. Constraint violation is after the solution of the optimization problem at step *i*. If it is detected, then the algorithm remains at iteration *i* and the violated constraints are added to the monitored set $\alpha_i$ and the *i*-th iteration problem is re-solved with the new constraint set. This procedure is repeated until no constraints are violated.

The resulting optimization problem at iteration *i* is the following:

$$\{\mathbf{X}_i^*, \mathbf{U}_i^*\} = \underset{\mathbf{X},\mathbf{U}}{\operatorname{argmin}} \sum_{k=1}^{K} c(\mathbf{X}_k, \mathbf{U}_k) + \mu \sum_{k=1}^{K} \left\| \nu_k \mathbf{I}_{mk}^{i-1} \right\|$$

subject to

$$\begin{aligned}
\mathbf{g}(\mathbf{X}_{k-1}, \mathbf{U}_{k-1}, \mathbf{X}_k, \mathbf{U}_k \mid \mathbf{P}_k) &= \nu_k \mathbf{I}_{mk}^{i-1} && k = 1,2,\ldots,K \\
\mathbf{U}_{\min} \le \mathbf{U}_k &\le \mathbf{U}_{\max} && k = 1,2,\ldots,K \\
\mathbf{X}_{\min} \le \mathbf{X}_k &\le \mathbf{X}_{\max} && k = 1,2,\ldots,K \\
\mathbf{X}_0 &= \mathbf{X}_{init} && k = 1,2,\ldots,K \\
\mathbf{U}_0 &= \mathbf{U}_{init} && k = 1,2,\ldots,K \\
h_j(\mathbf{X}_{k-1}, \mathbf{U}_{k-1}, \mathbf{X}_k, \mathbf{U}_k \mid \mathbf{P}_k) &\le 0 && k = 1,2,\ldots,K \;\&\; j \in a_{i-1} \\
0 \le \nu_k &\le \nu_{\max} && k = 1,2,\ldots,K
\end{aligned} \tag{34}$$

It should be noted that, at each iteration, solution is repeated until no inequality constraint violations are found for the given level of mismatch variables. This guarantees that iterations and further loading of the system will not proceed unless a solution that satisfies all inequality constraints is not found. Hence, each intermediate solution yields a

dispatch of control variables and a load shedding schedule that collectively result in a feasible solution with respect to the inequality constraints.

If a feasible solution can be attained, outer iterations are repeated until mismatch variables become sufficiently small, so as to make load shedding infinitesimally small. This corresponds to an overall feasible solution. The added by-product is that the set of enforced inequality constraints is not the entire set of constraints, but only a subset that were violated during the execution of the algorithm. This allows for a slight alleviation of the computational cost of the iterative algorithm.

If a feasible solution is not possible then the solver will fail at some level of mismatch variables whose magnitude is not negligible. In that case, the algorithm retrieves the previous successful solution, which corresponds to a larger value of mismatch variables for which a solution was possible. Hence, even in infeasible cases, the algorithm outputs a Remedial Action Scheme that restores feasibility.

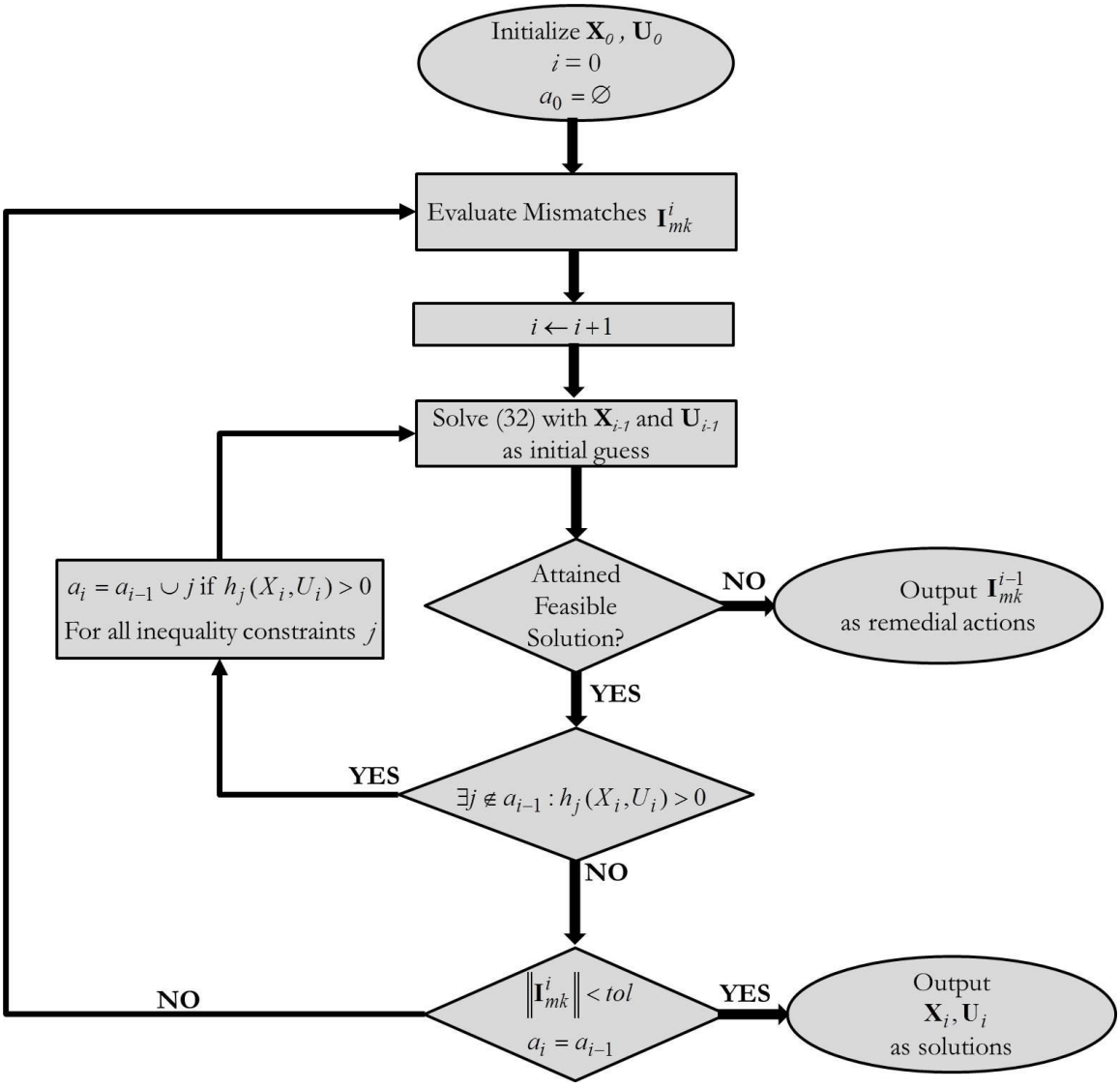


**Figure 5.1: Gradual Enforcement algorithm with adaptive inequality constraint set**

A flow chart outlining the stepwise de-relaxation algorithm is shown in Figure 5.1. It should be stressed that this algorithm is sensitive to the manner with which the mismatch variables are initialized, i.e. the manner with which the initial controls and states are chosen. In this framework, we initialize the control variables of all devices so that current injections in (1a) from generating devices are zero, all voltage variables are at 1 pu and all imaginary parts of voltages are at zero. This means that all loads are consuming power at their rated value and thus mismatch variables are initialized at the value of the system's

loads. Hence, at the initial step, $\mathbf{I}_{m,k}^{0}$ is initialized at the value of the system's loads at step *k* of the multi-step formulation and they are subsequently reduced at further steps.

The intermediate problem at step *i* in (34), is solved using the primal-dual interior point algorithm for NLP, using IPOPT, as detailed in Chapter 3. The optimal solutions $\{\mathbf{X}_i^*, \mathbf{U}_i^*\}$ at iteration *i* are used as the initial guess for the primal-dual interior point.

It should be noted that, using this methodology, the same variable $\nu_k$ is shared across all inequality constraint at each step *k*. Hence, the initial mismatch is relaxed evenly across all equality constraints at each step *k*, by a factor of at least $\nu_{\max}$ per iteration. Hence, in each step of the look-ahead OPF, Kirchhoff's law is enforced uniformly at each node in the system, which means that all loads in all buses will participate uniformly in load shedding if the algorithm of Figure 5.1 indeed terminates prematurely. This may lead to a load shedding with non-minimal magnitude, since this algorithm does not allow localization of load shedding in specific buses, in order to attain feasibility.

## 5.3. Sheddable Load Model

Since the above approach does not allow localization, it is reasonable to seek an alternative load shedding approach that restores feasibility, while also allowing for unequal load shedding percentages in all buses.

For this purpose, all rigid load models are replaced by sheddable load models in the formulation. In the sheddable load model, the rigid power consumption of active power $P_k$ and reactive power $Q_k$ is replaced by a relaxed power consumption of $(1-s_k)P_k$ and $(1-s_k)Q_k$. The control variable $s_k$ corresponds to the percentage of load shed. A single

variable is used for active and reactive power, signifying that load is shed uniformly. Separate curtailment of active and reactive power would not be an accurate representation of realistic load shedding capabilities. Namely, load is interrupted in bulk at substations, and a certain load interruption is expected to have a roughly equal effect in active and reactive power load. This approach is aligned with existing load shedding literature [75], [77].

Similar to standard form models detailed in Chapter 4, the sheddable load model is defined as:

$$\begin{bmatrix} I_r^k \\ I_i^k \\ 0 \\ 0 \end{bmatrix} = \begin{bmatrix} g_L(E_r^k - V_r^k) - b_L(E_i^k - V_i^k) \\ b_L(E_r^k - V_r^k) + g_L(E_i^k - V_i^k) \\ -g_L E_r^k V_r^k + b_L V_r^k E_i^k - g_L V_i^k E_i^k - b_L V_i^k E_r^k + g_L\left(V_r^k\right)^2 + g_L\left(V_i^k\right)^2 - P_k + s_k P_k \\ g_L V_r^k E_i^k + b_L V_r^k E_r^k - g_L V_i^k E_r^k + b_L V_i^k E_i^k - b_L\left(V_r^k\right)^2 - b_L\left(V_i^k\right)^2 - Q_k + s_k Q_k \end{bmatrix} \quad (35a)$$

$$0 \le s_k \le 1 \quad (35b)$$

Where the state and control vectors are given as:

$$\mathbf{x}_k = \begin{bmatrix} V_r^k \\ V_i^k \\ E_r^k \\ E_r^k \end{bmatrix} \quad (36a)$$

$$\mathbf{u}_k = [s_k] \quad (36b)$$

However, unlike the conventional constant power load, which does not participate in each period's objective function, in the sheddable load model load curtailment must be appropriately penalized, in order to guarantee that it does not take place under normal

operating conditions, when the OPF is feasible. For this purpose, a quadratic contribution is assumed, similar to that of generators in (14). It should be noted that the amount of active power shed at step *k*, which should be penalized, is equal to $s_k P_k$ , hence the cost function of the sheddable load model at step *k* is a quadratic function of that quantity:

$$f(\mathbf{x}_k, \mathbf{u}_k) = b_{sh} s_k P_k \tag{37}$$

A depiction of the differences between the rigid constant power load model and the sheddable load model with quadratic penalty is given in Figure 5.2.

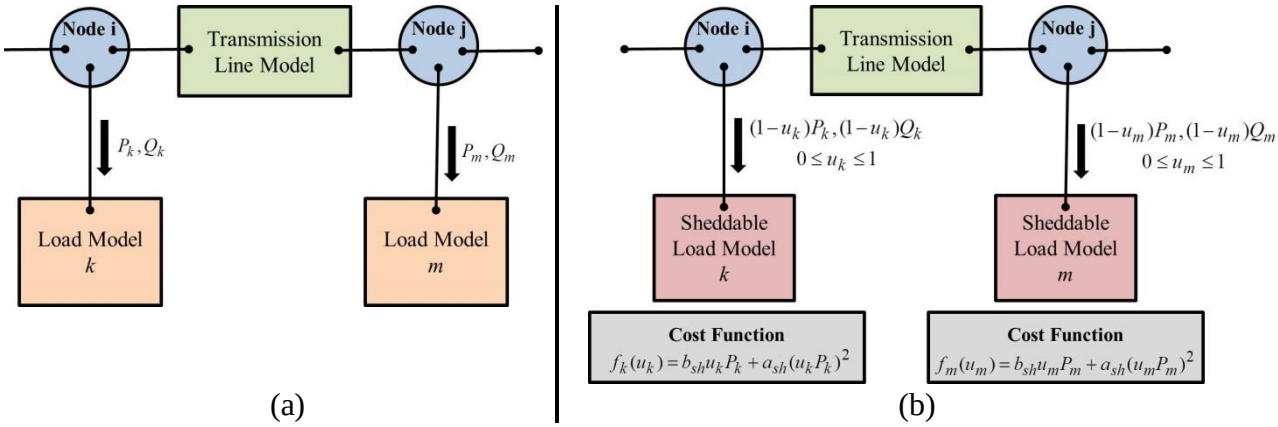


**Figure 5.2:** Load Models (a) Rigid Load Model (b) Sheddable Load Model

However, it is not evident what the choice for the penalty factors $b_{sh}$ should be. Unlike generator models, such cost data does not exist for load models, since the monetary value of load interruptions cannot be explicitly known. However, existing studies seem to indicate a significant cost for interruptions, exceeding by far the cost of energy by conventional generators [133], [134].

Hence, the choice of penalty factors for load shedding will be purely artificial; in order to ensure that load shedding is not activated unless it is required. For this purpose, marginal cost of load shedding must always be higher than marginal locational cost of power at any

bus, provided by normal means, i.e. by generating plants. For this purpose it would be appropriate if load shedding cost factors were strictly greater than the corresponding cost factors of the most expensive generator, plus a margin of safety in order to account for marginal cost of losses in the transmission network. Given that losses are not expected to exceed 10% in extreme cases, this margin of safety need not be larger than that amount. Hence, the choice of load shedding cost factors is:

$$b_{sh} = (1+\kappa)\max_{g\in G}\left\{2a_g P_g^{\max} + b_g\right\} \tag{38}$$

Where $\kappa$ is a safety factor larger than zero. The above heuristic suggests that a value of $\kappa$ close to 0.1 should be adequate to achieve the desired performance. This is a heuristic choice that guarantees the following fact for marginal cost of load shedding:

$$\begin{aligned}\frac{\partial f}{\partial(s_k P_k)} &= b_{sh} \\ &= 2\max_{g\in G}\left\{a_g P_g^{\max}\right\} + \max_{g\in G}\left\{b_g\right\} + 2\kappa\max_{g\in G}\left\{a_g P_g^{\max}\right\} + \kappa\max_{g\in G}\left\{b_g\right\} \\ &= (1+\kappa)\max_{g\in G}\left[\frac{\partial f}{\partial(P_g)}\right] \\ &> \max_{g\in G}\left[\frac{\partial f}{\partial(P_g)}\right]\end{aligned} \tag{39}$$

Hence the marginal cost of load shedding is larger than the marginal cost of any generator in the system, by a desired margin of safety. Due to the non-convexity of the problem, this does not guarantee that the globally minimal load shedding will be found. However, this is a reasonable heuristic, from which we expect good performance.

## 5.4. Minimal Load Shedding Formulation

By replacing the rigid load models with sheddable load models, the resulting look-ahead dispatch formulation changes, particularly with respect to its objective function. The control vector is also extended to include load shedding percentages for all loads. The resulting multi-step OPF formulation is:

$$\min_{\mathbf{X},\mathbf{U}}\left\{\sum_{k=1}^{K}\sum_{g\in G}\left(a_g P_{g,k}^2 + b_g P_{g,k} + c_g\right) + \sum_{k=1}^{K}\sum_{l\in L}\left[b_{sh} s_{l,k} P_{l,k}\right]\right\} = \min_{\mathbf{X},\mathbf{U}}\left\{c_G(\mathbf{Z}) + c_{sh}(\mathbf{Z})\right\}$$

$$\begin{aligned}
&\text{subject to}\\
&\mathbf{g}(\mathbf{X}_{k-1},\mathbf{U}_{k-1},\mathbf{X}_k,\mathbf{U}_k \mid \mathbf{P}_k) = 0 \quad k = 1,2,\ldots,K\\
&\mathbf{h}(\mathbf{X}_{k-1},\mathbf{U}_{k-1},\mathbf{X}_k,\mathbf{U}_k \mid \mathbf{P}_k) \le 0 \quad k = 1,2,\ldots,K\\
&\mathbf{U}_{\min} \le \mathbf{U}_k \le \mathbf{U}_{\max} \quad k = 1,2,\ldots,K\\
&\mathbf{X}_{\min} \le \mathbf{X}_k \le \mathbf{X}_{\max} \quad k = 1,2,\ldots,K\\
&\mathbf{X}_0 = \mathbf{X}_{init}\\
&\mathbf{U}_0 = \mathbf{U}_{init}
\end{aligned} \tag{40}$$

It should be reminded that $P_{g,k}$ and $s_{l,k}$ are elements of the control vector $\mathbf{U}_k$ and $P_{l,k}$ are elements of the parameter vector $\mathbf{P}_k$. The corresponding formulation without load shedding capabilities is:

$$\min_{\mathbf{X},\mathbf{U}}\left\{\sum_{k=1}^{K}\sum_{g\in G}\left(a_g P_{g,k}^2 + b_g P_{g,k} + c_g\right)\right\} = \min_{\mathbf{X},\mathbf{U}}\left\{c_G(\mathbf{Z})\right\}$$

$$\begin{aligned}
&\text{subject to}\\
&\mathbf{g}(\mathbf{X}_{k-1},\mathbf{U}_{k-1},\mathbf{X}_k,\mathbf{U}_k \mid \mathbf{P}_k) = 0 \quad k = 1,2,\ldots,K\\
&\mathbf{h}(\mathbf{X}_{k-1},\mathbf{U}_{k-1},\mathbf{X}_k,\mathbf{U}_k \mid \mathbf{P}_k) \le 0 \quad k = 1,2,\ldots,K\\
&\mathbf{U}_{\min} \le \mathbf{U}_k \le \mathbf{U}_{\max} \quad k = 1,2,\ldots,K\\
&\mathbf{X}_{\min} \le \mathbf{X}_k \le \mathbf{X}_{\max} \quad k = 1,2,\ldots,K\\
&\mathbf{X}_0 = \mathbf{X}_{init}\\
&\mathbf{U}_0 = \mathbf{U}_{init}
\end{aligned} \tag{41}$$

Where we defined the candidate solutions to (40), (41) as:

$$\mathbf{Z} = \begin{bmatrix} \mathbf{X}_1 \\ \mathbf{U}_1 \\ \vdots \\ \mathbf{X}_k \\ \mathbf{U}_k \end{bmatrix} \tag{42}$$

## 5.5. Results

It is of interest to compare the two Remedial Action Scheme methods that were proposed in this chapter, with respect to the amount of load shedding required in infeasible cases, as well as their performance in feasible (no load shedding required) cases. Furthermore, some results are presented regarding the convergence of the stepwise de-relaxation method, specifically emphasizing on the number of enforced constraints, to emphasize on the method's ability to consider a smaller set of constraints in the course of execution.

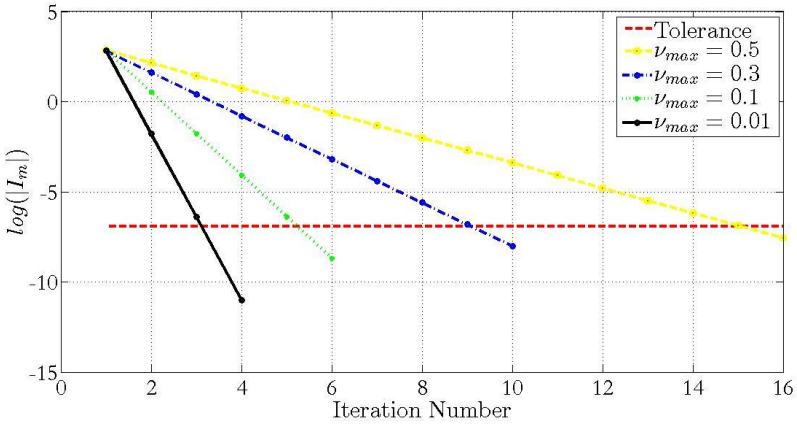

(a)

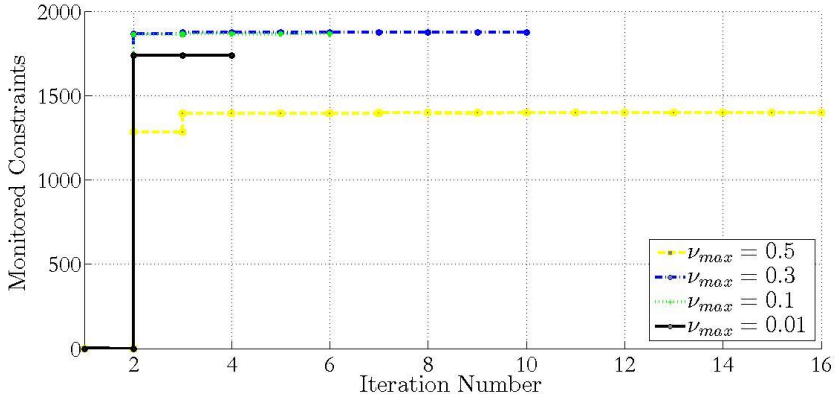


(b)

**Figure 5.3: PEGASE 1354 Bus System a. Missmatch Logarithm Per Iteration b. Number of active constraints**

An initial case study on the performance of the stepwise de-relaxation method is shown in Figure 5.3. The case study in question is a static (single-step) AC-OPF of the 1354 PEGASE System standard case. As expected, the choice of parameter $\nu_{\max}$ affects the rate of convergence. Lower value of $\nu_{\max}$ guarantees a faster convergence rate. As outlined in the algorithm definition, the algorithm is expected to multiply mismatches by a factor of at least $\nu_{\max}$ in every iteration of the algorithm. For this reason the logarithm of mismatches appears as a linear function of iteration number, with a seemingly constant slope in Figure 5.3a. The algorithm execution stops at a desired tolerance level. The algorithm does not fail before reaching the mismatch tolerance level, indicating this is a feasible (zero load shedding) case.

The total number of enforced constraints at the beginning of each iteration is shown in Figure 5.3b. We enter the algorithm with an empty constraint set, which is why all plots start at zero. As the system is loaded, i.e. the equality constraints at all buses are de-relaxed, more constraints are violated. It is of importance to note that most constraints are enforced in the first step. These are mostly bus voltage constraints, whose violation is very frequent,

even in unloaded cases. Our algorithm mostly fails to avoid enforcement of those constraints. However, the algorithm is very successful in avoiding consideration of line current limit and transformer current limit constraints. For all values of $\nu_{\max}$, less than 2,000 constraints are added in the monitored set, even though a total of 4,699 constraints exist in the system models. Our empirical observation regarding the correlation between system loading and constraint violation is true for current flows, but not so for voltage violations.

Another observation to be derived is that the smaller number of monitored constraints is achieved for the algorithm with the slowest convergence rate, i.e. for $\nu_{\max} = 0.5$. This is consistent with empirical expectation: smoother loading of the system means that constraints are violated gradually, unlike a more aggressive loading, where many lines are temporarily overloaded, before their constraints are eventually added in the monitored set. Hence, an execution of the algorithm with larger $\nu_{\max}$ is expected to enforce the critical line constraints. However, this is not generally the case, as the more aggressive $\nu_{\max} = 0.01$ version achieves a smaller monitored set than the other two, less aggressive, versions.

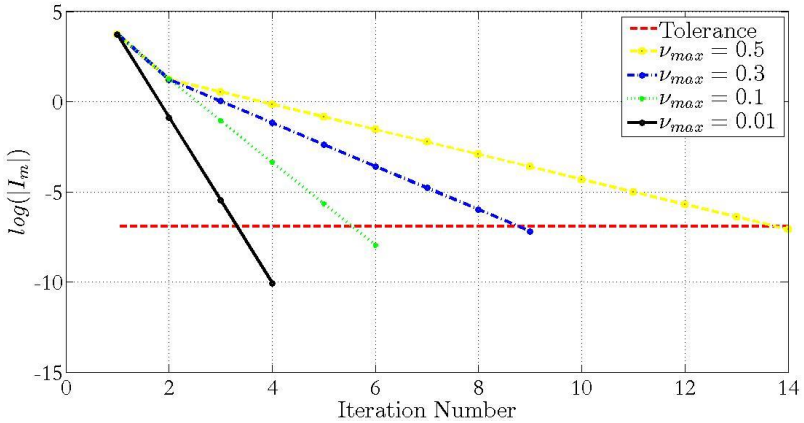

(a)

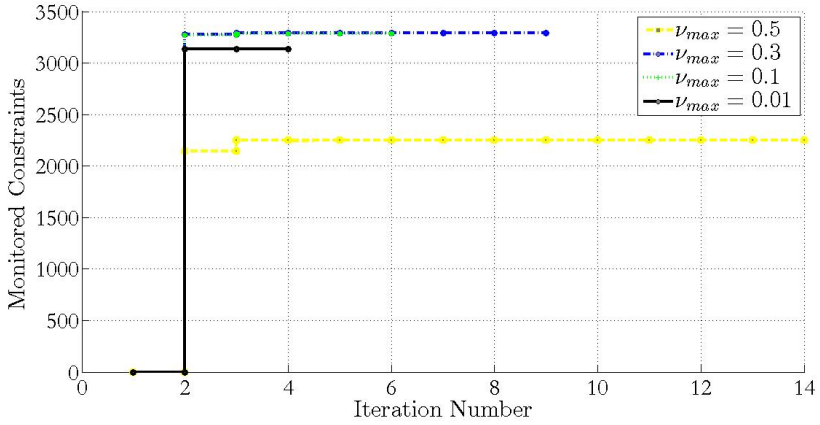


(b)

**Figure 5.4. Polish 3120 Spring PeakSystem a. Missmatch Logarithm Per Iteration b. Number of active constraints**

The corresponding results for the Polish 3120 Bus Spring Peak version are given in Figure 5.4, where similar observations can be drawn.

To highlight the capability of the method in reducing the number of enforced constraints, we provide Table 5.1, where the number of monitored inequality constraints at the conclusion of the algorithm is given for five feasible cases, as a function of $\nu_{\max}$. The de-relaxation approach achieves reduction of the monitored inequality set by at least 50% in all cases. In systems with a very large number of constraints, this may yield benefits in execution times of AC-OPF solutions. It should be noted, however, that even though cases with small $\nu_{\max}$ enforce a smaller number of inequality constraints in general, their convergence rate is smaller, thus presenting a tradeoff between size of monitored constraints set and number of iterations, which ultimately affects execution times. The choice of appropriate $\nu_{\max}$ remains an issue of trial and error.

**Table 5.1: Number of enforced constraints for various case studies – static OPF**

| System Case | $v_{max}$=0.5 | $v_{max}$=0.3 | $v_{max}$=0.1 | $v_{max}$=0.01 | Total Inequality Constraints |
|---|---|---|---|---|---|
| Pegase 1354 | **1,398** | **1,876** | **1,865** | **1,737** | **4,699** |
| Polish 2383 winter peak | **2,386** | **2,385** | **2,385** | **2,385** | **7,662** |
| IEEE 30 bus | **30** | **30** | **30** | **30** | **101** |
| Polish 3120 spring peak (110% load) | **2,251** | **3,291** | **3,284** | **3,137** | **9,933** |

Finally, it is interesting to compare the amount of total load shedding required for the stepwise de-relaxation and the minimal load shedding algorithms, for a suite of infeasible cases. For this purpose, we start with initially feasible system cases and we symmetrically increase the system loading, until load shedding is required. For the stepwise de-relaxation load shedding is equivalent to premature interruption of the algorithm, before the desired level of mismatch variables has been reached. For the minimal load shedding, load shedding means nonzero value of load shedding controls in sheddable load models. The results for three sample systems and various levels of loading, and a static AC-OPF problem, are shown in Table 5.2-5.4.

**Table 5.2: Load Shedding as a function of system loading – IEEE 30 Bus**

| | STEPWISE DERELAXATION | | MINIMAL LOAD SHEDDING | |
|---|---|---|---|---|
| LOADING (% OF BASE CASE) | Active Shed (MW) | Reactive Shed (MVAr) | Active Shed (MW) | Reactive Shed (MVAr) |
| 100% | **0.0017** | **9.0970e-04** | **8.1290e-06** | **4.1730e-06** |
| 102% | **0.0017** | **9.3114e-04** | **0.2588** | **0.2588** |
| 103% | **0.0018** | **9.4186e-04** | **0.5578** | **0.5578** |
| 105% | **2.1698** | **1.1629** | **1.1582** | **1.1582** |
| 110% | **11.0054** | **5.9151** | **2.6621** | **2.6621** |

**Table 5.3: Load Shedding as a function of system loading – Pegase 1354 Bus System**

| | Stepwise Derelaxation | | Minimal Load Shedding | |
|---|---|---|---|---|
| Loading (% of base Case) | Active Shed (MW) | Reactive Shed (MVAr) | Active Shed (MW) | Reactive Shed (MVAr) |
| 100% | **0.6561** | **-0.0082** | **0.0023** | **1.3891e-04** |
| 105% | **0.6927** | **-0.0015** | **2.6993e-04** | **1.1865e-04** |
| 110% | **0.7292** | **0.0052** | **2.0534e-05** | **2.0534e-05** |
| 115% | **0.7657** | **0.0119** | **1.9342e-05** | **6.2292e-06** |
| 120% | **0.8022** | **0.0186** | **8.6050e-04** | **8.6050e-04** |
| 121% | **0.8095** | **0.0200** | **6.7157e-04** | **8.6184e-05** |
| 122% | **0.8169** | **0.0213** | **3.6152** | **1.0444** |
| 123% | **571.1258** | **15.7059** | **18.5824** | **2.9129** |
| 124% | **1.2442e+03** | **35.9190** | **36.6521** | **4.8224** |
| 125% | **1.9225e+03** | **58.0919** | **56.9331** | **7.0939** |

**Table 5.4: Load Shedding as a function of System Loading – Polish 2383 Winter Peak**

| | Stepwise Derelaxation | | Minimal Load Shedding | |
|---|---|---|---|---|
| Loading (% of base Case) | Active Shed (MW) | Reactive Shed (MVAr) | Active Shed (MW) | Reactive Shed (MVAr) |
| 100% | **0.2207** | **0.0389** | **-0.0100** | **18.5478** |
| 105% | **0.2329** | **0.0430** | **-0.0019** | **26.8853** |
| 106% | **0.2354** | **0.0438** | **-0.0438** | **32.3027** |
| 108% | **0.2403** | **0.0454** | **-0.0138** | **40.5697** |
| 110% | **247.1916** | **47.4033** | **21.6716** | **52.6077** |

From these results we can safely conclude that the minimal load shedding formulations allows for smaller amounts of load shedding in general, than the stepwise de-relaxation algorithm. This is to be expected, based on the approach followed by the two algorithms. The de-relaxation algorithm relaxes all constraints uniformly, as noted before, since they share the same $\nu$ value. Hence, if congestion arises in a part of the system, the algorithm lacks the capability to localize load shedding in problematic areas, and iterations terminate with larger load shedding values. The opposite is true for the minimal load shedding formulation, which specifically ascribes a very high cost factor to load shedding quantities.

Also note that nonzero load shedding is signaled even in feasible cases. This is not an error, but merely an issue of finite accuracy of the algorithm. Higher accuracy would yield

load shedding values even closer to zero, but such accuracy is usually redundant in standard AC-OPF solvers (convergence tolerance does not exceed $10^{-5}$ in practice).

Finally, one disadvantage of the minimal load shedding algorithm is the failure to penalize reactive load shedding. For this reason, purely reactive loads are shed indiscriminately even in feasible cases, resulting in the nonzero reactive shedding values of Table 5.4.

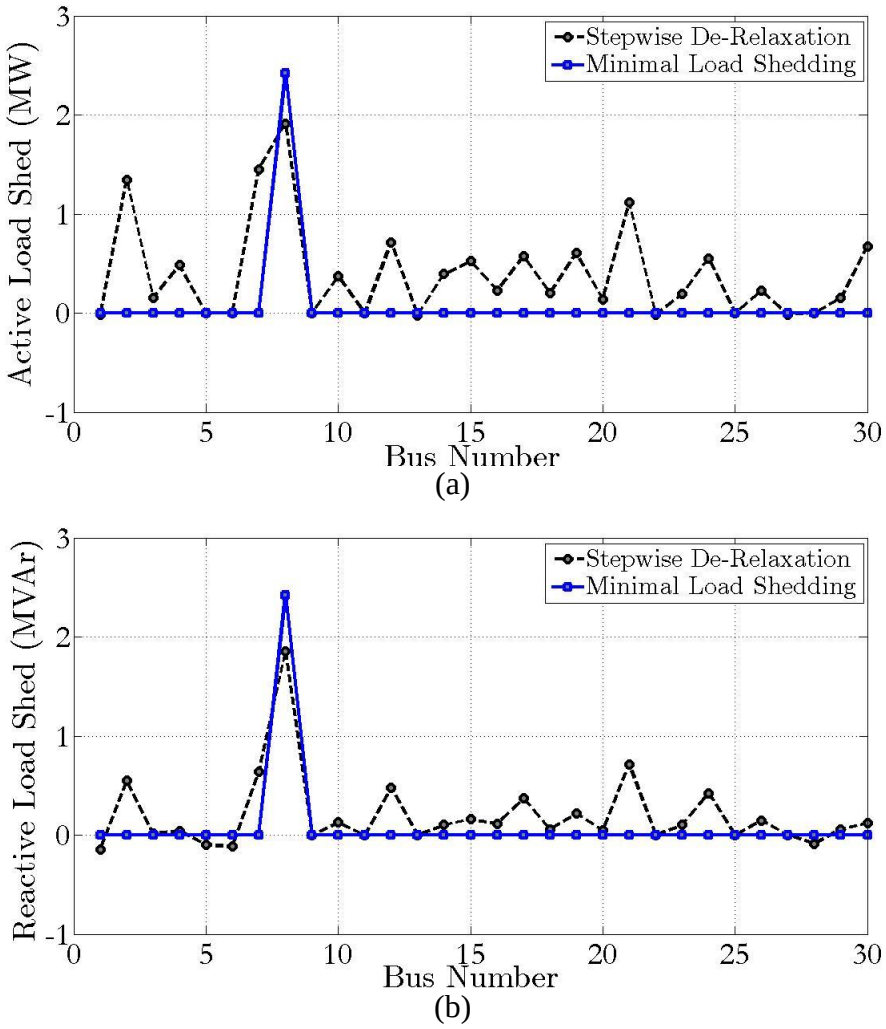


**Figure 5.5: Load Shedding Per Bus (a) Active Shed (b) Reactive Shed**

As mentioned, the minimal load shedding formulation minimizes total load shedding, and will tend to localize load shedding to buses where it will be most effective. For the

IEEE 30 bus system, this is bus 8, as shown in Figure 5.5, where the active shedding (figure a) and reactive shedding (figure b) per bus are plotted. Comparing with the corresponding results for the stepwise de-relaxation algorithm, we conclude that the latter tends to distribute load shedding between buses and thus will naturally yield larger load shedding outputs. However, a side benefit of that approach is that buses will share the burden for load shedding proportionally to their rated load values, hence not penalizing one bus in particular more than others. As shown in Figure 5.5, the load shedding required for bus 8, both active and reactive, is reduced in the stepwise de-relaxation case, compared to the minimal load shedding case.

# Chapter 6. Contingency Selection

## 6.1. Nomenclature

| | |
|---|---|
| $S_i$ | MVA loading of line *i* |
| $S_{r,i}$ | MVA rating of line *i* |
| $L$ | Set of transmission lines |
| $u_j$ | Contingency control variable of device *j* |
| $g_j^{ON}$ | Device *j* on model |
| $g_j^{OFF}$ | Device *j* off model |
| $N_d$ | Number of devices in the system |
| $\mathbf{u}$ | $N_d \times 1$ system-wide contingency control vector |
| $\mathbf{x}$ | $N_s \times 1$ system-wide state vector |
| $\mathbf{g}$ | $N_s \times 1$ System-wide (power-flow) equations |
| $\mathbf{h}$ | $N_h \times 1$ System-wide inequality constraints |
| $f$ | Performance index expression |
| $\overline{\mathbf{h}}$ | $N_h \times 1$ inequality limits |
| $(\mathbf{x}_0, \mathbf{u}_0)$ | Pre-outage operating point |
| $w_j$ | Weight of *j*-th constraint in margin index expression |
| $\mathbf{s}, \mathbf{y}, \mathbf{t}$ | $N_h \times 1$ auxiliary variable vectors |
| $\mathbf{z}$ | $3N_h \times 1$ concatenated auxiliary variable vector |
| $\mathbf{H}$ | $3N_h \times 1$ Auxiliary variable equations |
| $\hat{\mathbf{z}}$ | $3N_h \times 1$ costate vector |
| $\hat{\mathbf{x}}^T$ | $N_s \times 1$ costate vector |

| | |
|---|---|
| $P$ | The set $\{a,b,c\}$ of system phases |
| $I_j^{(p)}$ | RMS current through phase *p* circuit of line *j* |
| $I_{rated,j}$ | Rated current of line *j* |
| $B$ | Set of buses in the system |
| $V_{jp}$ | Voltage at phase *p* of bus *j* |
| $\overline{V}_j, \underline{V}_j$ | High and low voltage limit of bus *j* |
| $\Delta V_{band}$ | Width of voltage band $\overline{V}_j - \underline{V}_j$ |
| $G$ | Set of Generators in the system |
| $\overline{Q}_j, \underline{Q}_j$ | Reactive power limits of device *j* |
| $\overline{S}_{g,j}$ | MVA limit of generator *j* |
| $M$ | Number of criteria in multi-criterion algorithm |
| $K$ | Number of maximum misses until termination |
| $S$ | Number of misses until criterion switch |
| $r_{i,j}$ | *i*-th ranked outage by criterion *j* |
| $rnk$ | Multi-criterion ranked list |
| $Conn_j$ | Connectivity set of device *j* |
| $m_j$ | Number of (local) states in model of device *j* |
| $\mathbf{x}_j$ | $m_j \times 1$ local state vector for device *j* |
| $N_j$ | Connectivity matrix of device *j* |
| $\delta A^{(j-)}$ | $m_j \times m_j$ low rank correction of Jacobian upon outage of device *j* |

## 6.2. Introduction

A framework for performing fast online contingency selection in unbalanced power systems is presented in this Chapter. Selection methods are typically based on the principle of identifying the effect of contingencies on multiple normalized performance indices and ranking them using the results. Presently used performance indices are highly nonlinear and they are known to mask the effects of single contingencies leading to misclassifications. In this Chapter we propose two new methods, one relying on margin-based performance indices and another based on state sensitivity. New performance indices are proposed based on margins of (a) circuit loading, (b) bus voltages and (c) reactive power. In addition, a state sensitivity method is proposed which estimates a system's post contingency operating state via a single iteration of the Quadratized Power Flow model and provides estimates of post contingency line loading, bus voltages and reactive power levels. Numerical experiments on a three phase version of the IEEE Reliability Test System show that the proposed performance indices yield more accurate results, at a computational cost comparable to a single power flow iteration. The state sensitivity method is more accurate in identifying critical contingencies but its computational cost is higher. The method has been also demonstrated in the larger PEGASE systems.

While the existing literature has covered the topic of contingency selection and analysis for balanced networks using single-phase equivalent models for power system components, the application of contingency selection methodologies in unbalanced networks remains an unexplored area. Furthermore, existing PI methods use metrics such as the post-contingency real power line flows or the post contingency voltage deviation and reactive power injections [98]. However, for transmission lines, the actual thermal

constraint is expressed in terms of line current, and not line apparent power flow, hence the existing PI methods are potentially inaccurate predictors of post-contingency line limit violations when voltages are abnormal.

The methodologies proposed in this paper combine accuracy and speed and allow reliable selection of critical contingencies. The proposed margin indices: (1) directly quantify the distance from constraint violation and (2) the constraint is expressed in terms of the actual constraint physical quantity, for example electric current for thermal limits. The need for this approach is motivated by the fact that actual power transmission systems exhibit imbalance and they are limited by ampacity. Figure 6.1 illustrates a snapshot of a 345 kV transmission system. Note current imbalances as high as 23.9%, 7.7% and 7.09% for the three circuits respectively.

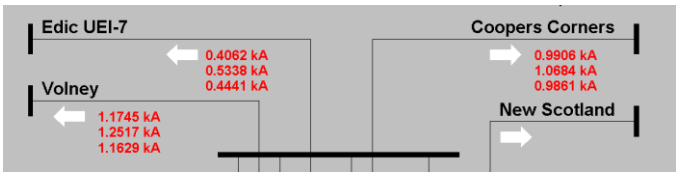


**Figure 6.1: Snapshot of an actual 345 kV System Indicating Imbalances**

The three-phase formulation allows separate treatment of each phase, addressing unbalanced cases. Second, the proposed state sensitivity method is characterized by decreased computations, due to the application of the compensation method for low-rank corrections of the Jacobian (see 6.2). Furthermore, the proposed methods assign a different weight to each constraint, based on the pre-outage proximity to the limit. Finally, both the index-based filtering and the state sensitivity indices discussed here constitute an extension and improvement of current filtering techniques [87], [135], with respect to accuracy and speed.

The proposed methodologies have been implemented using a three-phase unbalanced solver (quadratized power flow) and are applicable to unbalanced power system operation. Results on accuracy and execution time in various systems highlight the applicability of the discussed contingency filters. A detailed examination of contingency analysis results on the IEEE 72 bus system also helps reveal the potential need for three phase security analysis in transmission networks. The performance of the methods in large systems is demonstrated on the PEGASE systems. Regarding notation, note that the subscript 0 denotes the value of each quantity before any outage occurs and the superscript ($j$-) denotes the value of each quantity after the outage of device $j$.

## 6.3. Margin Index Method

The legacy performance index methods are described in the literature. One of the traditional criteria described in [88] is the following:

$$J_{LPI} = \sum_{i \in L} \left( \frac{S_i}{S_{r,i}} \right)^2 \tag{43}$$

In the generalized contingency selection method discussed here, the effect of contingencies must be modeled in the device level, and the system level effects of the outage will be determined upon combining and solving the system level equations (network model). The proposed contingency modeling approach as well as the proposed approximate first-order PI method is discussed in this section.

### 6.3.1. Contingency Modeling

In order to model the effects of the contingencies in the device level, the use of contingency control variables $u$ has been proposed [96], [136]. These are defined as follows:

$$u_j = \begin{cases} 1 & , \text{ if device is operational} \\ 0 & , \text{ if device is outaged} \end{cases} \tag{44}$$

Using the contingency control variable approach, each device model is extended to include the device outage model, in addition to the standard operational model of the device, obtaining the Device Switching Model (DSM):

$$\begin{bmatrix} \mathbf{i} \\ \mathbf{0} \end{bmatrix}_j = u_j g_j^{ON}(\mathbf{x}_j) + (1-u_j) g_j^{OFF}(\mathbf{x}_j) \tag{45}$$

The Device Outage Model $g_j^{OFF}$ describes the behavior of the device when it is outaged and is typically straight-forward to obtain. For transmission lines, the outage model is characterized by zero currents in all terminals (open circuits) while for more complex devices, such as synchronous generators, the outage model becomes slightly more involved as the outage of a generator requires that the remaining generators change their output or that the voltage controls for a bus may change, as it transitions from PV to PQ.

Upon combination of the device models, using KCL at each node to combine each terminal's current equations, a set of system equations is obtained:

$$0 = \mathbf{g}(\mathbf{x}, \mathbf{u}) \tag{46}$$

### 6.3.2. Margin Index Method

Suppose a feasible operating point is characterized by the power flow equations (46) and a set of operational constraints:

$$\bar{\mathbf{h}} \geq \mathbf{h}(\mathbf{x},\mathbf{u}) \tag{47}$$

Suppose the system is operating at a pre-contingency solution defined by $(\mathbf{x}_0, \mathbf{u}_0)$ that satisfies (46) and (47). In order to define an aggregate performance index suitable for quantifying the likelihood of constraint violations at a given operating point, we define the following margin index:

$$J = \sum_{j=1}^{N_h} w_j \max\left(\bar{h}_j - h_j(\mathbf{x},\mathbf{u}), 0\right) \tag{48}$$

The first step is elimination of the max function from (48) by introducing auxiliary variables $\mathbf{s}, \mathbf{y}, \mathbf{t}$ for each constraint:

$$\begin{aligned} 0 &= s_j - \left[\bar{h}_j - h_j(\mathbf{x},\mathbf{u})\right] \\ 0 &= y_j - \left(s_j + t_j^2\right) \\ 0 &= y_j t_j \end{aligned} \tag{49}$$

This auxiliary model ensures that $y_j$ becomes zero if and only if $s_j$ is negative, otherwise $t_j$ is zero and $y_j = s_j$.

The additional equations defined at (49) are symbolized as $\mathbf{H}(\mathbf{x},\mathbf{u},\mathbf{s},\mathbf{y},\mathbf{t})$. We refer to $\mathbf{s}, \mathbf{y}, \mathbf{t}$ collectively as auxiliary variables **z.** Note that equations (49) are analytic while equation (48) is not. The margin index can now be re-written as:

$$J = f(\mathbf{z}) = \sum_{j=1}^{N_h} w_j y_j \tag{50}$$

Using a first-order approximation the resulting changes in the margin index, the following set of linear equations is obtained:

$$\Delta\mathbf{x} = -\left[\frac{\partial \mathbf{g}}{\partial \mathbf{x}}\right]^{-1} \frac{\partial \mathbf{g}}{\partial \mathbf{u}} \Delta\mathbf{u} \tag{51a}$$

$$\Delta \mathbf{z} = -\left[\frac{\partial \mathbf{H}}{\partial \mathbf{z}}\right]^{-1} \frac{\partial \mathbf{H}}{\partial \mathbf{x}} \Delta \mathbf{x} - \left[\frac{\partial \mathbf{H}}{\partial \mathbf{z}}\right]^{-1} \frac{\partial \mathbf{H}}{\partial \mathbf{u}} \Delta \mathbf{u} \tag{51b}$$

$$\Delta J = \frac{\partial f}{\partial \mathbf{z}} \Delta \mathbf{z} \tag{51c}$$

The resulting expression for the change in the performance index caused by a change in the contingency control vector is:

$$\Delta J = \left\{ \frac{\partial f}{\partial \mathbf{z}} \left( \frac{\partial \mathbf{H}}{\partial \mathbf{z}} \right)^{-1} \left[ \frac{\partial \mathbf{H}}{\partial \mathbf{x}} \left( \frac{\partial \mathbf{g}}{\partial \mathbf{x}} \right)^{-1} \frac{\partial \mathbf{g}}{\partial \mathbf{u}} - \frac{\partial \mathbf{H}}{\partial \mathbf{u}} \right] \right\} \Delta \mathbf{u} \tag{52}$$

Define the following co-state vectors:

$$\hat{\mathbf{z}}^T = \frac{\partial f}{\partial \mathbf{z}} \left( \frac{\partial \mathbf{H}}{\partial \mathbf{z}} \right)^{-1} \tag{53a}$$

$$\hat{\mathbf{x}}^T = \hat{\mathbf{z}}^T \frac{\partial \mathbf{H}}{\partial \mathbf{x}} \left( \frac{\partial \mathbf{g}}{\partial \mathbf{x}} \right)^{-1} \tag{53b}$$

Note that these vectors do not depend on the specific outage and hence can be evaluated only once, reducing computational cost. The first order estimate of the margin index change becomes:

$$\Delta J = \left( \hat{\mathbf{x}}^T \frac{\partial \mathbf{g}}{\partial \mathbf{u}} - \hat{\mathbf{z}}^T \frac{\partial \mathbf{H}}{\partial \mathbf{u}} \right) \Delta \mathbf{u} \tag{54}$$

Given the co-state vectors and the sparsity of the Jacobian matrix $\partial \mathbf{g} / \partial \mathbf{x}$ and the auxiliary equation Jacobian matrix $\partial \mathbf{H} / \partial \mathbf{z}$, the calculation of $\Delta J$ is computationally efficient with sparse operations.

The choice of constraint weights $w_j$ is important. In this paper, constraints are weighted adaptively, based on proximity of each constraint to the limit in the pre-outage operating point. Suppose that at the pre-outage operating point we have:

$$0 = \mathbf{g}(\mathbf{x}_0, \mathbf{u}_0) \tag{55a}$$

$$\bar{\mathbf{h}} \geq \mathbf{h}_0 = \mathbf{h}(\mathbf{x}_0, \mathbf{u}_0) \tag{55b}$$

A violation of constraint *j* will occur at $(\mathbf{x}, \mathbf{u})$ if the following condition holds:

$$\begin{aligned} h_j(\mathbf{x}, \mathbf{u}) - h_j(\mathbf{x}_0, \mathbf{u}_0) &\geq \bar{h}_j - h_{0,j} \\ \Rightarrow \frac{1}{\bar{h}_j - h_{0,j}} \Delta h_j &\geq 1 \end{aligned} \tag{56}$$

Note that the advantage of the above condition is the constant right hand side. Hence, the factor at the left hand side is a good heuristic weight for the "severity" of a change in constraint value, as the system moves from $(\mathbf{x}_0, \mathbf{u}_0)$ to $(\mathbf{x}, \mathbf{u})$. For this reason, the weight is selected as follows:

$$w_j = \frac{1}{\bar{h}_j - h_{0,j}} \tag{57}$$

### 6.3.3. Current Margin Index

One proposed MI is a three phase index defined as the margin between the ampacity limit of each phase of the device and the actual current flowing through that phase.

Suppose that the inequality constraints are defined as:

$$\begin{aligned} h_j(\mathbf{x}, \mathbf{u}) &= I_j^{(p)} \\ \bar{h}_j &= I_{rated,j} \end{aligned} \tag{58}$$

Note that the phase currents in (58) are functions of system voltages and hence functions of **x**. The set *L* is the set of all circuits in the system. A Margin Index that quantifies the total Current Margin Index (CMI) for the system is given, according to (50), as:

$$J_{CMI} = \sum_{j \in L} \sum_{p \in \{a,b,c\}} w_{j,p} \max(I_{rated,j} - I_j^{(p)}, 0) \tag{59}$$

Elimination of the max function is addressed as in (49).

Equation (57) defines the expression for the MI. The weights $w_{j,p}$ are chosen as in (57). Hence, they prioritize the margin variables for circuits and phases that are more heavily loaded in the base case operating point and thus are more likely to be overloaded after a contingency. According to (57), the weights would be defined as:

$$\hat{w}_{j,p} = \frac{1}{I_{rated,j} - I_{j,0}^{p}} \tag{60}$$

It is also a good idea to normalize the expression for the weights so that they sum up to 1:

$$w_{j,p} = \frac{\hat{w}_{j,p}}{\sum_{k \in L} \sum_{p' \in P} \hat{w}_{k,p'}} \tag{61}$$

### 6.3.4. Weighted Voltage Margin

To quantify voltage limit violations, we define another MI as the weighted sum of the distance of the system's bus voltages from their maximum and minimum limits. Focusing on lower limit voltage violation, the Low Voltage Margin Index (LVMI) is:

$$J_{LVMI} = \sum_{j \in B} \sum_{p \in P} w_{j,p} \frac{\max(\left|V_{jp}\right| - \underline{V}_j, 0)}{\Delta V_{band}} \tag{62}$$

The weights are chosen as:

$$w_{j,p} = \frac{\frac{1}{\left(\left|V_{jp,0}\right| - \underline{V}_j\right)}}{\sum_{j' \in B} \sum_{p' \in P} \frac{1}{\left(\left|V_{j'p',0}\right| - \underline{V}_{j'}\right)}} \tag{63}$$

The LVMI is used to rank contingencies similarly to the CMI index, with lower values signifying more critical contingencies.

### 6.3.5. Reactive Power Margin Index

Critical contingencies may be associated with violation of generators' reactive power limits. If a device providing reactive support hits its capability limit, voltage support capability in its region is reduced, and voltage-related problems may emerge. To quantify this, we introduce a MI that quantifies the weighted margin from Reactive Power Limits (Reactive Margin Index – RMI):

$$J_{RMI} = \sum_{j \in G} w_j \frac{\max(\overline{Q}_j - Q_j, 0)}{\overline{S}_{g,j}} \tag{64}$$

The weights are chosen as:

$$w_j = \frac{S_{g,j}}{\overline{Q}_j - Q_{j,0}} \tag{65}$$

Of course, the weights are normalized, similarly to the CMI weights (63).

## 6.4. Multi-Criterion (MI) Contingency Selection

It is evident that the proposed criteria must be combined in a single ranking algorithm, given that they are heterogeneous in nature. Another complication is that a disproportionate amount of critical outages may be of a certain kind. Hence, an algorithm that assigns more weight to the corresponding criterion in the selection process should be defined.

The algorithm starts from the first criterion and successively performs full power flow analysis in the top ranked outages. If the outage is critical, it is considered a "hit" and the same criterion is used, proceeding to its next ranked outage. However, if *S* successive "misses" are recorded, the algorithm switches criteria, moving to the next. At the same time, the multi-criterion ranking list *rnk* is maintained. An outage is added in *rnk* only if it

has not been examined by another criterion before. The algorithm terminates after $K$ consecutive misses for all criteria.

This algorithm, using criterion switch, allows criteria with a high number of critical contingencies to remain active and be used for more checks. Thus, they are implicitly assigned more weight in the contingency selection.

Notice that the maximum number of allowed "misses" and the number of misses for criterion switch are algorithmic parameters and they affect the performance of the algorithm. A pseudocode for the algorithm is given in Figure 6.2 and a visualization of algorithm execution is shown in Figure 6.3.

**Input**: $K$, $S$
**Data**: $N$,$M$, Ranking list from each contingency $j$: $r_{i,j}$
**Output**: Multi-Criterion Ranking $rnk_i \; \forall i \in 1,\ldots,N$
// Initializations
$k \leftarrow 0$ , $Ind \leftarrow (1,1,1)$ , $j \leftarrow 1$, $n \leftarrow 1$
$TotalErr \leftarrow 0$ , $Err \leftarrow (0,0,0)$
// Multi - Criterion Ranking
**while** $k < K$ **do**
  $Outage \leftarrow r_{Ind(j),j}$ ; // Get next ranked outage for criterion $j$
  $Ind(j) \leftarrow Ind(j) + 1$
  Perform full power flow analysis of $Outage$
  // Check Outage Criticality
  **if** *Outage is not critical* **then**
    $Err(j) \leftarrow Err(j) + 1$
    $TotalErr \leftarrow TotalErr + 1$
    $k \leftarrow k + 1$
  **else**
    $Err(j) \leftarrow 0$
    $k \leftarrow 0$
  **end**
  // Criterion switch - if needed
  **if** $Err(j) == S$ **then**
    $Err(j) \leftarrow 0$
    $j \leftarrow mod(j, M) + 1$
  **end**
  // Update Ranking List $rnk$
  **if** *Outage is not already in* $rnk$ **then**
    $rnk_n \leftarrow Outage$
    $n \leftarrow n + 1$
  **end**
**end**

**Figure 6.2: Pseudocode for Multi-Criterion Contingency Selection**

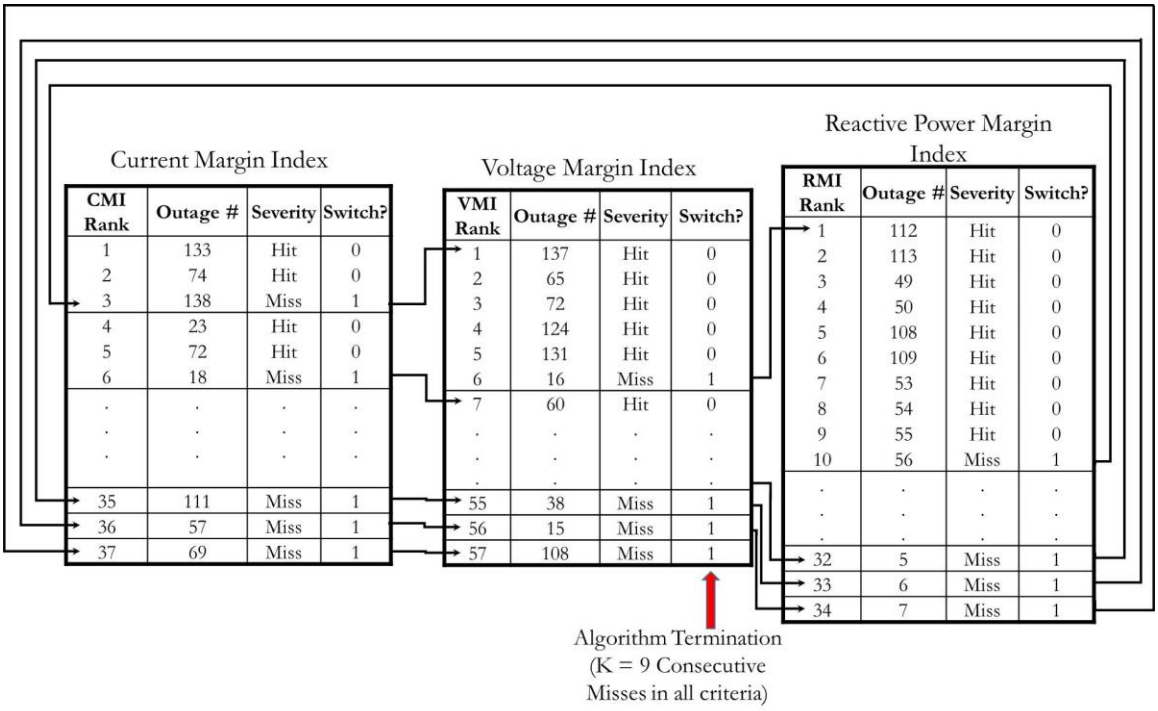


**Figure 6.3: Visualization of Contingency Ranking algorithm (S = 1, K = 9)**

## 6.5. Sensitivity – Based Contingency Selection

While contingency ranking based on Margin Performance Indices is characterized by increased computational speed, it could generate miss-rankings. The reason for the missed cases is that each contingency's criticality is evaluated based on a system-wide index. Another approach to address this issue would be to develop a sensitivity-based framework to examine the effects of each outage on each individual constraint.

The approach is based on obtaining the first order estimate for the post contingency state vector. An accurate first order approximation to the contingency selection problem would involve performing a power flow iteration on the post – contingency system, using the pre-contingency operating state as the initial guess. After a post-contingency state estimate is obtained, one can use appropriate metrics to rank the severity of each outage.

Suppose each device $j$ is modeled by its DSM model (44). Also, suppose that the connectivity mapping between the local device state numbers and equations to the global state numbers and equations is given by the following set:

$$Conn_j = \{(k,m) : \text{local state } m \text{ maps to global state } k\} \tag{66}$$

Then the $N_s \times m_j$ matrix $N_j$ is defined, whose element in the $k$-th row and $m$-th column is given as:

$$N_{km} = \begin{cases} 1, & (k,m) \in S_j \\ 0, & \text{otherwise} \end{cases} \tag{67}$$

Also define the following $m_j \times m_j$ matrix for each outage:

$$\delta A^{(j-)} = -\left.\frac{\partial g_j^{ON}}{\partial \mathbf{x}_j}\right|_{\mathbf{x}_0,\mathbf{u}_0} + \left.\frac{\partial g_j^{OFF}}{\partial \mathbf{x}_j}\right|_{\mathbf{x}_0,\mathbf{u}_0} \tag{68}$$

One can readily define the effect of outage of device $j$ in the system's Jacobian as a low rank modification of the original Jacobian:

$$\left.\frac{\partial \mathbf{g}}{\partial \mathbf{x}}\right|_{\mathbf{x}_0,\mathbf{u}_0^{(j-)}} = \left.\frac{\partial \mathbf{g}}{\partial \mathbf{x}}\right|_{\mathbf{x}_0,\mathbf{u}_0} + N_j \delta A^{(j-)} N_j^T \tag{69}$$

Where $u^{(j-)}$ is $u_0$ with device $j$ removed.

This modified version of the Jacobian matrix is used to obtain a single Newton iterate of the post-contingency power flow:

$$\hat{\mathbf{x}}^{(j-)} = \mathbf{x}_0 - \left[\left.\frac{\partial \mathbf{g}}{\partial \mathbf{x}}\right|_{\mathbf{x}_0,\mathbf{u}^{(j-)}}\right]^{-1} \mathbf{g}(\mathbf{x}_0, \mathbf{u}^{(j-)}) \tag{70}$$

Thus, a single iteration estimate $\hat{\mathbf{x}}^{(j-)}$ is evaluated for each contingency $j$. Subsequently, the margin index is evaluated by directly evaluating margins from constraint violation at this point:

$$J_{sens} = \min_j \left[ \bar{h}_j - h_j(\hat{\mathbf{x}}^{(j-)}, \mathbf{u}^{(j-)}) \right] \tag{71}$$

Note that the computation of $\hat{\mathbf{x}}^{(j-)}$ involves the solution of a linear system that represents a low-rank modification of the linear system Jacobian (69). Hence, compensation methods can be used to speed up this computation. **Compensation methods will not be covered here, but they are covered extensively in Chapter 7**. Compensation methods achieve considerable speed-up of this approach, as shown in the results section.

The physical meaning of $J_{sens}$ depends on the nature of the monitored inequality constraints $\mathbf{h}$. As discussed in Paragraph 6.3, circuit currents, phase voltages and generator reactive powers are of interest here. Applied to these three different types of constraints, the sensitivity criterion (71) takes one of three forms, the Current Limit Index (CLI), Voltage Limit Index (VLI) and Reactive Limit Index (RLI):

$$CLI^{(j-)} = \min_{l \in L,\, p \in P} \left[ 1 - \frac{\left| I_{l,p}(\mathbf{x}^{(j-)}) \right|}{I_{l,rated}} \right] \tag{72a}$$

$$VLI^{(j-)} = \min_{b \in B,\, p \in P} \left[ \min\left( V_{b,p}^{(j-)} - \underline{V}_b, \bar{V}_b - V_{b,p}^{(j-)} \right) \right] \tag{72b}$$

$$RLI^{(j-)} = \min_{g \in G} \left[ \min\left( Q_g^{(j-)} - \underline{Q}_g, \bar{Q}_g - Q_g^{(j-)} \right) \right] \tag{72c}$$

The multi-criterion method of Paragraph 6.4 can be applied to switch between these three criteria, if needed.

With the application of compensation methods, this approach requires a computational effort that is considerably reduced compared to full power flow analysis. As motivated in the results section, for most cases it provides an answer very close to the actual solution of the power flow equations. The reason for this accuracy level is that the quadratized power

flow method is used, which consists of linear and quadratic equation. Since this approach corresponds to one iteration of a Newton's method and the nonlinearities are at maximum quadratic, one iteration of the second order Newton's method provides a result very close to the final solution. Therefore, it is a very good predictor of critical contingencies.

## 6.6. Results

The contingency ranking methodology was applied to a three-phase model of the IEEE 72 bus reliability test system and the PEGASE 89/1354/2869 bus study cases. A three-phase model of the IEEE 72 bus system has not been proposed in the literature, but one was created by combining three versions of the breaker oriented model of the 24 Bus RTS proposed in [138].

The methods are compared with the following metrics:

$$\text{Efficiency} = 1 - \frac{\text{simulated outages}}{\text{total outages}} \tag{73a}$$

$$\text{Accuracy} = \frac{\text{critical outages}}{\text{simulated outages}} \tag{73b}$$

$$\text{Capture Ratio} = \frac{\text{critical outages identified}}{\text{total critical outages}} \tag{73c}$$

The performance of the Margin Index Contingency Ranking for the selection of the critical contingencies in this system is shown in Table 6.1

The Multi-Criteria Contingency Selection Algorithm was used with $S$ = 1 and $K$ = 9. In table 6.1, the performance of the proposed method is reported. In table 6.2 the margin index results are compared with those of the legacy PI described in [88] and also given in (43). This PI is referred to as Loading Performance Index (LPI). Table 6.1 reports the Margin Index values for each critical outage, and the result of the selection method –

whether the outage was missed or not. To compare the linearity of the LPI with the Margin Index for currents (49), a gradual outage of a given transmission line is enforced by changing $u_j$ continuously from one to zero in small incremental steps. The results are shown in Figure 6.4.

Note that the margin index is much smoother than the legacy PI index, because the margin index is defined in terms of line currents, while the legacy PI is defined in terms of apparent power with an exponent of 2 or 4.

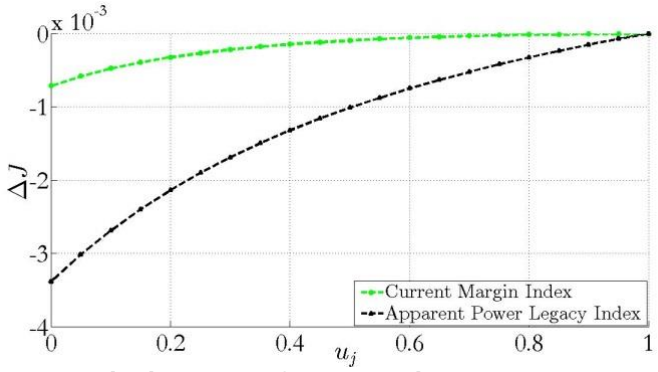


**Figure 6.4: Gradual Outage of 913-7762 in PEGASE 89 System.**

Table 6.2 reports the LPI for each critical outage, and whether a selection method utilizing exclusively the LPI would miss the outage. For the evaluation of the LPI, we assume the contingency analysis will stop after 10 consecutive successes.

**Table 6.1: Margin Index Ranking for Critical Outages – RTS 72 Bus**

| OUTAGE | CMI | LVMI | RMI | RANK | MISS? |
|---|---|---|---|---|---|
| 115 to 124 | -0.0134 | -0.0249 | -0.0138 | 2 | NO |
| 307 to 308 | -0.0028 | -0.0229 | -0.0115 | 3 | NO |
| 312 to 323 | -0.016 | -0.0216 | -0.0277 | 4 | NO |
| 107 to 108 | -0.0008 | -0.0213 | -0.0086 | 5 | NO |
| 112 to 123 | -0.0142 | -0.0213 | -0.0235 | 6 | NO |
| Gen-1, 302 | -0.0006 | -0.0051 | -0.0433 | 8 | NO |
| Gen-2, 302 | -0.0006 | -0.0051 | -0.0433 | 9 | NO |
| Gen – 1,201 | -0.0006 | -0.0046 | -0.0416 | 10 | NO |
| Gen-2, 201 | -0.0006 | -0.0044 | -0.0416 | 11 | NO |
| Gen-1, 301 | -0.0001 | -0.0048 | -0.0399 | 12 | NO |
| Gen-2, 301 | -0.0001 | -0.0048 | -0.0399 | 13 | NO |
| Gen-1, 202 | -0.001 | -0.0047 | -0.0312 | 14 | NO |
| Gen-2, 202 | -0.001 | -0.0047 | -0.0312 | 15 | NO |
| 302 to 304 | -0.0014 | -0.0197 | 0.01 | 9 | NO |
| 315 to 324 | -0.0101 | -0.0188 | -0.0131 | 18 | NO |
| 202 to 204 | -0.0014 | -0.0183 | 0.0093 | 19 | NO |
| 215 to 224 | -0.0094 | -0.018 | -0.0128 | 20 | NO |
| 207 to 208 | -0.0041 | -0.0169 | -0.0111 | 21 | NO |
| Tfmr 103-124 | -0.0022 | -0.0139 | -0.0112 | 26 | NO |
| 102-104 | -0.0005 | -0.0122 | 0.0021 | 34 | NO |
| 301-305 | -0.0022 | -0.0117 | 0.0053 | 40 | NO |
| 313-323 | -0.0118 | -0.0076 | -0.0163 | 49 | NO |
| 311-313 | -0.0057 | -0.0107 | -0.0085 | 53 | NO |
| 201-205 | -0.002 | -0.0108 | 0.0053 | 58 | NO |
| 113-123 | -0.0108 | -0.0079 | -0.0144 | 59 | NO |
| 113-215 | -0.0057 | -0.0044 | -0.0099 | | YES |
| 111-113 | -0.0043 | -0.0099 | -0.0069 | | YES |
| Tfmr 303-324 | -0.0005 | -0.0099 | -0.011 | | YES |
| Tfmr 203-224 | 0.0001 | -0.0098 | -0.0109 | | YES |
| 116-119 | -0.002 | -0.0001 | -0.0024 | | YES |

**Table 6.2: Comparison of Margin Index Ranking with Loading PI**

| OUTAGE | LPI | RANK | MISS? | MI MISS? |
|---|---|---|---|---|
| 312 - 323 | 9.4036 | 3 | NO | NO |
| 112 - 123 | 8.6158 | 4 | NO | NO |
| 313 - 323 | 6.6939 | 14 | NO | NO |
| 113 - 123 | 6.2927 | 15 | NO | NO |
| 115 - 124 | 6.2693 | 16 | NO | NO |
| 315 - 324 | 4.9905 | 19 | NO | NO |
| 215 - 224 | 4.2938 | 21 | NO | NO |
| 113 - 215 | 3.291 | 26 | NO | YES |
| 311 - 313 | 2.8302 | 29 | NO | NO |
| 207 - 208 | 2.2006 | 34 | NO | NO |
| 111 - 113 | 2.15 | 36 | NO | YES |
| 107 - 108 | 1.7319 | 43 | NO | NO |
| 307 - 308 | 1.7248 | 44 | NO | NO |
| Tfmr 103 - 124 | 1.5108 | 46 | NO | NO |
| 116 - 119 | 0.7779 | 63 | YES | YES |
| Tfmr 303 - 324 | 0.6876 | 65 | YES | YES |
| Gen-1, 202 | 0.4909 | 73 | YES | NO |
| Gen-2, 202 | 0.4909 | 73 | YES | NO |
| 301 - 305 | 0.3976 | 78 | YES | NO |
| Gen 1, 201 | 0.3895 | 79 | YES | NO |
| Gen 2, 201 | 0.3877 | 80 | YES | NO |
| 201 - 205 | 0.3137 | 81 | YES | NO |
| Gen 1, 302 | 0.2668 | 88 | YES | NO |
| Gen 2, 302 | 0.2668 | 88 | YES | NO |
| 302 - 304 | 0.2522 | 90 | YES | NO |
| 102 - 104 | 0.2339 | 91 | YES | NO |
| 202 - 204 | 0.2276 | 93 | YES | NO |
| Tfmr, 203 - 224 | 0.2238 | 95 | YES | YES |
| Gen 1, 301 | 0.116 | 109 | YES | NO |
| Gen 2, 302 | 0.116 | 109 | YES | NO |

**Table 6.3. Sensitivity Method Ranking for Critical Outages – RTS 72 Bus**

| OUTAGE | CLI | VLI | RLI | RANK | MISS? |
|---|---|---|---|---|---|
| Tfmr 103-124 | -0.1754 | -0.0381 | 0.0787 | 1 | NO |
| 115-124 | -0.1752 | -0.0389 | 0.075 | 2 | NO |
| 313-323 | -0.0852 | 0.0238 | 0.2158 | 3 | NO |
| 315-324 | -0.0756 | -0.0043 | 0.1087 | 5 | NO |
| Tfmr 303-324 | -0.075 | -0.0037 | 0.1112 | 7 | NO |
| 112-123 | -0.0629 | 0.0186 | 0.2146 | 8 | NO |
| 312-323 | -0.0622 | 0.0184 | 0.1761 | 9 | NO |
| 113-123 | -0.0584 | 0.0225 | 0.2142 | 10 | NO |
| 111-113 | -0.0402 | 0.0207 | 0.2166 | 12 | NO |
| 207-208 | -0.0387 | -0.032 | 0.0045 | 13 | NO |
| 116-119 | -0.0295 | 0.0233 | 0.2187 | 14 | NO |
| 311-313 | -0.0077 | 0.0184 | 0.2169 | 15 | NO |
| 113-215 | -0.0076 | 0.0232 | 0.2024 | 16 | NO |
| 107-108 | 0.0146 | -0.0573 | 0.1794 | 18 | NO |
| 307-308 | 0.0164 | -0.048 | -1.5787 | 20 | NO |
| 302-304 | 0.0759 | -0.0357 | 0.2174 | 23 | NO |
| 202-204 | 0.0759 | -0.0318 | 0.2831 | 24 | NO |
| 301-305 | 0.0773 | -0.0123 | 0.2183 | 25 | NO |
| 102-104 | 0.0728 | -0.0107 | 0.2169 | 26 | NO |
| 201-205 | 0.0782 | -0.0096 | 0.2829 | 27 | NO |
| 215-224 | 0.0606 | -0.0046 | 0.0104 | 28 | NO |
| Tfmr 203-224 | 0.0609 | -0.0041 | 0.0128 | 29 | NO |
| Gen - 1, 302 | 0.0665 | 0.025 | -0.2228 | 32 | NO |
| Gen - 2, 302 | 0.0665 | 0.025 | -0.2228 | 33 | NO |
| Gen - 2, 201 | 0.0982 | 0.0246 | -0.1487 | 34 | NO |
| Gen - 1, 201 | 0.0982 | 0.0246 | -0.1487 | 35 | NO |
| Gen - 1, 301 | 0.0671 | 0.025 | -0.1434 | 36 | NO |
| Gen - 2, 301 | 0.0671 | 0.025 | -0.1434 | 37 | NO |
| Gen - 1, 202 | 0.0983 | 0.0239 | -0.1362 | 38 | NO |
| Gen - 2, 202 | 0.0983 | 0.0239 | -0.1362 | 39 | NO |

In the proposed margin-based approach, 68 out of 221 contingencies are fully analyzed yielding an efficiency of 69.23%. The accuracy is 36.76%, since 25 out of 68 examined outages are critical. The capture ratio is 83.33% since 25 out of 30 critical contingencies were captured. Hence, the majority of the critical outages are uncovered by examining less than one third of the contingencies.

On the other hand, the traditional LPI method required 56 full AC power flow solutions out of 221 possible outages, yielding an efficiency of 74.67%. The accuracy is 25%, since 14 of 56 examined outages are critical, and the capture ratio is 46.7%. This

result indicates the superiority of the multi-criterion, margin-index method outlined in this work over traditional PI methods. With a small decrease in efficiency, better accuracy and capture ratio was recorded. Table 6.3 shows the performance of the sensitivity method in ranking critical contingencies. In this case the multi-criterion contingency ranking algorithm was used with $S = 3$ and $K = 6$. The accuracy of the sensitivity method is 66.7% (30 critical out of 45 examined were critical). The capture ratio is 100%, with an efficiency of 79.64%.

The performance of the sensitivity method in achieving high capture ratios can be explained using the convergence properties of the Quadratized Power Flow used for our implementation. To demonstrate this, we utilize the 72 bus RTS as a case study, and plot the histograms of the per unit current errors in the most heavily loaded conductor, for various iterations of the Quadratized Power Flow, defined as:

$$e_{i,k} = \frac{\left\| I^{k}_{j^*,p^*} - I_{j^*,p^*} \right\|}{I^{rated}_{j^*,p^*}} \tag{74}$$

Where $e_{i,k}$ is the per unit current error for outage *i* at iteration *k*, $I_{j^*,p^*}$ is the true value of the current through the most heavily loaded line conductor (line $j^*$ and phase $p^*$), and $I^{k}_{j^*,p^*}$ is its estimated value at the *k-th* iteration.

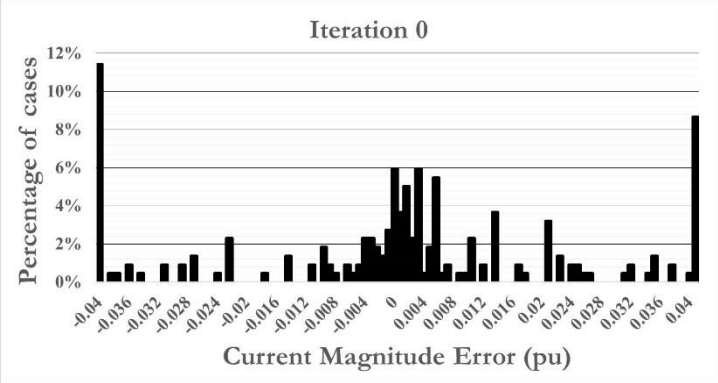

(a)

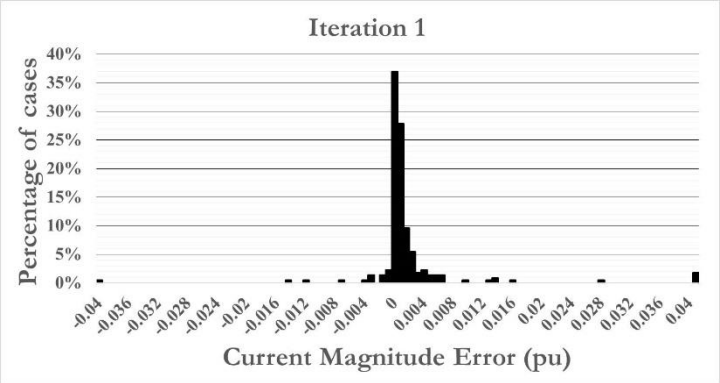


(b)

**Figure 6.5. Histogram of Current error at most heavily loaded conductor per iteration number (a) Error at initialization (b) Error after single iteration**

From Figure 6.5, it is clear that, with a single iteration, the quantity of interest (the current in the most heavily loaded conductor) can be estimated with high degree of accuracy. Namely, for 96.28% of outages, the single iteration estimate of the most heavily loaded conductor has an error less than 1% and for 98.61% of outages, the error is less than 1.5%.

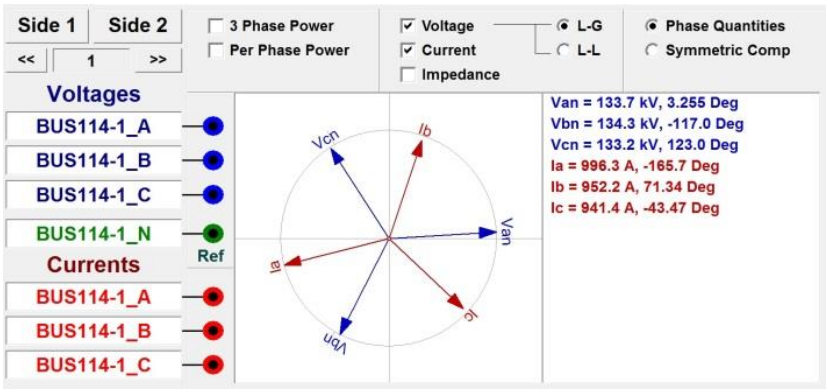


(a)

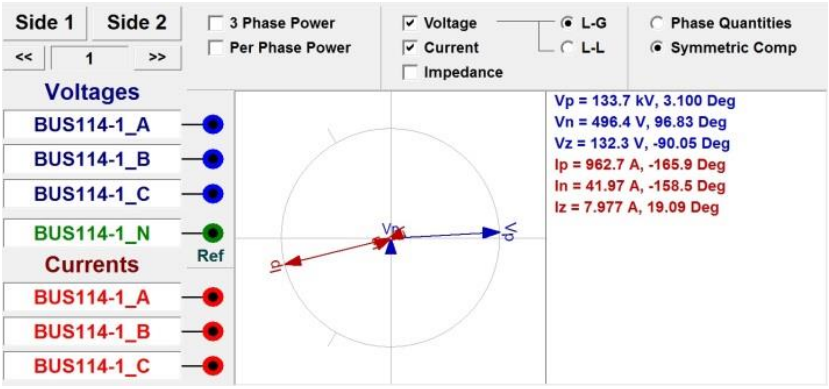


(b)

**Figure 6.6. Voltage and Current in Circuit 114-116 after the outage of circuit 116-119 (a) Phase Voltage and Current (b) Sequence Voltages and Currents**

These results also highlight the utility of unbalanced security analysis. For this system, several critical outages, such as the outage of line 112-123 and 116-119 would not be identified by a positive sequence solver even if a full power flow was solved. For example, outage of line 116-119 causes an overcurrent of 996.3A in phase A of 114-116, with a limit of 970 A. However, the positive sequence current is 962.7A, which is below the limit, even though the current imbalance does not exceed 5%. These results are shown with a snapshot from the simulator software in Figure 6.6.

A detailed summary of the performance of both methods in the PEGASE 1354 bus case study is presented in Table 6.4 and Table 6.5. It should be stressed that islanding outages are removed from consideration, resulting in 1430 considered outages, with 108 critical indicates that over 75% of outages can be filtered with a capture ratio of roughly 88%. As *K* increases, filtering performance – as measured by efficiency – deteriorates, while the capture ratio increases.

**Table 6.4: PEGASE 1354 – Margin Index Method Performance**

| K | POWER FLOWS | CRITICAL FOUND | EFFICIENCY | ACCURACY | CAPTURE RATIO |
|---|---|---|---|---|---|
| 4 | 60 | 39 | 0.9580 | 0.65 | 0.3611 |
| 8 | 100 | 55 | 0.9301 | 0.55 | 0.5093 |
| 12 | 104 | 55 | 0.9273 | 0.5288 | 0.5093 |
| 16 | 108 | 55 | 0.9245 | 0.5093 | 0.5093 |
| 20 | 211 | 79 | 0.8524 | 0.3744 | 0.7315 |
| 25 | 332 | 95 | 0.7678 | 0.2861 | 0.8796 |
| 30 | 408 | 101 | 0.7147 | 0.2475 | 0.9352 |
| 35 | 413 | 101 | 0.7112 | 0.2446 | 0.9352 |
| 50 | 502 | 103 | 0.6490 | 0.2052 | 0.9537 |

**Table 6.5: PEGASE 1354 – State Sensitivity Method Performance**

| K | POWER FLOWS | CRITICAL FOUND | EFFICIENCY | ACCURACY | CAPTURE RATIO |
|---|---|---|---|---|---|
| 1 | 66 | 65 | 0.9538 | 0.9848 | 0.6019 |
| 2 | 107 | 104 | 0.9252 | 0.9720 | 0.9630 |
| 10 | 115 | 104 | 0.9196 | 0.9043 | 0.9630 |
| 20 | 151 | 107 | 0.8944 | 0.7086 | 0.9907 |
| 50 | 181 | 107 | 0.8734 | 0.5912 | 0.9907 |
| 80 | 320 | 108 | 0.7762 | 0.3375 | 1.0000 |

The corresponding results for the larger, 2869 bus, PEGASE system are shown in Table 6.6 and Table 6.7. With 74.55% efficiency, a 87.74% of the 3804 critical non-islanding outages can be captured. The state sensitivity method performs very well. One of the outages is miss-ranked and a decrease in efficiency must be tolerated to get a 100% capture ratio.

The corresponding results for the larger, 2869 bus, PEGASE system are shown in Table 6.6 and Table 6.7. With 74.55% efficiency, a 87.74% of the 3804 critical non-islanding outages can be captured. The state sensitivity method performs very well. One of the outages is miss-ranked and a decrease in efficiency must be tolerated to get a 100% capture ratio.

**Table 6.6: PEGASE 2869 – Margin Index Method Performance**

| K | VISITED | CRITICAL FOUND | EFFICIENCY | ACCURACY | CAPTURE RATIO |
|---|---|---|---|---|---|
| 8 | 151 | 88 | 0.9603 | 0.5828 | 0.5677 |
| 12 | 155 | 88 | 0.9593 | 0.5677 | 0.5677 |
| 16 | 258 | 107 | 0.9322 | 0.4147 | 0.6903 |
| 20 | 359 | 116 | 0.9056 | 0.3231 | 0.7484 |
| 30 | 433 | 124 | 0.8862 | 0.2864 | 0.8000 |
| 40 | 443 | 124 | 0.8835 | 0.2799 | 0.8000 |
| 50 | 453 | 124 | 0.8809 | 0.2737 | 0.8000 |
| 80 | 968 | 136 | 0.7455 | 0.1405 | 0.8774 |

A summary of execution times for systems of various system cases is provided in Table 6.8. The margin index method is a very fast filtering approach, exhibiting low computational cost even for large systems. The state sensitivity approach coupled with the compensation method is slower, but achieves great time savings compared to a full N-1 analysis. The results were obtained with a modest 2GHz Intel i7 processor 4510.

**Table 6.7: PEGASE 2869 – Sensitivity Method Performance**

| K | POWER FLOWS | CRITICAL FOUND | EFFICIENCY | ACCURACY | CAPTURE RATIO |
|---|---|---|---|---|---|
| 1 | 147 | 146 | 0.9614 | 0.9932 | 0.9419 |
| 2 | 157 | 154 | 0.9587 | 0.9809 | 0.9935 |
| 3 | 160 | 154 | 0.9579 | 0.9625 | 0.9935 |
| 100 | 255 | 154 | 0.9330 | 0.6039 | 0.9935 |
| 500 | 655 | 154 | 0.8278 | 0.2351 | 0.9935 |
| 750 | 1509 | 155 | 0.6033 | 0.1027 | 1.0000 |

**Table 6.8: Execution Times for different methods & systems**

| | | Execution Times (seconds) | | |
|---|---|---|---|---|
| Case Name | Total Outages | Margin Index | State Sensitivity | Full Analysis |
| IEEE 24 bus | 37 | 0.0074 | 0.0537 | 0.3832 |
| PEGASE 89 | 194 | 0.0422 | 0.3486 | 3.5791 |
| PEGASE 1354 | 1430 | 0.4518 | 15.9726 | 493.7839 |
| PEGASE 2869 | 3804 | 1.0890 | 47.1750 | 1973.5944 |

Table 6.8 highlights the need for a fast contingency filter, especially within the context of a computationally demanding framework, such as the security constrained AC-OPF. For the larger system examined, the PEGASE 2869, a full power flow analysis costs 1973 seconds. Parallelization will improve speed, but in real life systems, with a realistic set of millions of credible contingencies, it is clear that parallelization is limited by the number of cores in the computing hardware.

# Chapter 7. Compensation Methods for Contingency Analysis

## 7.1. Nomenclature

| | |
|---|---|
| $N$ | Dimension of system state variable vector |
| $D$ | Number of devices connected to the system |
| $\mathbf{X}^*$ | Optimal Multi-Step State Vector |
| $\mathbf{U}^*$ | Optimal Multi-Step Control Vector |
| $\mathbf{X}_k^*$ | Optimal State Vector at step $k$ |
| $\mathbf{U}_k^*$ | Optimal Control Vector at step $k$ |
| $\mathbf{g}_d$ | Algebraic Equations of device $d$ in operational mode |
| $\mathbf{g}_d^{off}$ | Algebraic Equations of device $d$ in outaged mode |
| $\mathbf{g}_d^*$ | Algebraic Equations of device $d$ for previous state vectors and current state controls fixed to the optimal values |
| $s_d$ | A variable equal to 1 if the device is ON and 0 if it is OFF |
| $n_d$ | Dimension of device $d$ state variable vector |
| $N_d$ | Device $d$ connectivity matrix |

| | |
|---|---|
| $\mathbf{g}^*(\mathbf{X}\mid\mathbf{P}_k)$ | System equality constraint expressions at step *k* with the previous step states and controls, as well as the current step controls fixed at optimal values |
| $\mathbf{g}^*_{(d-)}(\mathbf{X}\mid\mathbf{P}_k)$ | System equality constraint expressions at step *k* with the previous step states and controls, as well as the current step controls fixed at optimal values, **with device *d* removed from the system** |
| $\tilde{\mathbf{X}}^k_{d-}$ | First order estimate of system state vector after the outage of device *d* at step *k* |
| $S_d$ | Device *d* sensitivity matrix |
| $\left.\frac{\partial \mathbf{g}^*(\mathbf{X}\mid\mathbf{P}_k)}{\partial \mathbf{X}}\right\|_{\mathbf{X}^*,\mathbf{U}^*} = J$ | Jacobian matrix of single-step equality constraints, evaluated at the optimal point |
| $\left.\frac{\partial \mathbf{g}^*_{(d-)}(\mathbf{X}\mid\mathbf{P}_k)}{\partial \mathbf{X}}\right\|_{\mathbf{X}^*,\mathbf{U}^*} = J_{d-}$ | Jacobian matrix of single-step equality constraints, evaluated at the optimal point, after the removal of device *d* from the system |
| $B_J$ | Matrix of LU factors of *J*, including any permutations and fill-in reduction re-orderings |
| $\mathbf{h}^*_{c-}$ | Vector of inequality constraint expressions, evaluated at the optimal solution & disregarding all inequality constraints of devices $d \in c$ |

## 7.2. Introduction

The sensitivity method proposed in the previous chapter relied on a single iteration of the Newton method which was obtained using the updated post-outage Jacobian. It was mentioned that this approach has significant advantages in terms of accuracy and speed. However, while compensation methods where mentioned, they were not covered in detail in Chapter 6. In this Chapter, we formulate the theoretical basis for the application of the

compensation method to contingency analysis. Our emphasis is on theoretical justification of the expected speedup from the compensation method, as well as the timing results for various systems. Furthermore, a low-cost necessary & sufficient condition for post-outage Jacobian singularity is also obtained. Using this condition islanding outages, i.e. outages that disconnect the network's graph, can be identified and removed from the analysis, since a valid load flow solution cannot be obtained for these cases. This results in a complete *N*-1 compensation-based contingency analysis framework, which is eventually extended to a generalized *N-k* multi-device framework. The results are verified in a group of standard test cases, ranging from small sample systems, to the realistic PEGASE 9000+ bus case study.

## 7.3. Contingency Analysis based on sensitivity factors

The multi-step optimization problem without security constraints is given in (75):

$$\begin{aligned} &\min_{\mathbf{X},\mathbf{U}} \sum_{k=1}^{K} c(\mathbf{X}_k, \mathbf{U}_k) \\ &\text{subject to} \\ &\mathbf{g}(\mathbf{X}_{k-1}, \mathbf{U}_{k-1}, \mathbf{X}_k, \mathbf{U}_k \mid \mathbf{P}_k) = 0 \quad k = 1,2,\ldots,K \\ &\mathbf{h}(\mathbf{X}_{k-1}, \mathbf{U}_{k-1}, \mathbf{X}_k, \mathbf{U}_k \mid \mathbf{P}_k) \le 0 \quad k = 1,2,...,K \\ &\mathbf{U}_{\min} \le \mathbf{U}_k \le \mathbf{U}_{\max} \quad k = 1,2,...,K \\ &\mathbf{X}_{\min} \le \mathbf{X}_k \le \mathbf{X}_{\max} \quad k = 1,2,...,K \\ &\mathbf{X}_0 = \mathbf{X}_{init} \\ &\mathbf{U}_0 = \mathbf{U}_{init} \end{aligned} \tag{75}$$

At each step *k* of the multi-step Optimal Power Flow, the set of algebraic constraints $g(\cdot)$ is enforced.

$$\mathbf{g}(\mathbf{X}_{k-1}^{*}, \mathbf{U}_{k-1}^{*}, \mathbf{X}_k^{*}, \mathbf{U}_k^{*} \mid \mathbf{P}_k) = \mathbf{0} \tag{76}$$

However, given $\mathbf{X}_{k-1}$, $\mathbf{U}_{k-1}$ and $\mathbf{U}_k$ the system state $\mathbf{X}_k$ yields a solution to the algebraic constraints *only under the nominal configuration of the system*, i.e. with all devices operational. If any combination of devices is outaged, the system state at step *k* will change. In the remaining of this text it is assumed that the control vector at step *k*, as well as the previous step(s) decisions and controls are fixed to the value yielded by the optimization problem solution.

The security analysis problem consists of identifying the set of critical outages at every step *k*, i.e. the set of outages that will cause a post-outage system state vector $\mathbf{X}$ that violates any controls at step *k*, we are implicitly assuming that the system does not have the capability to perform an emergency re-dispatch – i.e. to adjust its control variables – after the outage occurs.

The algebraic equations of device *d* at step *k*, for a given (optimal) choice of previous step decisions and current step controls, are given as:

$$\begin{bmatrix} \mathbf{i}_k \\ \mathbf{0} \end{bmatrix} = \mathbf{g}_d(\mathbf{x}^*_{k-1}, \mathbf{u}^*_{k-1}, \mathbf{x}_k, \mathbf{u}^*_k \mid \mathbf{p}_k) \tag{77}$$

In order to model the effect of a device outage in the system, we modify (77) to include both the *operational* and the *outaged* model of the device:

$$\begin{bmatrix} \mathbf{i}_k \\ \mathbf{0} \end{bmatrix} = \mathbf{g}^*_d(\mathbf{x}_k \mid \mathbf{p}_k) = s_d \mathbf{g}_d(\mathbf{x}^*_{k-1}, \mathbf{u}^*_{k-1}, \mathbf{x}_k, \mathbf{u}^*_k \mid \mathbf{p}_k) + (1 - s_d)\mathbf{g}^{off}_d(\mathbf{x}^*_{k-1}, \mathbf{u}^*_{k-1}, \mathbf{x}_k, \mathbf{u}^*_k \mid \mathbf{p}_k) \tag{78}$$

Where $\mathbf{g}^{off}_d$ is the set of device equations when the device is off (outage mode) and $s_d$ is a variable taking the value of zero if the device is outaged and one if it is operational.

In order to map the effect of device outages in the system equations, the device connectivity matrix $N_d \in M_{N \times n_d}$ needs to be defined. Specifically, $N_d = [\nu_{ij}]$, where

$$v_{ij}^{d} = \begin{cases} 1 & \text{if local device state } x^{j} \text{ maps to global state } X^{\mathrm{i}} \\ 0 & \text{otherwise} \end{cases} \tag{79}$$

Note that we make the implicit assumption that the mapping between the states of device *d* and the global states is identical to the mapping between local device equation numbers and global equation numbers. Hence, the matrix $N_d$ can be used to map local states & equations to their global equivalents.

The system's algebraic equations are synthesized by enforcing the internal algebraic constraints for each device – i.e. the expressions with a zero on the left hand side in (78) – and enforcing Kirchhoff's Current Law by equating the summation of currents corresponding to the same node to zero –i.e. the expressions with **I** on the left hand side in (78). Given the definition of $N_d$, the algebraic constraints at step *k* can be written as:

$$0 = \mathbf{g}^{*}(\mathbf{X}_k \mid \mathbf{P}_k) = \sum_{d=1}^{D} N_d \mathbf{g}_d^{*}(N_d^T \mathbf{X}_k \mid \mathbf{p}_k) \tag{80}$$

This formulation of the system's equality constraints as a summation of the algebraic expressions of all of the system's devices is referred to as *device oriented system equations* expressions and it proves very useful in contingency analysis.

Contingency analysis requires the solution to (80) after device *d* is outaged. Instead of obtaining the exact solution, which would require solving the nonlinear system of equations, a *sensitivity method* can be formulated. The system equations after the outage of device *d* can be obtained considering that, during the outage, the device transitions from its operational model to its outaged model, according to (78). In mathematical terms:

$$0 = \mathbf{g}^*_{(d-)}(\mathbf{X}_k \mid \mathbf{P}_k) = \mathbf{g}^*(\mathbf{X}_k \mid \mathbf{P}_k) - N_d \mathbf{g}^*_d(N_d^T \mathbf{X}_k \mid \mathbf{p}_k)$$
$$= \mathbf{g}^*(\mathbf{X}_k \mid \mathbf{P}_k) \tag{81}$$
$$- N_d \left[ s_d \mathbf{g}_d(\mathbf{x}^*_{k-1}, \mathbf{u}^*_{k-1}, N_d^T \mathbf{X}_k, \mathbf{u}^*_k \mid \mathbf{p}_k) + (1 - s_d)\mathbf{g}_d^{off}(\mathbf{x}^*_{k-1}, \mathbf{u}^*_{k-1}, N_d^T \mathbf{X}_k, \mathbf{u}^*_k \mid \mathbf{p}_k) \right]$$

A first-order Taylor expansion around the current solution $\mathbf{X}^*$ is written as follows:

$$0 = \mathbf{g}^*_{(d-)}(\mathbf{X}_k \mid \mathbf{P}_k) \cong \mathbf{g}^*_{(d-)}(\mathbf{X}^* \mid \mathbf{P}_k) + \left. \frac{\partial \mathbf{g}^*_{(d-)}}{\partial \mathbf{X}} \right|_{\mathbf{X}^*, \mathbf{U}^*} \Delta \mathbf{X} \tag{82}$$

It is worth noting a fact regarding the values of the equality constraints evaluated at the optimal solution, after the outage of device *d*. Namely, from (81) we obtain:

$$\mathbf{g}^*_{(d-)}(\mathbf{X}^*_k \mid \mathbf{P}_k) = \mathbf{g}^*(\mathbf{X}^*_k \mid \mathbf{P}_k) - N_d \mathbf{g}^*_d(N_d^T \mathbf{X}^*_k \mid \mathbf{p}_k) \tag{83}$$

However, from (76) we have:

$$\mathbf{g}^*(\mathbf{X}^*_k \mid \mathbf{P}_k) = \mathbf{0} \tag{84}$$

Hence:

$$\mathbf{g}^*_{(d-)}(\mathbf{X}^*_k \mid \mathbf{P}_k) = -N_d \mathbf{g}^*_d(N_d^T \mathbf{X}^*_k \mid \mathbf{p}_k) \tag{85}$$

This is a vector in $R^N$ which has $n_d$ nonzero elements. This vector will be henceforth referred to as $\mathbf{g}^*_{(d-)}$ in order to simplify notation. Hence, the first order estimate for the post-outage system state vector is given us:

$$\left. \frac{\partial \mathbf{g}_{(d-)}}{\partial \mathbf{X}} \right|_{\mathbf{X}^*, \mathbf{U}^*} \left( \tilde{\mathbf{X}}^k_{d-} - \mathbf{X}^*_k \right) = N_d \mathbf{g}^*_d(N_d^T \mathbf{X}^*_k \mid \mathbf{p}_k) \tag{86}$$

which leads to:

$$\tilde{\mathbf{X}}^k_{d-} = \mathbf{X}^*_k + \left[ \left. \frac{\partial \mathbf{g}^*_{d-}}{\partial \mathbf{X}} \right|_{\mathbf{X}^*, \mathbf{U}^*} \right]^{-1} N_d \mathbf{g}^*_d(N_d^T \mathbf{X}^*_k \mid \mathbf{p}_k) \tag{87}$$

Even though obtaining $\tilde{\mathbf{X}}_{d-}$ through (87) explicitly is straight-forward, it is well-known that calculating explicit inverses is not numerically efficient. However, given low-rank structure of the change in the Jacobian matrix after the removal of device *d*, expression (87) can be modified to yield a numerically efficient implementation.

**Theorem 6.1.** Suppose $\left.\frac{\partial \mathbf{g}_{(d-)}}{\partial \mathbf{X}}\right|_{\mathbf{X}^*,\mathbf{U}^*}$ is non-singular. Then, the first order estimate for the state of the system after the outage of device *d* is given by:

$$\tilde{\mathbf{X}}_{d-}^{k} = \mathbf{X}_k^* + S_d \left[ -\left( \left.\frac{\partial \mathbf{g}_d^*(\mathbf{x}_d \mid \mathbf{p}_k)}{\partial \mathbf{x}_d}\right|_{\mathbf{x}_d^*,\mathbf{u}_d^*} \right)^{-1} + N_d^T S_d \right]^{-1} \left( \left.\frac{\partial \mathbf{g}_d^*(\mathbf{x}_d \mid \mathbf{p}_k)}{\partial \mathbf{x}_d}\right|_{\mathbf{x}_d^*,\mathbf{u}_d^*} \right)^{-1} \mathbf{g}_{(d-)}^* \quad (88)$$

Where

$$S_d = \left[ \left.\frac{\partial \mathbf{g}^*(\mathbf{X} \mid \mathbf{P}_k)}{\partial \mathbf{X}}\right|_{\mathbf{X}^*,\mathbf{U}^*} \right]^{-1} N_d \quad (89)$$

*Proof.* Taking the partial derivatives with respect to ***X*** in (83), we have:

$$\left.\frac{\partial \mathbf{g}_{(d-)}^*(\mathbf{X} \mid \mathbf{P}_k)}{\partial \mathbf{X}}\right|_{\mathbf{X}^*,\mathbf{U}^*} = \left.\frac{\partial \mathbf{g}^*(\mathbf{X} \mid \mathbf{P}_k)}{\partial \mathbf{X}}\right|_{\mathbf{X}^*,\mathbf{U}^*} - N_d \left.\frac{\partial \mathbf{g}_d^*(\mathbf{x}_d \mid \mathbf{p}_k)}{\partial \mathbf{x}_d}\right|_{\mathbf{x}_d^*,\mathbf{u}_d^*} N_d^T \quad (90)$$

Hence, after the removal of device *d*, the Jacobian of the algebraic expressions $\mathbf{g}_{(d-)}^*(\mathbf{X} \mid \mathbf{P}_k)$ evaluated at the optimal state point is a low rank modification of the Jacobian of the algebraic expressions with the device operational $\mathbf{g}^*(\mathbf{X} \mid \mathbf{P}_k)$. Using the Matrix Inversion Lemma, which is given as:

$$(A + XBY)^{-1} = A^{-1} - A^{-1}X(B^{-1} + YA^{-1}X)^{-1}YA^{-1} \quad (91)$$

To simplify notation, we define the following:

$$\left.\frac{\partial \mathbf{g}^*_{(d-)}(\mathbf{X}\,|\,\mathbf{P}_k)}{\partial \mathbf{X}}\right|_{\mathbf{X}^*,\mathbf{U}^*} = J_{d-} \tag{92a}$$

$$\left.\frac{\partial \mathbf{g}^*(\mathbf{X}\,|\,\mathbf{P}_k)}{\partial \mathbf{X}}\right|_{\mathbf{X}^*,\mathbf{U}^*} = J \tag{92a}$$

Hence we have:

$$J_{d-}^{-1} = J^{-1}\left\{I - N_d\left\{-\left[\left.\frac{\partial \mathbf{g}^*_d(\mathbf{x}_d\,|\,\mathbf{p}_k)}{\partial \mathbf{x}_d}\right|_{\mathbf{x}^*_d,\mathbf{u}^*_d}\right]^{-1} + N_d^T J^{-1} N_d\right\}^{-1} N_d^T J^{-1}\right\} \tag{93}$$

By substituting (93) to (87) we have:

$$\tilde{\mathbf{X}}^k_{d-} = \mathbf{X}^*_k + J^{-1}\left\{I - N_d\left\{-\left[\left.\frac{\partial \mathbf{g}^*_d}{\partial \mathbf{x}_d}\right|_{\mathbf{x}^*_d,\mathbf{u}^*_d}\right]^{-1} + N_d^T J^{-1} N_d\right\}^{-1} N_d J^{-1}\right\} N_d^T \mathbf{g}^*_d(N_d^T \mathbf{X}^*_k\,|\,\mathbf{p}_k) \tag{94}$$

However, it is evident that:

$$\begin{aligned}&\left\{-\left[\left.\frac{\partial \mathbf{g}^*_d}{\partial \mathbf{x}_d}\right|_{\mathbf{x}^*_d,\mathbf{u}^*_d}\right]^{-1} + N_d^T J^{-1} N_d\right\}^{-1} N_d^T J^{-1} N_d \mathbf{g}^*_d(N_d^T \mathbf{X}^*_k\,|\,\mathbf{p}_k)\\ &= I - \left\{-\left[\left.\frac{\partial \mathbf{g}^*_d}{\partial \mathbf{x}_d}\right|_{\mathbf{x}^*_d,\mathbf{u}^*_d}\right]^{-1} + N_d^T J^{-1} N_d\right\}^{-1}\left[-\left.\frac{\partial \mathbf{g}^*_d}{\partial \mathbf{x}_d}\right|_{\mathbf{x}^*_d,\mathbf{u}^*_d}\right]^{-1} \mathbf{g}^*_d(N_d^T \mathbf{X}^*_k\,|\,\mathbf{p}_k)\end{aligned} \tag{95}$$

Substituting (95) to (94) we have:

$$\tilde{\mathbf{X}}^k_{d-} = \mathbf{X}^*_k + J^{-1} N_d\left\{-\left[\left.\frac{\partial \mathbf{g}^*_d}{\partial \mathbf{x}_d}\right|_{\mathbf{x}^*_d,\mathbf{u}^*_d}\right]^{-1} + N_d^T J^{-1} N_d\right\}^{-1}\left[-\left.\frac{\partial \mathbf{g}^*_d}{\partial \mathbf{x}_d}\right|_{\mathbf{x}^*_d,\mathbf{u}^*_d}\right]^{-1} \mathbf{g}^*_d(N_d^T \mathbf{X}^*_k\,|\,\mathbf{p}_k)) \tag{96}$$

Which is the required expression ■

It is worth noting that the sensitivity matrix for each device *d* is obtained by solving for an $N \times n_d$ matrix with the pre-outage Jacobian $J$ on the left hand side. The fact that the (common) sparse pre-outage Jacobian can be used to calculate the sensitivity factors for all outages means that a single factorization is required, and their computation requires less computations that brute force re-factorization of each modified post outage Jacobian $J_{d-}$ for each $d \in D$.

Due to ill-conditioning issues, it is impractical to invert $\left.\frac{\partial \mathbf{g}_d^*}{\partial \mathbf{x}_d}\right|_{\mathbf{x}_d^*, \mathbf{u}_d^*}$. For this reason, we define $\mathbf{z}_d$:

$$\begin{aligned}
\mathbf{z}_d &= \left\{ -\left[ \left.\frac{\partial \mathbf{g}_d^*}{\partial \mathbf{x}_d}\right|_{\mathbf{x}_d^*, \mathbf{u}_d^*} \right]^{-1} + N_d^T J^{-1} N_d \right\}^{-1} \left[ -\left.\frac{\partial \mathbf{g}_d^*}{\partial \mathbf{x}_d}\right|_{\mathbf{x}_d^*, \mathbf{u}_d^*} \right]^{-1} \mathbf{g}_d^*(N_d^T \mathbf{X}_k^* \,|\, \mathbf{p}_k)) \\
&\Rightarrow \left[ \left.\frac{\partial \mathbf{g}_d^*}{\partial \mathbf{x}_d}\right|_{\mathbf{x}_d^*, \mathbf{u}_d^*} \right] \left\{ \left[ \left.\frac{\partial \mathbf{g}_d^*}{\partial \mathbf{x}_d}\right|_{\mathbf{x}_d^*, \mathbf{u}_d^*} \right]^{-1} + N_d^T J^{-1} N_d \right\} \mathbf{z}_d = \mathbf{g}_d^*(N_d^T \mathbf{X}_k^* \,|\, \mathbf{p}_k)) \qquad (97) \\
&\Rightarrow \left[ I - \left.\frac{\partial \mathbf{g}_d^*}{\partial \mathbf{x}_d}\right|_{\mathbf{x}_d^*, \mathbf{u}_d^*} N_d^T J^{-1} N_d \right] \mathbf{z}_d == \mathbf{g}_d^*(N_d^T \mathbf{X}_k^* \,|\, \mathbf{p}_k))
\end{aligned}$$

The matrix in the left hand side of (97) does not have conditioning issues under a non-islanding condition (see below), and thus the preferred approach is to compute $\mathbf{z}_d$ and subsequently find the first-order estimate as:

$$\tilde{\mathbf{X}}_{d-}^k = \mathbf{X}_k^* + J^{-1} N_d \mathbf{z}_d \qquad (98)$$

### 7.3.1. Post – Outage Jacobian Singularity and Islanding Outages

The derivation of Theorem 1 is performed under the assumption that the post-outage Jacobian is non-singular, and the sensitivity matrix can be computed. Even in practical power system case studies, it often happens that this Jacobian is singular. In fact, this singularity is strongly coupled with islanding conditions, i.e. outages that cause the underlying graph of the power network to become disconnected into two (or more) components. The implications and conditions for Jacobian singularity are examined in this section.

We first prove the following rather evident fact:

**Theorem 6.2.** Suppose the pre-outage equality constraint Jacobian $J$ is non-singular. Then the post-outage system equality constraint Jacobian matrix defined in (90) is singular if and only if the following $n_d \times n_d$ matrix is singular:

$$M_d = I - \left.\frac{\partial \mathbf{g}_d^*}{\partial \mathbf{x}_d}\right|_{\mathbf{x}_d^*, \mathbf{u}_d^*} N_d^T J^{-1} N_d \tag{99}$$

*Proof.* We need to prove the if and only if statement:

a. Let us assume $J_d$ is singular. Then there exists a right eigenvector $\mathbf{u} \in R^N$ of $J_d$ such that $J_d \mathbf{u} = \mathbf{0}$. By substituting to (90) we have:

$$\begin{aligned} & J_{d\_}\mathbf{u} = J\mathbf{u} - N_d \left.\frac{\partial \mathbf{g}_d^*(\mathbf{x}_d \mid \mathbf{p}_k)}{\partial \mathbf{x}_d}\right|_{\mathbf{x}_d^*, \mathbf{u}_d^*} N_d^T \mathbf{u} = 0 \\ & \Rightarrow J\mathbf{u} = N_d \left.\frac{\partial \mathbf{g}_d^*(\mathbf{x}_d \mid \mathbf{p}_k)}{\partial \mathbf{x}_d}\right|_{\mathbf{x}_d^*, \mathbf{u}_d^*} N_d^T \mathbf{u} \end{aligned} \tag{100}$$

Now let us define the $n_d \times 1$ vector:

$$\mathbf{u}^* = \left.\frac{\partial \mathbf{g}_d^*(\mathbf{x}_d \mid \mathbf{p}_k)}{\partial \mathbf{x}_d}\right|_{\mathbf{x}_d^*, \mathbf{u}_d^*} N_d^T \mathbf{u} \tag{101}$$

By substituting (101) to (100) we have:

$$J\mathbf{u} = N_d \mathbf{u}^* \tag{102}$$

We can prove that $M_d$ is singular, with $\mathbf{u}^*$ being the right eigenvector corresponding to the zero eigenvalue. Specifically:

$$\begin{aligned} M_d \mathbf{u}^* &= \mathbf{u}^* - \left.\frac{\partial \mathbf{g}_d^*}{\partial \mathbf{x}_d}\right|_{\mathbf{x}_d^*, \mathbf{u}_d^*} N_d^T J^{-1} N_d \mathbf{u}^* \\ &= \mathbf{u}^* - \left.\frac{\partial \mathbf{g}_d^*}{\partial \mathbf{x}_d}\right|_{\mathbf{x}_d^*, \mathbf{u}_d^*} N_d^T J^{-1} J\mathbf{u} \\ &= \mathbf{u}^* - \left.\frac{\partial \mathbf{g}_d^*}{\partial \mathbf{x}_d}\right|_{\mathbf{x}_d^*, \mathbf{u}_d^*} N_d^T \mathbf{u} \\ &= \mathbf{u}^* - \mathbf{u}^* \\ &= 0 \end{aligned} \tag{103}$$

b. Singularity of $M_d$ implies singularity of $J_{d-}$ following exactly the reverse reasoning. Namely, let us assume that $M_d$ is singular, so there exists $\mathbf{u}^* \in R^{n_d}$ such that:

$$M_d \mathbf{u}^* = 0 \tag{104}$$

By substituting (104) to (99) we have:

$$\begin{aligned} 0 = M_d \mathbf{u}^* &= \mathbf{u}^* - \left.\frac{\partial \mathbf{g}_d^*}{\partial \mathbf{x}_d}\right|_{\mathbf{x}_d^*, \mathbf{u}_d^*} N_d^T J^{-1} N_d \mathbf{u}^* \\ \Rightarrow \mathbf{u}^* &= \left.\frac{\partial \mathbf{g}_d^*}{\partial \mathbf{x}_d}\right|_{\mathbf{x}_d^*, \mathbf{u}_d^*} N_d^T J^{-1} N_d \mathbf{u}^* \end{aligned} \tag{105}$$

Let us define:

$$\mathbf{u} = J^{-1} N_d \mathbf{u}^* \Rightarrow J\mathbf{u} = N_d \mathbf{u}^* \tag{106}$$

It is clear by (105) that:

$$\mathbf{u}^* = \left.\frac{\partial \mathbf{g}_d^*}{\partial \mathbf{x}_d}\right|_{\mathbf{x}_d^*, \mathbf{u}_d^*} N_d^T \mathbf{u} \tag{107}$$

Now $\mathbf{u}$ is an eigenvector of $J_{d-}$ corresponding to the zero eigenvalue:

$$\begin{aligned} J_{d-}\mathbf{u} &= J\mathbf{u} - N_d \left.\frac{\partial \mathbf{g}_d^*(\mathbf{x}_d \mid \mathbf{p}_k)}{\partial \mathbf{x}_d}\right|_{\mathbf{x}_d^*, \mathbf{u}_d^*} N_d^T \mathbf{u} \\ &= J\mathbf{u} - N_d \mathbf{u}^* \\ &= \mathbf{0} \end{aligned} \tag{108}$$

Which is the required result ■

The practical importance of this proof is that the singularity of the post-outage Jacobian, which would not permit the use of the first-order sensitivity method for this particular outage, can be efficiently checked by checking the singularity of the $n_d \times n_d$ matrix $M_d$. Hence our statement in the previous chapter that (97) can be used to implement the sensitivity method without risking running into unexpected ill-conditioning issues is valid, as long as the post-outage Jacobian itself is non-singular. This fact, however, would disallow the use of the sensitivity method for this outage. Hence, (97) can be used for all non-singularity inducing outages.

In fact, even the singularity of $M_d$ is important information. It means that the outage of device *d* can be an *islanding outage*, i.e. it disconnects the power system's graph into separate components, inducing the singularity of the post-outage Jacobian.

### 7.3.2. Computational Efficiency of Low-Rank Correction Method

In this Section, the computational advantages of using (96) to obtain first-order estimates of the post-outage state vector. It is important to note that the explicit matrix

inverses in (96) involve "low" dimension $n_d \times n_d$ matrices, which depend on the size of the *device model* and *not the size of the system's algebraic equations*. This indicates that these operations have a flat O(1) cost for constant $n_d$ and they do not scale badly with an increase in system size. In order to extract computational complexity bounds we are going to adopt the assumption that the number of nonzero elements in *n*-dimensional sparse Jacobian matrices, such as $J$ and $J_{d-}$, increases linearly with the size of the matrix:

$$J \in M_{n\times n} \Rightarrow nnz(J) = O(n) \tag{109}$$

There are no guarantees that this will hold for an arbitrary Jacobian matrix stored in sparse matrix form. In fact, one can easily define power networks for which this fact does not hold. However, *practical experience from common power network designs suggests that this assumption is relevant.* The cost of most important sparse matrix operations is given in Table 7.1 below:

**Table 7.1: Computational Complexity of Common Matrix Operations**

| MATHEMATICAL OPERATION | DESCRIPTION | WORST – CASE COMPUTATIONAL COST |
|---|---|---|
| $Bx = b, B = LU$ | Forward - Backward Substitution with factorized matrix | $O(nnz(B))$ |
| $B = LU(J)$ | LU factorization of matrix (with reordering for fill-ins) | $O(n \cdot nnz(B))$ |
| $C = A^{-1}$ | Explicit inverse of full $m \times m$ matrix | $O(m^3)$ (standard implementation) |

Let us assume that a factorization of the Jacobian at the base-case (pre-contingency optimal) point $\mathbf{X}_k^*$ is already available. This assumption is absolutely acceptable from an implementation perspective, because this matrix is normally factorized in order to solve the optimization problem. Also, let us define the factorization of that Jacobian as:

$$B_J = lu(J) \tag{110}$$

In order to obtain the first order estimate of the post-contingency state vector using the low-rank correction technique (97)-(98), with sparse matrix techniques, we need, to perform the following operations:

1. Solution of $n_d$ linear systems to obtain $S_d$, where $JS_d = N_d$ - costs $O(n_d \cdot nnz(B_J))$ operations
2. Solve for $z_d$, including factorizing the left hand side of (97)– costs $O(n_d{}^3)$ operations
3. Solve linear system $J\Delta\tilde{\mathbf{X}}_d = N_d\mathbf{z}_d$ - costs $O(nnz(B_J))$ operations
4. Perform vector addition $\tilde{\mathbf{X}}^k_{d-} = \mathbf{X}^*_k + \Delta\tilde{\mathbf{X}}_d$ - costs $O(n)$ operations

Hence, the entire procedure of obtaining $\tilde{\mathbf{X}}^k_{d-}$ costs $O(n_d \cdot nnz(B_J))$ operations. If we further assume that the number of nonzero elements of the factor matrix $B_J$ increases linearly with $n$, and noticing that $n_d$ is a given value, typically not exceeding 10-20, the cost of the algorithm can be given as $O(n)$ operations.

In order to quantify the computational advantages of the approach, we need to compare this result with the computational complexity bound of other approaches to find $\tilde{\mathbf{X}}^k_{d-}$. Here we will assume that the factor matrix of $J_{d-}$, symbolized by $B_{Jd-}$ has a number of nonzero elements of the same order as $B_J$, an assumption that is not at all restrictive, given that small corrections to $J$ are needed to obtain $J_{d-}$. The simplest, straight-forward approach to compute $\tilde{\mathbf{X}}^k_{d-}$ would be to:

1. Obtain $J_{d-}$ by (90) and re-factorize it – costs $O(n \cdot nnz(B_J))$ operations
2. Solve linear system $J_{d-}\Delta\tilde{\mathbf{X}}_d = N_d \mathbf{g}_d^*(N_d^T \mathbf{X}_k^* \mid \mathbf{p}_k)$ - costs $O(nnz(B_J))$ operations
3. Perform vector addition $\tilde{\mathbf{X}}_{d-}^k = \mathbf{X}_k^* + \Delta\tilde{\mathbf{X}}_d$ - costs $O(n)$ operations

The above approach, which does not exploit the low rank corrections to $\boldsymbol{J}$, costs $O(n \cdot nnz(B_J))$ operations which is already a higher order bound than the one for the low-rank correction approach. If we repeat the assumption that $nnz(B_J) = O(n)$, then we arrive to the conclusion that this approach costs $O(n^2)$ operations. This means that the computational cost of just solving for one device outage could scale much worse with this straight-forward algorithm, versus using the low-rank correction technique.

Finally, it is worth noting that for detailed contingency analysis, the post-outage state needs to be calculated for all devices. Such an approach would require $O(n^2)$ for the low-rank correction approach and $O(Dn^2)$ for the naïve approach, which translates to $O(n^3)$ if we assume $D = O(n)$.

### 7.3.3. Timing Statistics of Low-Rank Correction Method

The timing results for the implementation of the low-rank correction sensitivity method and the naïve Jacobian re-factorization method are given in Table 7.2. It should be stressed that the timing results for the low-rank method **do not include** the time needed for the factorization of the base case Jacobian, as this is performed only once for all outages, and it is an output of the pre-outage power flow. The results are summarized in Figure 7.7.

**Table 7.2: Timing Results for Single – Device Contingency Analysis**

| DEVICE | DEVICE # | METHOD 1 (SEC) | METHOD 2 (SEC) |
|---|---|---|---|
| **PEGASE 9241** | | | |
| Trans. Line 5147-3097 | 13668 | 0.0052 | 0.0933 |
| Trans. Line 1161-2990 | 15790 | 0.0054 | 0.0980 |
| Trans. Line 1928-269 | 22054 | 0.0050 | 0.0927 |
| Trans. Line 7287-7755 | 18802 | 0.0056 | 0.0966 |
| Trans. Line 7596-2305 | 23229 | 0.0055 | 0.0983 |
| Transfmer 7695-3936 | 27493 | 0.0056 | 0.0970 |
| Generator 3113 | 12713 | 0.0057 | 0.0929 |
| Generator 7279 | 13385 | 0.0061 | 0.0968 |
| | | **0.0055** | **0.0957** |
| **Polish 2383** | | | |
| Generator 1106 | 1975 | 0.001195 | 0.018573 |
| Generator 2272 | 2134 | 0.001288 | 0.019145 |
| Trans Line 22-4 | 2165 | 0.001488 | 0.019343 |
| Trans Line 715-1190 | 3218 | 0.001494 | 0.019017 |
| Trans. Line 912-1572 | 3492 | 0.001280 | 0.020264 |
| Trans. Line 1914-1907 | 4627 | 0.001683 | 0.019903 |
| Trans. Line 2364-2367 | 5045 | 0.001564 | 0.018146 |
| Trfmer 716-49 | 2282 | 0.001476 | 0.018597 |
| Trfmer 1748-121 | 2431 | 0.001610 | 0.018814 |
| | | **0.001453** | **0.019089** |
| **PEGASE 1354** | | | |
| Generator 2197 | 1813 | 7.3292e-04 | 8.5956e-03 |
| Generator 5781 | 1925 | 7.4329e-04 | 9.2523e-03 |
| Trans. Line 7351-5441 | 2016 | 8.2324e-04 | 8.9280e-03 |
| Trans. Line 564-7903 | 2367 | 8.8976e-04 | 8.5836e-03 |
| Trans. Line 5441-7098 | 2998 | 7.7640e-04 | 9.5088e-03 |
| Trans. Line 314-4300 | 3450 | 7.9442e-04 | 8.7351e-03 |
| Trfmer 2359-8005 | 3937 | 8.0590e-04 | 8.6683e-03 |
| Trfmer 1642-687 | 4001 | 7.7015e-04 | 8.7307e-03 |
| | | **7.9201e-04** | **8.8753e-03** |
| **IEEE 300** | | | |
| Generator 220 | 264 | 3.8114e-04 | 2.0390e-03 |
| Generator 7044 | 285 | 4.4814e-04 | 2.1789e-03 |

**Table 7.3 continued**

| | | | |
|---|---|---|---|
| Trans. Line 1-5 | 338 | 4.5112e-04 | 2.1612e-03 |
| Trans. Line 77-80 | 432 | 4.3393e-04 | 2.2164e-03 |
| Trans. Line 193-205 | 569 | 4.5384e-04 | 2.1398e-03 |
| Trans. Line 220-218 | 601 | 4.4890e-04 | 2.1425e-03 |
| Trfmer 223-224 | 685 | 4.5121e-04 | 2.1076e-03 |
| Trfmer 121-115 | 657 | 4.9789e-04 | 2.2114e-03 |
| | | **4.4577e-04** | **2.1496e-03** |
| **Polish 3120 Spring** | | | |
| Trans- Line 390-793 | 3182 | **2.2156e-03** | **2.6430e-02** |
| **PEGASE 2869** | | | |
| Trans. Line 5280-2343 | 4606 | **0.0018** | **0.0212** |
| **IEEE 118** | | | |
| Trans. Line 53-54 | 241 | **5.7929e-4** | **0.0012** |
| **Polish 2736** | | | |
| Trans. Line 1755-1091 | 4000 | **0.0017** | **0.0234** |

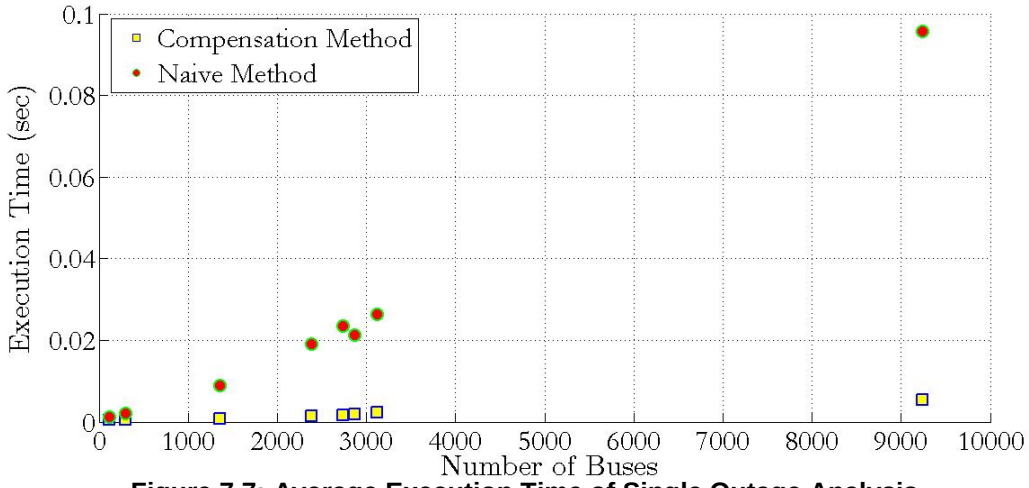


**Figure 7.7: Average Execution Time of Single Outage Analysis**

The results indicate a severe reduction in the computational burden of analyzing a single outage, if the compensation method is used. In fact, the difference in the execution time increases with system size, which is consistent with our theoretical expectations, as discussed in 7.3.2.

### 7.3.4. Sparsity Statistics

The computational complexity results of paragraph 7.3.2 were based on assumptions regarding the sparsity pattern of the system's Jacobian and their relationship with system size. In Table 7.4 and Figure 7.8 a justification for these assumptions is provided. Specifically, it can be seen that the number of nonzero elements in the equality constraint Jacobian and the associated LU factorization (with pivoting) indeed scales roughly linearly with system size.

**Table 7.4: Statistics for Nonzero Elements in Equality Constraint Jacobian**

| CASE | # OF BUSES | NNZ (J) | NNZ(B) |
|---|---|---|---|
| **IEEE RTS 24** | 24 | 361 | 569 |
| **Pegase 89** | 89 | 2001 | 3517 |
| **IEEE 118** | 118 | 1890 | 3002 |
| **IEEE 300 bus** | 300 | 4468 | 8361 |
| **PEGASE 1354** | 1354 | 19085 | 36564 |
| **Polish 2383** | 2383 | 32603 | 80809 |
| **Polish 2736** | 2736 | 37037 | 94387 |
| **Pegase 2869** | 2869 | 43209 | 92105 |
| **Polish 3120 spring** | 3120 | 41941 | 105353 |
| **Pegase 9241** | 9241 | 150609 | 368806 |

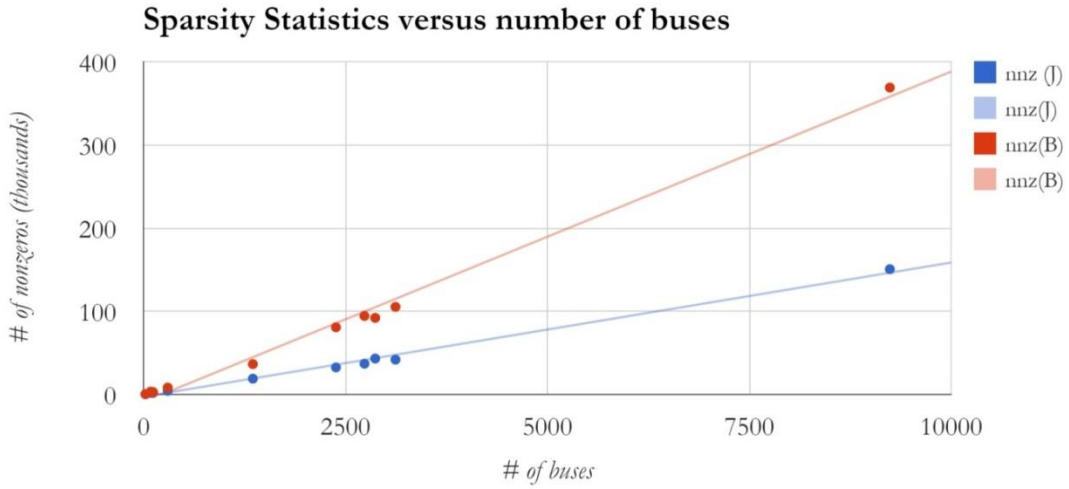


**Figure 7.8: Number of Nonzero Elements versus number of buses**

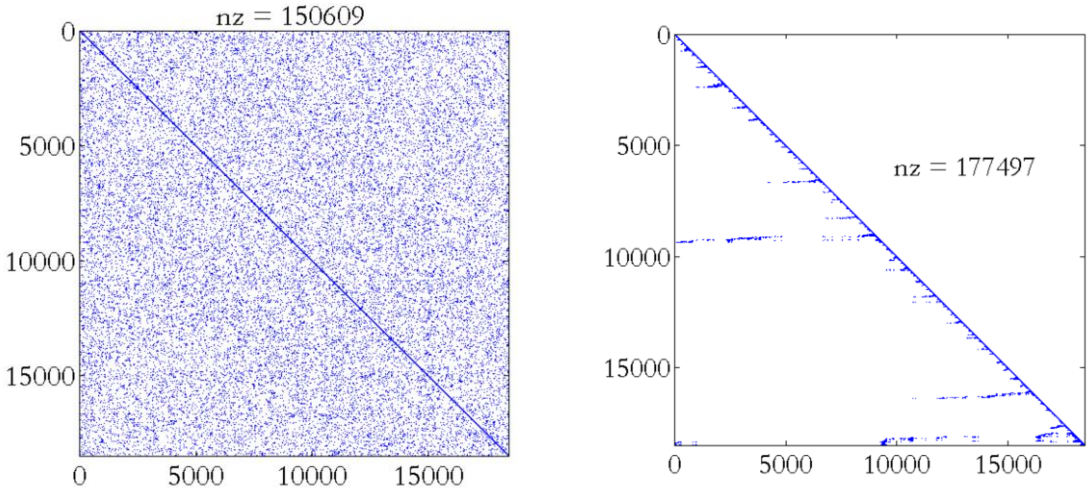


**(a)** **(b)**

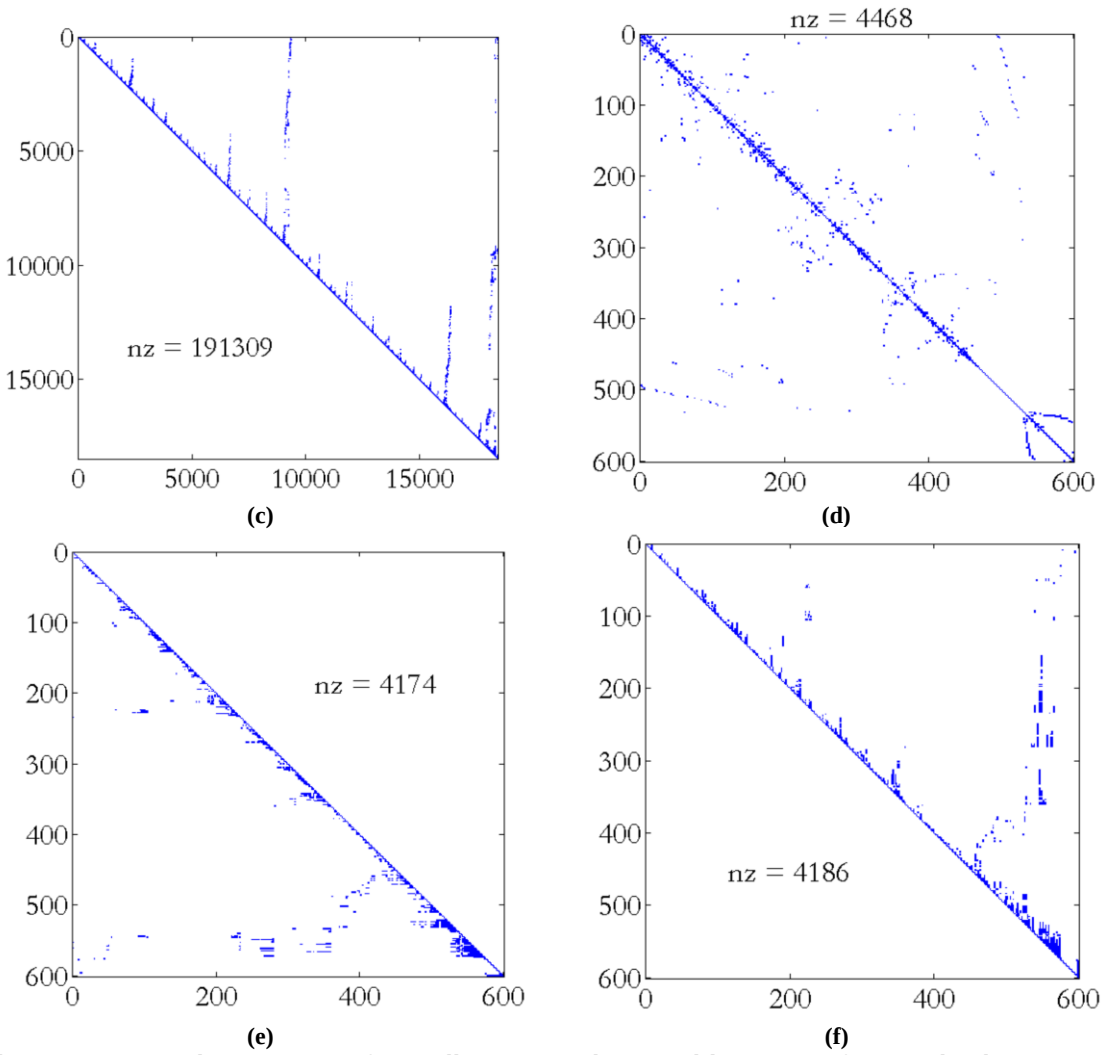


**Figure 7.9: Sparsity patterns of Equality Constraint Jacobians & LU factors (a-c) PEGASE 9241 Jacobian, L and U respectively (d-f) IEEE 300 bus Jacobian, L and U respectively**

In Figure 7.9 a pictorial representation of these matrices in terms of their sparsity pattern is also provided, for the PEGASE 9241 and the IEEE 300 systems. Figure 7.9a & d show the initial un-factorized Jacobian sparsity pattern for these two systems respectively, while Figure 7.9b and Figure 7.9e show the lower triangular matrix of the LU factorization and Figure 7.9c & Figure 7.9f show the upper triangular matrix. It can be seen from this section that, although the LU factorization does introduce new nonzero elements

in the sparsity pattern, due to fill-ins in the elimination process, the number of nonzero elements in the factor matrix *B* retains a linear relationship with system size.

## 7.4. Extension for N-1 contingency analysis and multi-device outages

The previous Chapter was concerned with good performance algorithms for a single device outage security analysis. In this section we extend the framework by proposing an *N*-1 contingency analysis algorithm and simple extension for *k* component outages.

### 7.4.1. Full N-1 contingency analysis

In order to obtain the first order estimate for the post-outage state vector, (97) and (98) need to be solved. This requires $n_d$ forward-backward substitutions for (97) and a single forward-backward substitution for (98). The LU factorization of the pre-outage Jacobian needs to be performed once for all outages, a fact which constitutes the major computational advantage of the approach.

An important increase in performance can be achieved by noticing that (97) requires a sub-matrix of the Jacobian inverse $N_d^T J^{-1} N_d$. For a single outage it would be unacceptable to obtain $J^{-1}$ explicitly because it is a dense matrix, and sparse matrix operations were chosen instead. However, in a full N-1 contingency analysis, all the elements of $J^{-1}$ will be needed, since (97) will be solved for all outages. Several of these elements will be re-used, since various device equations share the same variables (e.g. transmission lines connected to the same node). Given this observation, it will be faster to pre-compute $J^{-1}$ before analyzing any single outage and re-use its elements as needed. Hence, the algorithm proposed in this section is composed of a preparatory step that

involves the explicit computation of the Jacobian inverse and a contingency analysis step that iterates (97) and (98), using that matrix. The computational bottleneck of that algorithm is obviously the inversion of the Jacobian, which under out assumptions for the nonzero elements of $J$, costs $O(n^2)$ operations.

In Table 7.5, the Low-Rank correction technique is compared to the naïve technique, where the Jacobian matrix is re-factorized after each outage.

**Table 7.5: Timing Results for full N-1 Contingency Analysis**

| Case | # of busses | # of outages | Low-Rank Method Execution Time (s) | Naïve Method Execution Time (s) |
|---|---|---|---|---|
| **IEEE RTS 24** | 24 | 71 | 0.029440 | 0.042585 |
| **Pegase 89** | 89 | 222 | 0.139945 | 0.276742 |
| **IEEE 118** | 118 | 240 | 0.126626 | 0.288448 |
| **IEEE 300 bus** | 300 | 480 | 0.436563 | 1.335959 |
| **PEGASE 1354** | 1354 | 2251 | 3.386278 | 23.887899 |
| **Polish 2383** | 2383 | 3223 | 8.789590 | 78.423165 |
| **Polish 2736** | 2736 | 3539 | 9.320747 | 103.905093 |
| **Pegase 2869** | 2869 | 5092 | 10.627910 | 118.218754 |
| **Polish 3120sp** | 3120 | 3991 | 12.054053 | 136.9957 |
| **Pegase 9241** | 9241 | 17494 | 95.489861 | 1674.2 |

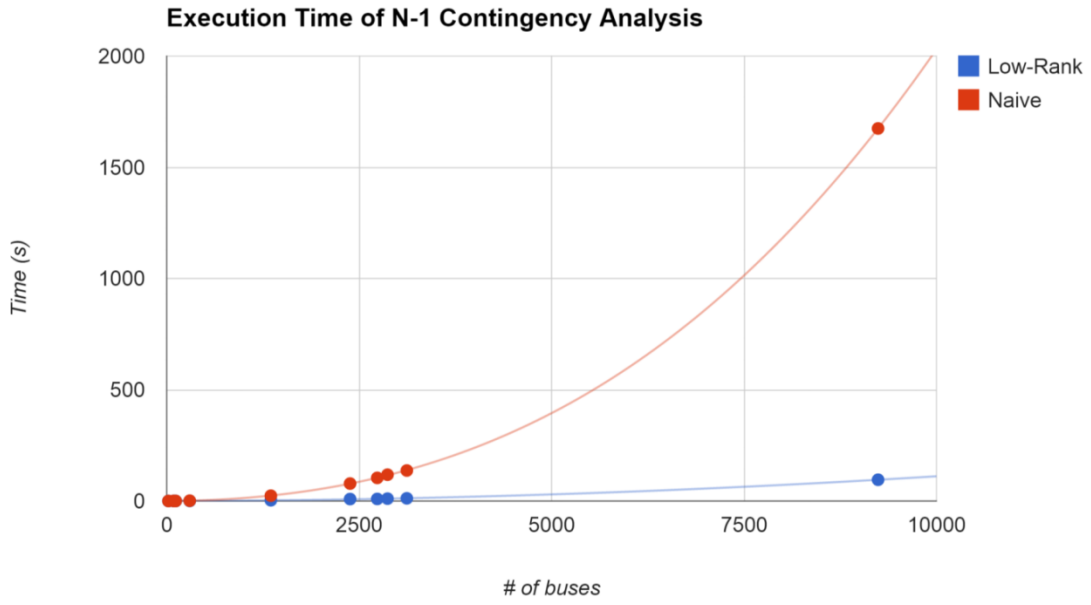

**Figure 7.10. Execution Time for N-1 contingency analysis: Naïve versus Low-Rank Modification Approach**

### 7.4.2. Multi – Device Outage Analysis

In many cases, N-1 contingency analysis may not be enough and multi-component outages need to be examined for constraint violations as well. This is due to extreme events that may cause the outage of multiple devices in the system or due to cascading component outages. Furthermore, in many cases a single cause or event may cause the outage of multiple components, as is the case for parallel circuits of transmission lines (these outages are also known as "common mode" outages).

One of the advantages of the low-rank correction sensitivity approach is that it is easily extended to multi-component outages. Let $c$ be a set of device in an *m*-component outage:

$$c = \{d_1, d_2, \ldots, d_M\} \tag{111}$$

If we define the following matrices and vectors for *c*:

$$N_c = \begin{bmatrix} N_{d_1} & N_{d_2} & \cdots & N_{d_M} \end{bmatrix} \tag{112a}$$

$$\mathbf{x}_c = \begin{bmatrix} \mathbf{x}_{d_1} & \mathbf{x}_{d_2} & \cdots & \mathbf{x}_{d_M} \end{bmatrix}^T \tag{112b}$$

$$\mathbf{g}_c^*(\mathbf{x}_c \mid \mathbf{P}_k) = \begin{bmatrix} \mathbf{g}_{d_1}^*(\mathbf{x}_{d_1} \mid \mathbf{P}_k) & \mathbf{g}_{d_2}^*(\mathbf{x}_{d_1} \mid \mathbf{P}_k) & \cdots & \mathbf{g}_{d_m}^*(\mathbf{x}_{d_1} \mid \mathbf{P}_k) \end{bmatrix}^T \tag{112c}$$

Then we can formulate a multi-component version of (97) & (98), as:

$$\mathbf{z}_c = \left\{ -\left[ \left. \frac{\partial \mathbf{g}_c^*}{\partial \mathbf{x}_c} \right|_{\mathbf{x}_c^*} \right]^{-1} + N_c^T J^{-1} N_c \right\}^{-1} \left[ -\left. \frac{\partial \mathbf{g}_c^*}{\partial \mathbf{x}_c} \right|_{\mathbf{x}_c^*} \right]^{-1} \mathbf{g}_c^*(N_c^T \mathbf{X}_k^* \mid \mathbf{P}_k))$$

$$\Rightarrow \left[ -\left. \frac{\partial \mathbf{g}_c^*}{\partial \mathbf{x}_c} \right|_{\mathbf{x}_c^*} \right]^{-1} \left\{ -\left[ \left. \frac{\partial \mathbf{g}_c^*}{\partial \mathbf{x}_c} \right|_{\mathbf{x}_c^*} \right]^{-1} + N_c^T J^{-1} N_c \right\}^{-1} \mathbf{z}_d = \mathbf{g}_c^*(N_c^T \mathbf{X}_k^* \mid \mathbf{P}_k)) \tag{113}$$

$$\Rightarrow \left[ I - \left. \frac{\partial \mathbf{g}_c^*}{\partial \mathbf{x}_c} \right|_{\mathbf{x}_c^*} N_c^T J^{-1} N_c \right] \mathbf{z}_c == \mathbf{g}_c^*(N_c^T \mathbf{X}_k^* \mid \mathbf{P}_k)$$

$$\tilde{\tilde{\mathbf{X}}}_{c-}^k = \mathbf{X}_k^* + J^{-1} N_c \mathbf{z}_c \tag{114}$$

Where $\tilde{\tilde{\mathbf{X}}}_{c-}^k$ is now the sensitivity method estimate for the system's state after the outage of all devices in set *c*. The proof of this claim is completely analogous to the derivation of (97) and it is omitted for brevity.

We should note that (113) requires forward-backward substitution of $\sum_{d \in c} n_d$ linear systems with the Jacobian $J$ on the right hand side. This will inevitably cause a deterioration of the performance of the method compared to re-factorization if *c* contains too many devices. However, for two component outages, which is the most usual case of multi-device outage, the desirable characteristics of the low-rank correction method, as described in previous sections, are expected to remain.

As a final observation, we must remark that, within a full contingency analysis framework for the entire system, including a potential list of credible multi-component outages, the explicit calculation of the Jacobian inverse remains the most favorable

approach. In that case, calculation of $N_c^T J^{-1} N_c$ does not incur substantial computational burden.

## 7.5. Critical Outage Identification based on the Sensitivity Method

The low-rank method for contingency analysis derived in previous sections serves as a step in a critical contingency identification framework. The procedure for identifying critical outages consists of obtaining

1. Obtain $\tilde{\mathbf{X}}_{c-}^k$ for each contingency *c* a set of potential critical outages *C*
2. For each outage $c \in C$, define the list of inequality constraints, excluding contingency *c*

$$\mathbf{h}_{c-}^*(\mathbf{X}^k \mid \mathbf{P}_k) = \left\lfloor \mathbf{h}_{d_i}^*(N_{d_i}^T \mathbf{X}^k \mid \mathbf{P}_k) \right\rfloor_{d_i \notin c} \tag{115}$$

   This step is needed, in order to make sure that we do not enforce constraints associated with the device that is outaged.

3. Identify contingencies *c* that yield an $\mathbf{h}_{c-,j}^*(\tilde{\mathbf{X}}_{c-}^k \mid \mathbf{P}_k)$ with at least one element exceeding a certain tolerance value and add them to the critical contingency set *CCS*:

$$\text{if } \max_{\text{j}} \left\{ \mathbf{h}_{c-,j}^*(\tilde{\mathbf{X}}_{c-}^k \mid \mathbf{P}_k) \right\} > tol \Rightarrow CCS \leftarrow CCS \cup \{c\} \tag{116}$$

These outages are the ones for which the security criterion is violated, since they cause a post-outage operating state that is expected to cause violations in the operating limits of other devices.

Note that, in addition to identifying critical outages using (116), the overall framework must also be able to identify islanding outages by identifying ill-conditioning issues with the matrix $M_d$ in (99). In case such issues appear, the outage is identified as islanding, and constraint violation is not checked for that outage. The reason is that the sensitivity method is not applicable to such outages, and any first order sensitivity results will not be valid. Nevertheless, for the practical purposes of critical outage identification this is not a crucial problem because islanding outages are de facto critical, i.e. they require some special attention in terms of corrective measures.

The principles of the low-rank correction method, as well as critical and islanding outage identification are combined in the algorithm shown in Figure 7.11. The algorithm consists of a preparatory stage, where the equations are defined, the pre-outage Jacobian is pre-factorized and the rows $b_i$ of its inverse are pre-computed, defining matrix $B$. Subsequently, each outage $c \in C$ is checked for islanding and criticality and added to the appropriate set (*ISL* or *CCS* respectively).

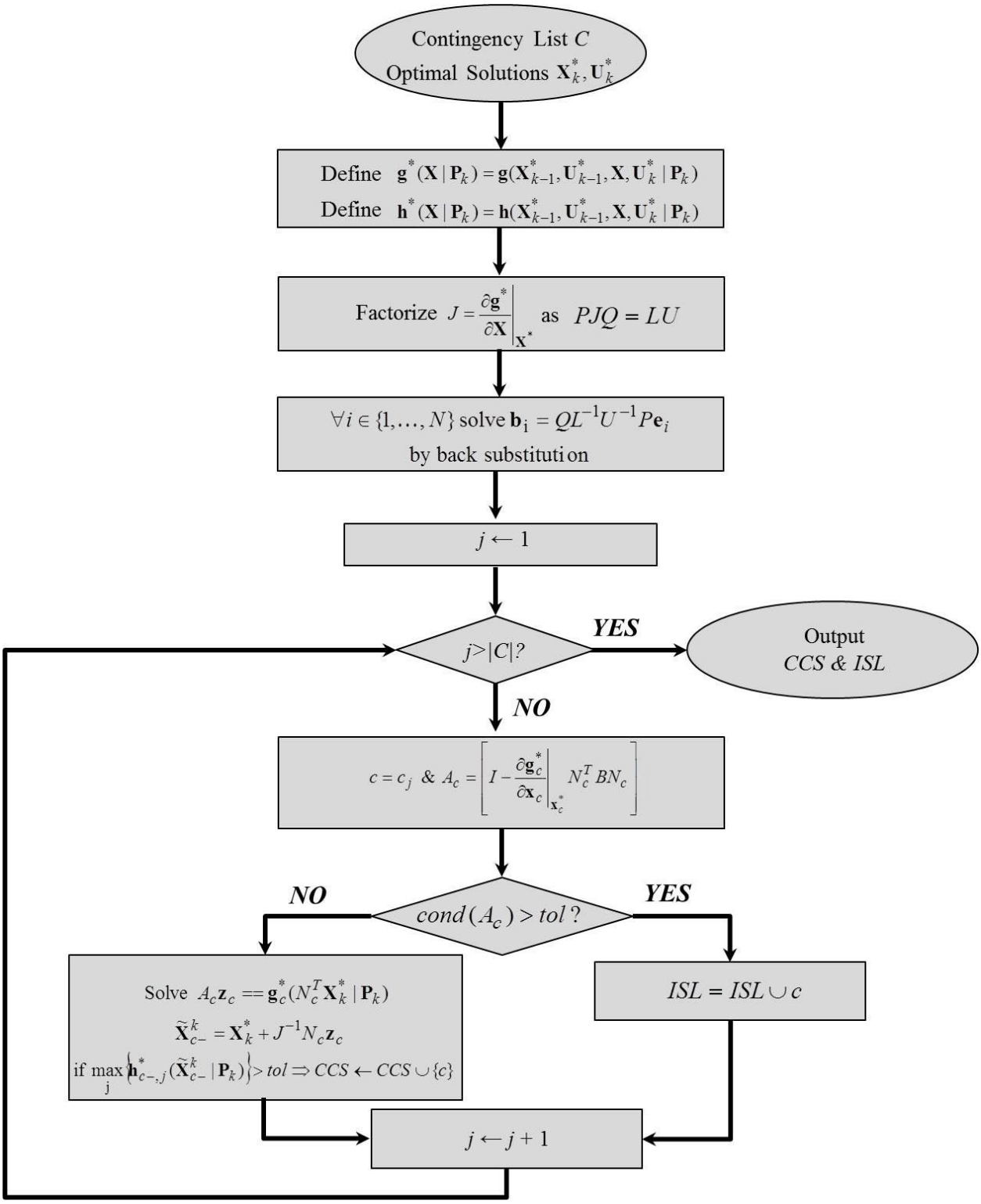


**Figure 7.11:** Low-Rank Correction Method for Identification of Critical and Islanding Outages

# Chapter 8. Conclusion and Future Research Directions

## 8.1. Conclusions

In this thesis, a real time operations framework for enhancing power system flexibility was presented and modeling of flexible resources was expanded. The following is a summary of the conclusions drawn from this body of work.

With respect to the study of the look-ahead dispatch problem, the AC-OPF and the DC-OPF version of the problem were formulated and studied. It was verified that the AC-OPF version can be substantially more accurate, yielding to decreased costs, mainly due to accurate congestion modeling. However, it was also seen that the DC-OPF is a much more tractable model, with attractive convexity properties, and does not display the sensitivity to initial conditions that is an adverse characteristic of the AC-OPF. This explains its attractiveness for power system operators, who almost exclusively base their operating models on the DC-OPF formulation. While current AC-OPF solvers are not robust enough to justify a transition to AC-OPF look-ahead scheduling, this research provided enough evidence to justify its benefits in terms of producing solutions that are feasible in real time. Furthermore, the proposed AC-OPF formulation is applicable as a necessary operating tool for issues of voltage control which the DC-OPF is incapable of modeling.

As a next step of this thesis, several models were added to the look-ahead OPF procedure, and their benefits were analyzed. The first model added was a first-order dynamic TCL model for large-scale loads with thermal characteristics and temperature

constraints. The resulting analysis showed that, with 15% penetration of thermal loads, cost savings of 0.8% can be achieved simply by scheduling load operation, without violating their temperature constraints. The control did have an adverse effect (increase) in TCL energy consumption, which was around 10%, compared to the non-dispatched case.

Our study of Dynamic Line Ratings resulted in important findings regarding their benefits in multi-step operations algorithms. Specifically, when studying heavily loaded test-cases, it was found that implementing dynamic line ratings in selected critical lines could achieve significant reductions in the amount of load shedding needed to restore feasibility. In many cases, load shedding could be altogether avoided, because critical lines could be temporarily overloaded without violating their temperature constraints. A study of Lagrange multipliers in critical buses showed that dynamic line ratings allow for increased stability in locational marginal prices, by alleviating congestion. The cost benefits of dynamic line ratings, on the other hand, do not seem to be significant. Compared to existing literature, the Thermal Line Model developed here provides a physically-based background for exceeding the very harsh restrictions of static MVA ratings.

In terms of Aggregate Distribution System modeling and controls, a time-dependent ellipsoidal model was developed to capture the time-varying flexibility offered by active Distribution Networks. A model extraction procedure was developed, whereby thousands of small scale DER's were aggregated into a single model by maximizing the resulting feasible region volume. The model's linear nature & unavoidable aggregation gives rise to inaccuracies. However, it was verified that we can obtain a desirable response from aggregate active distribution systems – e.g. curtailed consumption during up-ramps and net load peaks. Also, a disaggregation algorithm was developed to dispatch the active &

reactive consumption targets to each individual distribution-connected device. The aggregation – optimization – disaggregation approach results in a viable hierarchical control scheme and solves the problem of scalability & dimensionality of the look-ahead optimization problem.

In terms of contingency analysis, a new framework for online contingency analysis has been presented. The framework is based on three new margin indices and a new sensitivity method using a three-phase unbalanced model of power system components. The sensitivity method performs a single iteration of the three-phase quadratized power flow and then ranks outages based on the proximity to constraint violations. A multi-criterion algorithm has been also presented to perform security assessment. Numerical experiments showed that the sensitivity method performs better in predicting post-contingency constraint violations than the MI-based method, but the MI method achieved very good results and high computational efficiency. Numerical experiments also suggest that unbalanced contingency selection and analysis methods can assist the reliable operation of the grid, given that a symmetric positive sequence solver failed to capture all violating contingencies. Benchmarking the computational intensity of contingency analysis using compensation methods within the quadratized power flow is an immediate future step of this research.

In the contingency analysis section, emphasis was given to a faster implementation of the post-outage solution, by observing that the outage causes low-rank modifications to the post-outage Jacobian. The so-called compensation method, revisited from existing literature, was generalized to $k$ component outages, and a check for islanding conditions was added. The resulting method allowed for faster studies of single-component and

multiple-component outages compared to naïve methods. A study of N-1 security analysis documented the effectiveness of the developed approach in severely reducing execution times for security analysis. It should be noted that the developed compensation method is directly applicable to the sensitivity method that was discussed in the contingency selection section, where it was shown that is has very good filtering and accuracy performance as a contingency filter.

## 8.2. Future Research Directions

Many open problems associated with this research topic remain open. In the area of AC-OPF formulations, the presented algorithms obviously do not come with global optimality guarantees, and more work should be done towards obtaining a robust look-ahead AC-OPF solver. The benefits for transitioning from the DC-OPF to the AC-OPF have been documented here, but the AC-OPF must reach a maturity level consistent with the operator's current requirements.

In the area of dynamic line ratings, a very important next step would be to design to measurement infrastructure, particularly using PMU data, in order to identify and maintain thermal line models, in order to implement the approach. Dynamic state estimation may be a key element in order to acquire the data required to add dynamic line models to the system's scheduling algorithms. Validation of such models in the field should be an immediate first step, in order for the outlined modeling approach to hold any real value.

Related to aggregate modeling of distribution systems, two areas of research are the most promising: extending the approach to nonlinear models & including the distribution feeder's power flow equations will be important augmentations to the work presented here.

It is worth mentioning that the inclusion of all distribution customer models, as well as the feeder three-phase unbalanced power flow equations in the distribution-level optimization will give rise to a formulation with a very large number of constraints and variables. Leveraging high-performance computing methods will be very important in addressing the tractability of this problem. As we suggested in this work, including this level of accuracy of distribution system modeling to the transmission scheduling problem is prohibitive, and aggregate model extraction is of paramount importance.

Furthermore, experimental verification in pilot feeders should be a good first step in demonstrating the applicability of hierarchical optimization. Such a research endeavor would have to cover the very important issues of data acquisition & distribution state estimation, in order to obtain the data and models needed to implement the suggested approach. These issues were not covered in this thesis, but they are an important area of future research.

In the area of security analysis there is substantial open ground for future research. However, one key element in this topic would be to expand the static security analysis framework that we developed here to dynamic security assessment methods. In many cases, the system may be N-1 secure in terms of static constraints, but it may still be dynamically unstable if a component outage happens. In that case the system is not in a de facto secure state, and thus it does not meet NERC criteria for security. The computational burden for this problem is increased. However, advances in high-performance computing and parallelization, along with decomposition algorithms, should also be leveraged to make such a framework implementable in current real-life systems.

# References


[1] California Independent System Operator (2013). What the duck curve tells us about managing a green grid. Folsom, CA: California ISO. Accessed September 2014: http://www.caiso.com/documents/flexibleresourceshelprenewables_ fastfacts.pdf

[2] EirGrid, S. O. N. I. (2011). Ensuring a Secure, Reliable and Efficient Power System in a Changing Environment. A EIRGRID, SONI Report June.

[3] United State Department of Energy (2011). The importance of flexible electricity supply, DOE Solar Integration Series Report, May 2011

[4] Papaefthymiou, G.; Grave, K.; Dragoon, K. (2014), "Flexibility Options in Electricity Systems," ECOFYS report, March 2014

[5] International Energy Agency. (2009). Empowering Variable Renewables-Options for Flexible Electricity Systems. OECD Publishing.

[6] Adams, J., O'Malley, M., & Hanson, K. (2010). Flexibility requirements and potential metrics for variable generation: Implications for system planning studies. Princeton, NJ: NERC.

[7] North American Electric Reliability Corporation (2009). Accommodating High Levels of Variable Generation. Princeton, NJ: NERC., April 2009

[8] Cochran, J., Miller, M., Zinaman, O., Milligan, M., Arent, D., Palmintier, B., ... & Soonee, S. K. (2014). Flexibility in 21st Century Power Systems (No. NREL/TP-6A20-61721). National Renewable Energy Laboratory (NREL), Golden, CO.

[9] Troy, N.; Denny, E.; O'Malley, M. (2010). Base-Load Cycling on a System With Significant Wind Penetration, *IEEE Transactions on Power Systems*, vol.25, no.2, pp.1088-1097, May 2010

[10] Wan, Y. H. (2011). Analysis of wind power ramping behavior in ERCOT. Contract, 303, 275-3000.

[11] Georgilakis, P. S. (2008). Technical challenges associated with the integration of wind power into power systems. *Renewable and Sustainable Energy Reviews*, 12(3), 852-863, 2008

[12] Le Xie; Carvalho, P.M.S.; Ferreira, L.A.F.M.; Juhua Liu; Krogh, B.H.; Popli, N.; Ilic, M.D. (2011), Wind Integration in Power Systems: Operational Challenges and Possible Solutions, *Proceedings of the IEEE*, vol.99, no.1, pp.214,232, Jan. 2011

[13] Brouwer, A. S., van den Broek, M., Seebregts, A., & Faaij, A. (2014). Impacts of large-scale Intermittent Renewable Energy Sources on electricity systems, and how these can be modeled. *Renewable and Sustainable Energy Reviews*, 33, 443-466.

[14] Ma, J., Silva, V., Belhomme, R., Kirschen, D. S., & Ochoa, L. F. (2013, July). Evaluating and planning flexibility in sustainable power systems. *In Power and Energy Society General Meeting (PES)*, 2013 IEEE (pp. 1-11). IEEE.

[15] Lannoye, E., Flynn, D., & O'Malley, M. (2012). Evaluation of power system flexibility. *Power Systems, IEEE Transactions on*, 27(2), 922-931.

[16] Menemenlis, N.; Huneault, M.; Robitaille, A. (2011). Thoughts on power system flexibility quantification for the short-term horizon. *Power and Energy Society General Meeting, 2011 IEEE* , pp.1,8, 24-29 July 2011

[17] G. Andersson, P. Donalek, R. Farmer, N. Hatziargyriou, I. Kamwa, P. Kundur, N. Martins, J. Paserba, P. Pourbeik, J. Sanchez-Gasca, R. Schulz, A. Stankovic, C. Taylor, V. Vittal (2005). Causes of the 2003 major grid blackouts in North America and Europe, and recommended means to improve system dynamic performance. *Power Systems, IEEE Transactions on* , vol.20, no.4, pp.1922,1928, Nov. 2005

[18] R. Billinton, L. Salvaderi, J.D. McCalley, H. Chao, Th. Seitz, R.N. Allan, J. Odom, C. Fallon. (1997). Reliability issues in today's electric power utility environment. *Power Systems, IEEE Transactions on* , vol.12, no.4, pp.1708,1714, Nov 1997

[19] K. Morison, L. Wang, P. Kundur (2004). Power system security assessment. *Power and Energy Magazine, IEEE* , vol.2, no.5, pp.30,39, Sept.-Oct. 2004

[20] Albadi, M. H., & El-Saadany, E. F. (2008). A summary of demand response in electricity markets. *Electric Power Systems Research*, 78(11), 1989-1996.

[21] Bitar, E. Y., Rajagopal, R., Khargonekar, P. P., Poolla, K., & Varaiya, P. (2012). Bringing wind energy to market. *IEEE Transactions on Power Systems*, 27(3), 1225-1235, 2012.

[22] Rahimi, F.; Ipakchi, A. (2010). Demand Response as a Market Resource Under the Smart Grid Paradigm. *IEEE Transactions on Smart Grid*, vol.1, no.1, pp.82,88, June 2010

[23] Li, N., Chen, L., & Low, S. H. (2011). Optimal demand response based on utility maximization in power networks. *Power and Energy Society General Meeting, 2011 IEEE* (pp. 1-8).

[24] Papavasiliou, A., & Oren, S. S. (2014). Large-scale integration of deferrable demand and renewable energy sources. *IEEE Transactions on Power Systems*, 29(1), 489-499, 2014.

[25] Gayme, D., & Topcu, U. (2011). Optimal power flow with distributed energy storage dynamics. *American Control Conference (ACC)*, pp. 1536-1542, IEEE, June 2011.

[26] Pina, A., Silva, C., & Ferrão, P. (2012). The impact of demand side management strategies in the penetration of renewable electricity. *Energy*, 41(1), 128-137.

[27] Solomon, A. A., Kammen, D. M., & Callaway, D. (2014). The role of large-scale energy storage design and dispatch in the power grid: A study of very high grid penetration of variable renewable resources. *Applied Energy*, 134, 75-89.

[28] Brown, P. D., Peas Lopes, J. A., & Matos, M. A. (2008). Optimization of pumped storage capacity in an isolated power system with large renewable penetration. Power Systems, *IEEE Transactions on*, 23(2), 523-531.

[29] Denholm, P., & Hand, M. (2011). Grid flexibility and storage required to achieve very high penetration of variable renewable electricity. *Energy Policy*, 39(3), 1817-1830.

[30] Lannoye, E.; Flynn, D.; O'Malley, M. (2015). Transmission, Variable Generation, and Power System Flexibility. *Power Systems, IEEE Transactions on* , vol.30, no.1, pp.57,66, Jan. 2015

[31] Bo Lu; Shahidehpour, M. (2005). Unit commitment with flexible generating units. *Power Systems, IEEE Transactions on* , vol.20, no.2, pp.1022,1034, May 2005

[32] Tao Li; Shahidehpour, M. (2007). Dynamic Ramping in Unit Commitment. *Power Systems, IEEE Transactions on* , vol.22, no.3, pp.1379,1381, Aug. 2007

[33] Ruiwei Jiang; Jianhui Wang; Yongpei Guan. (2012). Robust Unit Commitment With Wind Power and Pumped Storage Hydro. *Power Systems, IEEE Transactions on* , vol.27, no.2, pp.800,810, May 2012

[34] Ferrero, R. W., & Shahidehpour, S. M. (1997). Dynamic economic dispatch in deregulated systems. *International Journal of Electrical Power & Energy Systems*, 19(7), 433-439.

[35] Sharif, S. S., & Taylor, J. H. (1998, June). Dynamic optimal reactive power flow. *In American Control Conference, 1998. Proceedings of the 1998* (Vol. 6, pp. 3410-3414). IEEE.

[36] Xie, K., & Song, Y. H. (2001, January). Dynamic optimal power flow by interior point methods. In Generation, Transmission and Distribution, *IEE Proceedings*- (Vol. 148, No. 1, pp. 76-84). IET.

[37] Lorca, A., & Sun, X. A. (2014). Adaptive Robust Optimization with Dynamic Uncertainty Sets for Multi-Period Economic Dispatch under Significant Wind.

[38] Cardell, J.B.; Anderson, C.L. "A Flexible Dispatch Margin for Wind Integration," *Power Systems, IEEE Transactions on* , no.99, pp.1,10

[39] Anderson, C.L.; Cardell, J.B. (2014). A Decision Framework for Optimal Pairing of Wind and Demand Response Resources. *Systems Journal, IEEE* , vol.8, no.4, pp.1104,1111, Dec. 2014

[40] Papadaskalopoulos, D.; Strbac, G.; Mancarella, P.; Aunedi, M.; Stanojevic, V. (2013). Decentralized Participation of Flexible Demand in Electricity Markets—Part II: Application With Electric Vehicles and Heat Pump Systems. *Power Systems, IEEE Transactions on* , vol.28, no.4, pp.3667,3674, Nov. 2013

[41] Yi Zong; Kullmann, D.; Thavlov, A.; Gehrke, O.; Bindner, H.W. (2012) Application of Model Predictive Control for Active Load Management in a Distributed Power System With High Wind Penetration. *Smart Grid, IEEE Transactions on* , vol.3, no.2, pp.1055,1062, June 2012

[42] Gayme, D., & Topcu, U. (2013). Optimal power flow with large-scale storage integration. *Power Systems, IEEE Transactions on*, 28(2), 709-717.

[43] Sortomme, E.; El-Sharkawi, M.A. (2009). Optimal Power Flow for a System of Microgrids with Controllable Loads and Battery Storage. *Power Systems Conference and Exposition, 2009. PSCE '09. IEEE/PES* , pp.1,5, 15-18 March 2009

[44] Bao, Z., Zhou, Q., Yang, Z., Yang, Q., Xu, L., & Wu, T. A Multi Time-Scale and Multi Energy-Type Coordinated Microgrid Scheduling Solution—Part II: Optimization Algorithm and Case Studies.

[45] Panigrahi, B. K., Ravikumar Pandi, V., & Das, S. (2008). Adaptive particle swarm optimization approach for static and dynamic economic load dispatch. *Energy conversion and management*, 49(6), 1407-1415.

[46] Zhou, W., Peng, Y., Sun, H., & Wei, Q. H. (2009). Dynamic economic dispatch in wind power integrated system [J]. *Proceedings of the CSEE*, 25, 006.

[47] Alguacil, N., & Conejo, A. J. (2000). Multiperiod optimal power flow using Benders decomposition. *Power Systems, IEEE Transactions on*, 15(1), 196-201.

[48] Ilic, M. D., Xie, L., & Joo, J. Y. (2011). Efficient coordination of wind power and price-responsive demand—Part I: Theoretical foundations. *Power Systems, IEEE Transactions on*, 26(4), 1875-1884.

[49] Le Xie; Ilić, M.D. (2009). Model predictive economic/environmental dispatch of power systems with intermittent resources. Power & Energy Society General Meeting, *2009. PES '09. IEEE* , pp.1,6, 26-30 July 2009

[50] Wang, D., Parkinson, S., Miao, W., Jia, H., Crawford, C., & Djilali, N. (2012). Online voltage security assessment considering comfort-constrained demand response control of distributed heat pump systems. *Applied Energy*, 96, 104-114.

[51] Callaway, D. S. (2009). Tapping the energy storage potential in electric loads to deliver load following and regulation, with application to wind energy. *Energy Conversion and Management*, 50(5), 1389-1400.

[52] J. Cochran, M. Miller, M. Milligan, E. Ela, D. Arent, A. Bloom, M. Futch, J. Kiviluoma, H. Holtinnen, A. Orths, E. Gmez-Lzaro, S. MartnMartnez, S. Kukoda, G. Garcia, K. Mller, Mikkelsen, Z. Yongqiang, and K. Sandholt. (2013). Market Evolution: Wholesale Electricity Market Design for 21st Century Power Systems. NREL/TP-6A20-57477, Oct. 2013, Tech. Rep., 21st Century Power Partnership.

[53] H. Wang (2007). On the computation and application of multi-period security-constrained optimal power flow for real-time electricity market operations. Ph.D. dissertation, Dept. Electr. Eng., Cornell Univ., Ithaca, 2007.

[54] Tao, Y., Xu, Z., Meliopoulos, A. P., & Hu, Z. (2013, July). Optimal power flow with flexible loading. *In Power and Energy Society General Meeting (PES)*, 2013 IEEE (pp. 1-5). IEEE.

[55] Lu, N., Chassin, D.P., & Widergren,S.E.(2005). Modeling uncertainties in aggregated thermostatically controlled loads using a state queueing model. *Power Systems, IEEE Transactions on*, 20(2), 725-733.

[56] Mathieu, J. L., Koch, S., & Callaway, D. S. (2013). State estimation and control of electric loads to manage real-time energy imbalance. *Power Systems, IEEE Transactions on*, 28(1), 430-440.

[57] Koch, S., Mathieu, J. L., & Callaway, D. S. (2011, August). Modeling and control of aggregated heterogeneous thermostatically controlled loads for ancillary services. *In Proceedings of the PSCC* (pp. 1-7).

[58] Hao, H., Sanandaji, B. M., Poolla, K., & Vincent, T. L. (2013). Aggregate flexibility of thermostatically controlled loads.

[59] Koch, S., Zima, M., & Andersson, G. (2009, July). Active coordination of thermal household appliances for load management purposes. *In IFAC Symposium on Power Plants and Power Systems Control*, Tampere, Finland.

[60] Kalsi, K., Elizondo, M., Fuller, J., Lu, S., & Chassin, D. (2012, January). Development and validation of aggregated models for thermostatic controlled loads with demand response. *In System Science (HICSS), 2012 45th Hawaii International Conference on* (pp. 1959-1966). IEEE.

[61] Thavlov, A.; Bindner, H.W. Utilization of Flexible Demand in a Virtual Power Plant Set-Up. *Smart Grid, IEEE Transactions on* , no.99, pp.1,1

[62] MacDougall, P., Roossien, B., Warmer, C., & Kok, K. (2013, July). Quantifying flexibility for smart grid services. *In Power and Energy Society General Meeting (PES)*, 2013 IEEE (pp. 1-5). IEEE.

[63] Mai, W.; Chung, C.Y. Economic MPC of Aggregating Commercial Buildings for Providing Flexible Power Reserve. *Power Systems, IEEE Transactions on*, no.99, pp.1,10

[64] Han, S., Han, S., & Sezaki, K. (2010). Development of an optimal vehicle-to-grid aggregator for frequency regulation. *Smart Grid, IEEE Transactions on*, 1(1), 65-72.

[65] Ruiz, N., Cobelo, I., & Oyarzabal, J. (2009). A direct load control model for virtual power plant management. *Power Systems, IEEE Transactions on*, 24(2), 959-966.

[66] Jansen, B., Binding, C., Sundstrom, O., & Gantenbein, D. (2010, October). Architecture and communication of an electric vehicle virtual power plant. *In Smart Grid Communications (SmartGridComm), 2010 First IEEE International Conference on* (pp. 149-154). IEEE.

[67] Bertsch, J., Carnal, C., Karlson, D., McDaniel, J., & Vu, K. (2005). Wide-area protection and power system utilization. *Proceedings of the IEEE*, 93(5), 997-1003.

[68] Wen, J., Arons, P., & Liu, W. H. E. (2010, January). The role of remedial action schemes in renewable generation integrations. *In Innovative Smart Grid Technologies (ISGT), 2010* (pp. 1-6). IEEE.

[69] Venkatasubramanian, V. M., Yue, X., Liu, G., Sherwood, M., & Zhang, Q. (2009, March). Wide-area monitoring and control algorithms for large power systems using synchrophasors. *In Power Systems Conference and Exposition, 2009. PSCE'09*. IEEE/PES (pp. 1-5). IEEE.

[70] Shandilya, A., Gupta, H., & Sharma, J. (1993, September). Method for generation rescheduling and load shedding to alleviate line overloads using local optimisation. In Generation, Transmission and Distribution, *IEE Proceedings C* (Vol. 140, No. 5, pp. 337-342). IET.

[71] Arnborg, S., Andersson, G., Hill, D. J., & Hiskens, I. A. (1997). On undervoltage load shedding in power systems. *International Journal of Electrical Power & Energy Systems*, 19(2), 141-149.

[72] Feng, Z., Ajjarapu, V., & Maratukulam, D. J. (1998). A practical minimum load shedding strategy to mitigate voltage collapse. *Power Systems, IEEE Transactions on*, 13(4), 1285-1290.

[73] Faranda, R., Pievatolo, A., & Tironi, E. (2007). Load shedding: a new proposal. Power Systems, *IEEE Transactions on*, 22(4), 2086-2093.

[74] Shah, S., & Shahidehpour, S. M. (1989). A heuristic approach to load shedding scheme. *Power Systems, IEEE Transactions on*, 4(4), 1421-1429.

[75] Granville, S., Mello, J., & Melo, A. C. G. (1996). Application of interior point methods to power flow unsolvability. *Power Systems, IEEE Transactions on*, 11(2), 1096-1103.

[76] Overbye, T. J. (1995). Computation of a practical method to restore power flow solvability. *Power Systems, IEEE Transactions on*, 10(1), 280-287.

[77] Barboza, L. V., & Salgado, R. (2001). Restoring solutions for unsolvable cases via minimum load shedding for a specified direction. In Power Industry Computer Applications, 2001. PICA 2001. *Innovative Computing for Power-Electric Energy Meets the Market. 22nd IEEE Power Engineering Society International Conference on (pp. 374-379)*. IEEE.

[78] Wang, P., & Billinton, R. (2000, January). Optimum load-shedding technique to reduce the total customer interruption cost in a distribution system. *In Generation, Transmission and Distribution, IEE Proceedings* (Vol. 147, No. 1, pp. 51-56). IET.

[79] Aponte, E. E., & Nelson, J. K. (2006). Time optimal load shedding for distributed power systems. *Power Systems, IEEE Transactions on*, 21(1), 269-277.

[80] Fernandes, T. S., Lenzi, J. R., & Mikilita, M. (2008). Load shedding strategies using optimal load flow with relaxation of restrictions. *Power Systems, IEEE Transactions on*, 23(2), 712-718.

[81] G.C. Ejebe, B.F. Wollenberg. (1979) Automatic Contingency Selection. *Power Apparatus and Systems, IEEE Transactions on* , vol.PAS-98, no.1, pp.97,109, Jan. 1979

[82] G.D. Irisarri, A.M. Sasson. (1981) An Automatic Contingency Selection Method for On-Line Security Analysis. *Power Apparatus and Systems, IEEE Transactions on* , vol.PAS-100, no.4, pp.1838,1844, April 1981

[83] NERC Reliability Standards for the Bulk Electric Systems of North America, Reliability Coordination Standard, Standard IRO-001, 2014

[84] Chen, Q., & McCalley, J. D. (2005). Identifying high risk nk contingencies for online security assessment. *Power Systems, IEEE Transactions on*, 20(2), 823-834.

[85] Ejebe, G. C., Van Meeteren, H. P., & Wollenberg, B. F. (1988). Fast contingency screening and evaluation for voltage security analysis. *Power Systems, IEEE Transactions on*, 3(4), 1582-1590.

[86] Fu, C., & Bose, A. (1999). Contingency ranking based on severity indices in dynamic security analysis. *Power Systems, IEEE Transactions on*, 14(3), 980-985.

[87] Capitanescu, F., Glavic, M., Ernst, D., & Wehenkel, L. (2007). Contingency filtering techniques for preventive security-constrained optimal power flow. *Power Systems, IEEE Transactions on*, 22(4), 1690-1697.

[88] T. A. Mikolinnas, B.F. Wollenberg. (1981). An Advanced Contingency Selection Algorithm. *Power Apparatus and Systems, IEEE Transactions on* , vol.PAS-100, no.2, pp.608,617, Feb. 1981

[89] S. Vemuri, R.E. Usher. (1983). On-Line Automatic Contingency Selection Algorithms. *Power Apparatus and Systems, IEEE Transactions on* , vol.PAS-102, no.2, pp.346,354, Feb. 1983

[90] J. Zaborszky, Keh-Wen Whang; K. Prasad. (1980). Fast Contingency Evaluation Using Concentric Relaxation. *Power Apparatus and Systems, IEEE Transactions on* , vol.PAS-99, no.1, pp.28,36, Jan. 1980

[91] V. Brandwajn (1988). Efficient bounding method for linear contingency analysis. *Power Systems, IEEE Transactions on* , vol.3, no.1, pp.38,43, Feb 1988

[92] V. Brandwajn, M.G. Lauby. (1989). Complete bounding method for AC contingency screening. *Power Systems, IEEE Transactions on* , vol.4, no.2, pp.724,729, May 1989

[93] O. Alsac, B. Stott, W.F. Tinney. (1983). Sparsity-Oriented Compensation Methods for Modified Network Solutions. *Power Engineering Review, IEEE* , vol.PER-3, no.5, pp.24,25, May 1983

[94] W.F. Tinney, V. Brandwajn, S.M. Chan. (1985). Sparse Vector Methods. *Power Apparatus and Systems, IEEE Transactions on* , vol.PAS-104, no.2, pp.295,301, Feb. 1985

[95] S.M. Chan, V. Brandwajn. (1986). Partial Matrix Refactorization. *Power Engineering Review, IEEE* , vol.PER-6, no.2, pp.44,45, Feb. 1986

[96] A.P.S. Meliopoulos, C.S. Cheng, X. Feng. (1994). Performance evaluation of static security analysis methods. *Power Systems, IEEE Transactions on*, vol.9, no.3, pp.1441,1449, Aug 1994

[97] A. P. S. Meliopoulos and C. Cheng. (1990). A hybrid contingency selection method. *Proceedings of the 10th Power System Computation Conference*, Graz, Austria, Aug. 1990, pp. 605-612.

[98] F. Albuyeh, A. Bose, B. Heath. (1982). Reactive Power Considerations in Automatic Contingency Selection. *Power Apparatus and Systems, IEEE Transactions on* , vol.PAS-101, no.1, pp.107,112, Jan. 1982

[99] S. Gerbex, R. Cherkaoui, A.J. Germond. (2003). Optimal location of FACTS devices to enhance power system security. *Power Tech Conference Proceedings, 2003 IEEE Bologna* , vol.3, no.7 pp. Vol.3,, 23-26 June 2003

[100] F. Bouffard, F.D. Galiana. (2008). Stochastic security for operations planning with significant wind power generation. *Power and Energy Society General Meeting - Conversion and Delivery of Electrical Energy in the 21st Century*, 2008 IEEE , pp.1,11, 20-24 July 2008

[101] H. Song, H., M. Kezunovic. (2007). A new analysis method for early detection and prevention of cascading events. *Electric Power Systems Research*, vol. 77, no. 8, pp. 1132-1142, 2007

[102] Kim, J., Maria, G., & Wong, V. (1985). Contingency ranking and simulation for on-line use. *Power Apparatus and Systems, IEEE Transactions on*, (9), 2401-2407.

[103] Lo, K. L., & Meng, Z. J. (2004, March). Newton-like method for line outage simulation. *In Generation, Transmission and Distribution, IEE Proceedings* (Vol. 151, No. 2, pp. 225-231). IET.

[104] Ruiz, P. A., & Sauer, P. W. (2007). Voltage and reactive power estimation for contingency analysis using sensitivities. *Power Systems, IEEE Transactions on*, 22(2), 639-647.

[105] Davis, C., & Overbye, T. J. (2011). Multiple element contingency screening. *Power Systems, IEEE Transactions on*, 26(3), 1294-1301.

[106] Meliopoulos, A. P., Cokkinides, G. J., & Stefopoulos, G. K. (2005, June). "Quadratic integration method", *Proceedings of the 2005 International Power System Transients Conference*, IPST 2005, pp. 19-23.

[107] D. P. Bertsekas, Nonlinear Programming, 2nd ed. Nashua, NH: Athena Scientific, 1999, pp. 95–97, 397-426.

[108] Wu, Y. C., Debs, A. S., & Marsten, R. E. (1994). A direct nonlinear predictor-corrector primal-dual interior point algorithm for optimal power flows. *Power Systems, IEEE Transactions on*, 9(2), 876-883.

[109] Jabr, R., Coonick, A. H., & Cory, B. J. (2002). A primal-dual interior point method for optimal power flow dispatching. *Power Systems, IEEE Transactions on*, 17(3), 654-662.

[110] Wächter, A., & Biegler, L. T. (2006). On the implementation of an interior-point filter line-search algorithm for large-scale nonlinear programming. *Mathematical programming*, 106(1), 25-57.

[111] Boyd, S., & Vandenberghe, L. (2004). Convex optimization. Cambridge university press.

[112] Zimmerman, R. D., Murillo-Sánchez, C. E., & Thomas, R. J. (2011). MATPOWER: Steady-state operations, planning, and analysis tools for power systems research and education. *Power Systems, IEEE Transactions on*, 26(1), 12-19.

[113] Wang, C., & Shahidehpour, S. M. (1993). Effects of ramp-rate limits on unit commitment and economic dispatch. *Power Systems, IEEE Transactions on*, 8(3), 1341-1350.

[114] Wang, J., Shahidehpour, M., & Li, Z. (2008). Security-constrained unit commitment with volatile wind power generation. *Power Systems, IEEE Transactions on*, 23(3), 1319-1327.

[115] Han, X. S., Gooi, H. B., & Kirschen, D. S. (2001). Dynamic economic dispatch: feasible and optimal solutions. *Power Systems, IEEE Transactions on*, 16(1), 22-28.

[116] Glover, J. D., Sarma, M., & Overbye, T. (2011). Power System Analysis & Design, SI Version. Cengage Learning.

[117] Foss, S. D., Lin, S. H., & Fernandes, R. A. (1983). Dynamic thermal line ratings part I dynamic ampacity rating algorithm. *Power Apparatus and Systems, IEEE Transactions on*, (6), 1858-1864.

[118] IEEE Standard for Calculating the Current-Temperature Relationship of Bare Overhead Conductors," IEEE Std 738-2012 (Revision of IEEE Std 738-2006 - Incorporates IEEE Std 738-2012 Cor 1-2013) , vol., no., pp.1,72, Dec. 23 2013

[119] Douglass, D. A., Lawry, D. C., Edris, A. A., & Bascom, E. C. (2000). Dynamic thermal ratings realize circuit load limits. *Computer Applications in Power, IEEE*, 13(1), 38-44.

[120] Douglass, D. A., & Edris, A. (1996). Real-time monitoring and dynamic thermal rating of power transmission circuits. *Power Delivery, IEEE Transactions on*, 11(3), 1407-1418.

[121] Black, W. Z., & Rehberg, R. L. (1985). Simplified model for steady state and real-time ampacity of overhead conductors. *Power Apparatus and Systems, IEEE Transactions on*, (10), 2942-2953.

[122] Black, M., & Strbac, G. (2007). Value of bulk energy storage for managing wind power fluctuations. *Energy conversion, IEEE transactions on*, 22(1), 197-205.

[123] Ipakchi, A., & Albuyeh, F. (2009). Grid of the future. *Power and Energy Magazine, IEEE*, 7(2), 52-62.

[124] El Ghaoui, L., Feron, E., & Balakrishnan, V. (1994). Linear matrix inequalities in system and control theory (Vol. 15, p. 1). Philadelphia: Society for industrial and applied mathematics.

[125] Vandenberghe, L., Boyd, S., & Wu, S. P. (1998). Determinant maximization with linear matrix inequality constraints. *SIAM journal on matrix analysis and applications*, 19(2), 499-533.

[126] Ben-Tal, A., & Nemirovski, A. (2001). Lectures on modern convex optimization: nalysis, algorithms, and engineering applications (Vol. 2). SIAM.

[127] A. P. Meliopoulos, E. Polymeneas, Zhenyu Tan, Renke Huang, and Dongbo Zhao. (2013). Advanced Distribution Management System. *IEEE Transactions on Smart Grid*, Vol 4, Issue 4, pp 2109-2117, 2013

[128] Fliscounakis, S., Panciatici, P., Capitanescu, F., & Wehenkel, L. (2013). Contingency ranking with respect to overloads in very large power systems taking into account uncertainty, preventive, and corrective actions. *Power Systems, IEEE Transactions on*, 28(4), 4909-4917.

[129] Löfberg, J. (2004, September). YALMIP: A toolbox for modeling and optimization in MATLAB. *In Computer Aided Control Systems Design, 2004 IEEE International Symposium on* (pp. 284-289). IEEE.

[130] Kvasnica, M., Grieder, P., Baotić, M., & Morari, M. (2004). Multi-parametric toolbox (MPT). *In Hybrid systems: computation and control* (pp. 448-462). Springer Berlin Heidelberg.

[131] Toh, K. C., Todd, M. J., & Tütüncü, R. H. (1999). SDPT3—a MATLAB software package for semidefinite programming, version 1.3. Optimization methods and software, 11(1-4), 545-581.

[132] Grant, M., Boyd, S., & Ye, Y. (2008). CVX: Matlab software for disciplined convex programming.

[133] Wacker, G., & Billinton, R. (1989). Customer cost of electric service interruptions. *Proceedings of the IEEE*, 77(6), 919-930.

[134] Caves, D. W., Herriges, J. A., & Windle, R. J. (1992). The cost of electric power interruptions in the industrial sector: estimates derived from interruptible service programs. *Land Economics*, 49-61.

[135] Capitanescu, F., & Wehenke, L. (2008). A new iterative approach to the corrective security-constrained optimal power flow problem. *Power Systems, IEEE Transactions on*, 23(4), 1533-1541.

[136] G.K. Stefopoulos, Y. Fang, G.J. Cokkinides, A.P.S. Meliopoulos. (2005). "Advanced contingency selection methodology," *Proceedings of the 37th Annual North American Power Symposium*, 2005. , pp.67,73, 23-25 Oct. 2005

[137] C. Grigg, P. Wong, P. Albrecht, R. Allan, M. Bhavaraju, R. Billinton, Q. Chen, C. Fong, S. Haddad, S. Kuruganty, W. Li, R. Mukerji, D. Patton, N. Rau, D. Reppen, A. Schneider, M. Shahidehpour, C. Singh. (1999). The IEEE Reliability Test System-1996. A report prepared by the Reliability Test System Task Force of the Application of Probability Methods Subcommittee. *Power Systems, IEEE Transactions on* , vol.14, no.3, pp.1010,1020, Aug 1999

[138] Q. Binh Dam, A.P.S. Meliopoulos, G.T. Heydt, A. Bose. (2010). A Breaker-Oriented, Three-Phase IEEE 24-Substation Test System. *Power Systems, IEEE Transactions on* , vol.25, no.1, pp.59,67, Feb. 2010